

Neurobiological aspects of depression- Antidepressant effects on glia-neuron interaction



DISSERTATION ZUR ERLANGUNG DES DOKTORGRADES DER
NATURWISSENSCHAFTEN (DR. RER. NAT.) DER FAKULTÄT FÜR BIOLOGIE UND
VORKLINISCHE MEDIZIN DER UNIVERSITÄT REGENSBURG

Vorgelegt von

Celia Roman de la Calle

Aus Segovia, Spanien

Im Jahr 2020

Neurobiological aspects of depression- Antidepressant effects on glia-neuron interaction



DISSERTATION ZUR ERLANGUNG DES DOKTORGRADES DER
NATURWISSENSCHAFTEN (DR. RER. NAT.) DER FAKULTÄT FÜR BIOLOGIE UND
VORKLINISCHE MEDIZIN DER UNIVERSITÄT REGENSBURG

Vorgelegt von

Celia Roman de la Calle

Aus Segovia, Spanien

Im Jahr **2020**

Das Promotionsgesuch wurde eingereicht am:

Die Arbeit wurde angeleitet von:

Prof. Dr. Inga D. Neumann und Dr. Barbara Di Benedetto

Unterschrift

Table of content

Abstract.....	9
1. Introduction	11
1.1 Major depressive disorder	11
1.1.1 Susceptibility to depression	11
1.2 Neurocircuitry of depression: brain areas implicated in depression	12
1.3 Etiopathogenesis of depression	14
1.4 Cellular changes in depressive disorder	16
1.5 Astrocytes	17
1.5.1 Origin of astrocytes	18
1.5.2 Neurogenesis, astrogenesis and synaptogenesis	19
1.5.3 Morphological characterization	20
1.5.4 Astrocytic markers and receptors	21
1.5.5 Functions of astrocytes	22
1.6 Phagocytosis and MEGF10 receptor	23
1.7 Astrocytes heterogeneity	26
1.8 Astrocytes in depression	28
1.9 Antidepressants act on the brain, focused on their action in astrocytes and synaptic plasticity	30
1.10 Animal models of depression	33
1.11 Aim	37
2 Materials and Methods.....	38
2.1 Animals	38
2.2 Drugs	39
2.3 Preparation of neurons	39
2.4 Preparation of astrocytes	39
2.5 Preparation of co-cultures	40
2.6 Antidepressant treatment	40
2.7 Harvesting astrocytes for western blot	40
2.8 Western blot experiments	41
2.9 Protein expression quantification	43
2.10 Immunofluorescence procedure and analysis	44
2.11 Confocal microscopy	48
2.12 Quantitative analysis	49
2.13 Sholl analysis	52
2.14 Short interfering RNAs (siRNAs) for the downregulation of MEGF10	53

2.15	RNA isolation, reverse transcription and qPCR	55
2.16	Statistical analysis.....	57
3	Results	58
3.1	Astrocytes as targets of antidepressant (AD) drugs	58
3.1.1	pERK protein expression in primary astrocytes	58
3.2	Synaptic remodelling	59
3.2.1	Analysis of synaptic densities <i>in vitro</i> and <i>in vivo</i>	59
3.2.2	Excitatory synaptic densities in a monoculture model	59
3.2.3	Inhibitory synaptic densities in a monoculture model.....	62
3.2.4	Excitatory synaptic densities in a co-culture model after 48h and 120h continuous AD treatment	64
3.2.5	Analysis of inhibitory synaptic densities in co-culture model.....	67
3.2.6	Examination amount of microglia in co-cultures	69
3.2.7	Excitatory synaptic densities in a monoculture model in the presence of Astrocyte Neuron Condition Media (ANCM)	70
3.2.8	Analysis synaptic densities ex vivo in the rat PFC : synaptic signal intensity	72
3.2.9	Analysis synaptic markers ex vivo in the rat PFC.....	74
3.2.10	Excitatory synaptic densities in the presence of hippocampal astrocytes.....	75
3.3	Evidences of the astrocyte-dependent remodelling of synapses	77
3.3.1	Analysis MEGF10 expression in the rat PFC	77
3.3.2	Analysis of MEGF10 protein amount in PFC.....	77
3.3.3	Analysis of MEGF10 in primary cortical astrocytes	78
3.3.4	Analysis of MEGF10 protein amount in astrocytes from cortical regions.....	79
3.3.5	Evidences MEGF10 is mediating the astrocyte-dependent remodelling of synapses ..	80
3.3.6	Effects of inhibitor U0126 on the number of synapses.....	80
3.3.7	MEGF10 knockdown via siRNA.....	82
3.3.8	Analysis of excitatory synaptic densities in the presence of knockdown MEGF10 astrocytes	86
3.3.9	Phagocytic properties of astrocytes <i>in vitro</i>	88
3.4	Studying astrocytes and their interaction with neurons in animal models for depression	90
3.4.1	Characteristics of the depressive-like phenotype in Wistar Kyoto rats on a cellular basis	90
3.4.2	Sholl analysis: Alteration of morphological properties and complexity of NAB neurons co-cultured with HAB or WKY astrocytes	92
3.4.3	Sholl analysis after AD treatment.....	94
3.4.4	Synaptic density in NAB Neurons co-cultured with HAB or WKY Astrocytes.....	94
3.4.5	MEGF10 levels in primary astrocytes derived from animal models of depression.....	96

4	Discussion	97
4.1	Synaptic remodelling and the implication of astrocytes.....	98
4.2	MEGF10 and its role in the remodelling of synapses	105
4.3	Animal models of depression and targeting astrocytes as therapeutic value	107
	Supplementary.....	111
	List of abbreviations	113
	References	116
	Acknowledgments.....	121

Abstract

Major depressive disorder (MDD) is a globally spread and complex neuropsychiatric disorder. The neurobiological underpinnings of MDD are a current matter of study. The strong heterogeneity of its clinical manifestations and the lack of response in some patients make the identification of new targets and the generation of novel treatments an important issue for the treatment of MDD. Therefore, the aim of this thesis was to contribute to the discovery of new targets for antidepressants (ADs) to improve MDD treatment. Recently, it was shown in *post-mortem* tissue of MDD patients that the number of glial cells is reduced, accompanied by atrophy of neuronal cells and decreased volume of the prefrontal cortex (PFC). Neuropsychiatric disorders also display disrupted synaptic communication and neuronal connectivity, which are reversed by ADs. Following the hypothesis that a dysregulation in the communication between glial cells and neurons is one of the key factors underlying the development of MDD, I aimed to see the effects of astrocytes on synapse homeostasis upon the effect of ADs.

I focused my study on the PFC and hippocampal areas, hence these areas are known to be highly involved in mood disorders. For examining cell-type specificity, I performed both *in vitro* and *ex vivo* experiments from naïve animals in order to not interfere with other physiological changes produced by the disease itself. In the present study, I could observe a reduction in excitatory synaptic densities *in vitro*, after 48h continuous AD treatment, when neurons were growing in the presence of cortical astrocytes but not when hippocampal astrocytes were present. In the absence of astrocytes or in the presence Astrocyte-Neuron Conditioned Media such effects were not seen, suggesting that a membrane-bound protein might have mediated those effects. *Ex vivo* experiments also revealed a reduction of synaptic markers in the adult rat PFC after short-term treatment with ADs, but not in other areas such as CA1 and CA3 of the hippocampus. Astrocytes could mediate this fast AD action as there are closely associated to synapses. For these reasons, MEGF10 receptor was studied. This molecule is a transmembrane receptor that participates in synapse elimination mostly during development. Indeed, treatment with ADs for 48 hours (h) triggered an increase in MEGF10 expression in the adult rat PFC and in primary cultured astrocytes. Therefore, the reduction in the number of synaptic densities I observed could be explained by an astrocyte-dependent

remodelling of synapses following acute AD treatment. In support of this hypothesis, the downregulation of MEGF10 was sufficient to block ADs effects, thus no reduction in synaptic densities was observed. Taken together, these data suggest that MEGF10 could be a potential novel candidate to develop alternative treatment options for diseases characterized by synaptic aberrancies, such as MDD.

Moreover, it is important to understand which major changes are produced in disease conditions. Therefore, part of this thesis aimed to demonstrate the neurobiological basis of the heterogeneity found in depression, using two different animal models with a depressive-like phenotype (HAB, *High Anxiety like Behaviour rat* and WK, *Wistar Kyoto rat*). Differences in the number of synaptic densities and in the morphology of neurons have been found in HAB and WK compared to control animals. Finally, further studies should reveal the contribution of MEGF10 to such changes and how a pharmacological treatment may help to re-establish some of those changes.

1. Introduction

1.1 Major depressive disorder

Major depressive disorder (MDD) is a psychiatric disorder that affects 264 million people worldwide, according to the data set by the World Health Organization (WHO). Moreover, this number has increased in more than 18% between 2005 and 2015 (WHO, 2017). In general, neuropsychiatric disorders account for 19.5% of the burden of disease in the European Region. The cost of mood disorders and anxiety in the European Union is about 170€ billion per year. Despite this fact, about 50% of major depressions are untreated (WHO, 2012) and current pharmacotherapies help many patients, but there are still high rates of a partial response or no response to antidepressant therapies. MDD is characterized by depressed mood or dysphoria, but in addition to this core experience, there are several other symptoms, including loss of interest in activities, sleep and appetite changes, guilt and hopelessness, fatigue, restlessness, concentration problems, and suicidal thoughts (Kanter et al., 2008). Clinicians find a standard criteria for the classification of mental disorders in “The Diagnostic and Statistical Manual of Mental Disorders” (DSM), published by the American Psychiatric Association (Kanter et al., 2008). The criteria to categorize the state and severity of depression are based on a diagnostic interview by the psychologist, indicating that this diagnosis is not based on concrete pathophysiological evidences. Improving treatment of depression requires properly organized treatment programs, regular patient follow-up and monitoring of treatments (Schulberg et al. 1998). Understanding the pathophysiology of depression is necessary, given the clinical heterogeneity of MDD, to obtain a more individual treatment response and novel treatment strategies (Heshmati and Russo, 1993).

1.1.1 Susceptibility to depression

A variety of genetic, epigenetic, endocrine and environmental factors may be risk factors of this disease (**figure 1** from Duman et al. 2016). For example, susceptible individuals exposed to traumatic or stressful life events may develop depression. Among the factors

that can trigger a depressive phenotype are: an abnormal function of the hypothalamic-pituitary-adrenal (HPA) axis, neurotrophic factors, sex steroids, and metabolic and/or inflammatory cytokines that can lead to alterations in neurotransmitters, intracellular signalling, gene transcription, and epigenetic changes that can contribute to short-term and long-lasting imbalances of neuronal function and behaviour. These systems lead to an increased incidence of depression, as well as to comorbid illnesses (Duman et al. 2016).

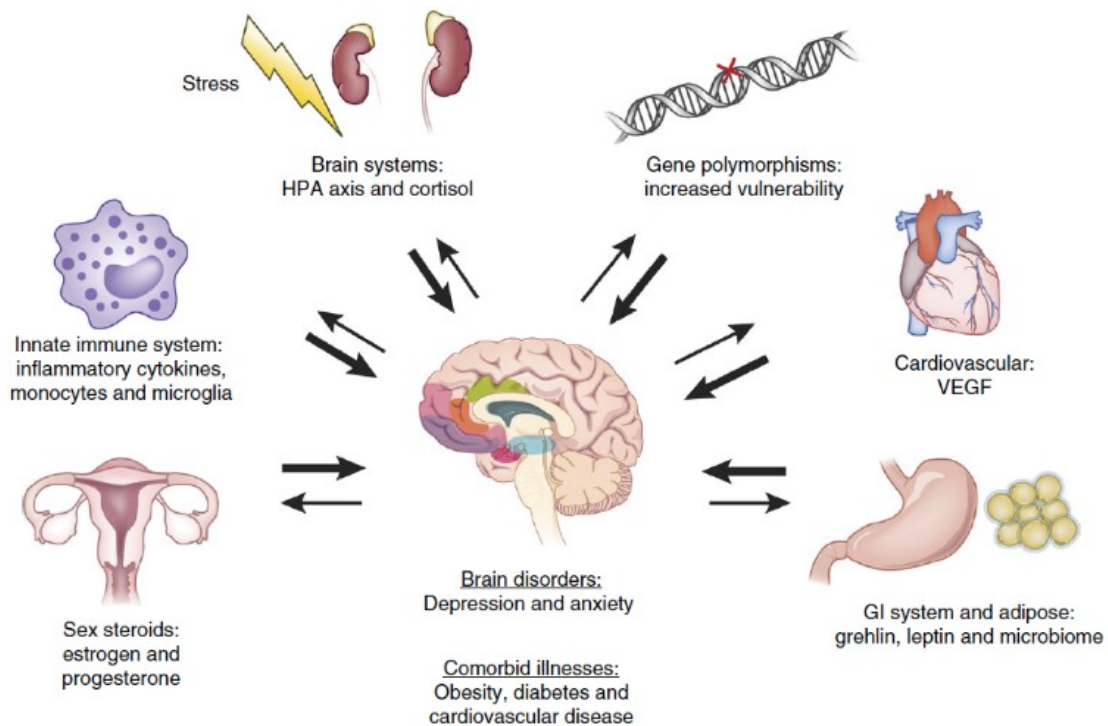


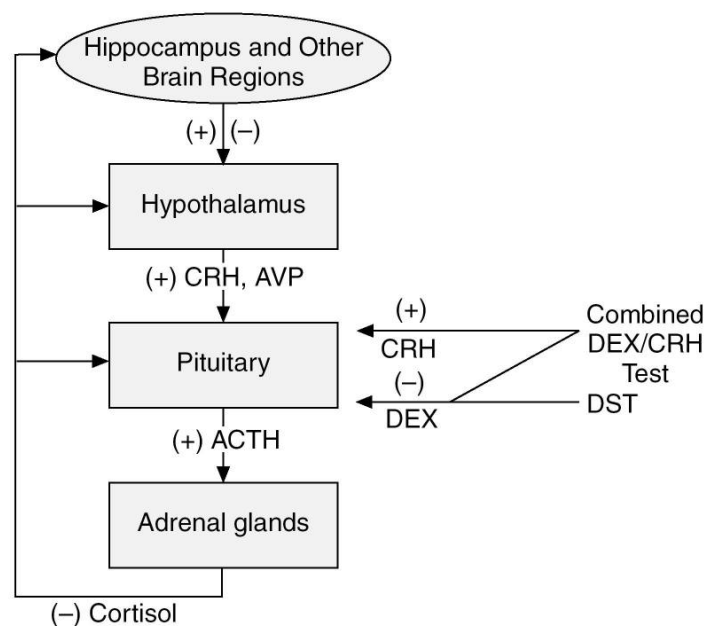
Figure 1. Factors influencing susceptibility to depression. The heterogeneity of depression results from one or more pathological determinants. Activation of the HPA axis and cortisol, the innate immune system and inflammatory cytokines, fluctuations of ovarian steroids, the gastrointestinal system, adipose tissue and related peptides, the microbiome, the cardiovascular system and gene polymorphisms may influence vulnerability (from Duman et al. 2016).

1.2 Neurocircuitry of depression: brain areas implicated in depression

Variations in hormones levels and the stress response have been studied in patients with a depressive phenotype. Abnormalities in the HPA axis have been analysed by psychiatrists and researches in order to understand the biology of depression. The HPA axis consists of a feedback circuits including the hypothalamus, pituitary and adrenal glands (**figure 2**). The hippocampus, amygdala, bed nucleus of the stria terminalis and

paraventricular nuclei (PVN) also participates in the regulation of this axis. During stress, the HPA axis is activated (Varghese and Brown, 2001). The hypothalamus secretes two hormones –corticotropin-releasing hormone (CHR) and arginine vasopressin (AVP)- that act on the pituitary to increase the release of adrenocorticotropin hormone (ACTH) that will be carried to the blood circuitry to interact with receptors on adrenocortical cells that finally will stimulate the release of cortisol in humans or corticosterone in other animals. Cortisol levels will influence the pituitary and hypothalamus and with this negative feedback the loop is completed (Varghese and Brown, 2001).

Elevated levels of cortisol have been found in depressive patients, this is the reason why those elevated levels may be involved in the etiology of mood disorders. Increased CHR levels after stressful events –i.e. maternal deprivation- or in experimental conditions when this hormone is administered to animals, give rise to a depressive phenotype (Varghese and Brown, 2001).



Abbreviations: ACTH = adrenocorticotropin hormone, AVP = arginine vasopressin, CRH = corticotropin-releasing hormone, DEX = dexamethasone, DST = dexamethasone suppression test.

Figure 2. Hypothalamic-pituitary-adrenal (HPA) axis and regulation (from Varghese and Brown, 2001).

The hippocampus is another brain structure that has been extensively studied due to its implications in depression and with regard to the actions of stress and antidepressant actions in this area (Czeh et al. 2001). This structure plays a critical role in learning and

memory (Sapolsky, 2015). Some imaging studies in humans have revealed that the hippocampus undergoes selective atrophy by reducing its volume in stress-related neuropsychiatric disorders (Czeh et al. 2001).

Other areas that integrates sensory information in humans are the orbital PFC, the medial PFC (mPFC) and the infralimbic PFC in rodents. These areas integrate information and modulate visceral reactions that are related to emotional processes through multiple outputs to other brain regions (Duman et al. 2016), like hippocampus, nucleus accumbens, ventral tegmental area and amygdala (AMY), that are part of the mesolimbic reward circuit together with the PFC (Heshmati and Russo, 1993). In patient with mood disorder, the medial prefrontal network and related regions have been shown to contain alterations in gray matter volume, cellular elements, neurophysiological activity, receptor pharmacology (Price and Drevets, 2010).

1.3 Etiopathogenesis of depression

Many studies have tried to explain the etiology of depression (**figure 3**). These are some of the hypothesis:

- i. **Monoamine hypothesis.** Monoamines are neurotransmitters that contain one amino group connected to an aromatic ring by a two-carbon chain, some monoamines in the brain are serotonin, noradrenaline and dopamine. Some neurons that use monoamine neurotransmitters, are involved in the regulation of processes such as emotion. Under pathological conditions, like MDD there is a deficiency of brain monoaminergic activity. Different antidepressants work by increasing the availability of brain monoamines (Elhwuegi 2004).
- ii. **Glutamatergic hypothesis.** Dysfunction of glutamatergic neurotransmission is increasingly considered to be a core feature of stress-related mental illnesses. Both stressors/glucocorticoid treatments acutely increase glutamate release in some brain areas as PFC and amygdala. For example, *in vivo* microdialysis studies have shown that exposure of rats certain stress: tail-pinch, restraint- or forced-swim stress induces a marked and transient increase of extracellular glutamate levels in the PFC (Popoli et al. 2012).

- iii. **Neurotrophic hypothesis.** MDD results from decreased neurotrophic support, leading to neuronal atrophy, decreased hippocampal neurogenesis and loss of glial cells. Antidepressant treatment blocks or reverses this neurotrophic factor deficit, and thereby reverses the atrophy and cell loss. Some studies have demonstrated that stress and depression decrease brain-derived neurotrophic factor (BDNF) expression and function in the PFC, hippocampus and in the blood of subjects with depression. It is known that BDNF infusion is sufficient to produce an antidepressant response in animal models, and that BDNF is required for a response to antidepressant treatment (Duman and Li, 2012; Duman et al. 2016)
- iv. **Immunological hypothesis.** The body activates an immune response against a threat to the subject's self-esteem. Stressors are known to activate key inflammatory pathways in peripheral blood, e.g. increasing circulating levels of pro-inflammatory cytokines, like interleukin-6 (IL-6). On the contrary, the greater the inflammatory response to a psychosocial stressor, the more probable the subject is to develop depression over time. In this way, individuals at high risk of developing depression (for example, e.g. after early-life trauma) show increased inflammatory responses compared with low-risk individuals (Miller and Raison 2016). Normal brain function requires low levels of inflammatory cytokines, therefore elevated levels contribute to damage, atrophy and loss of spine synapses in response to stress and depression (R. S. Duman et al. 2016).
- v. **Glia cell hypothesis.** Reduction in astrocytic proteins – glial fibrillary acidic protein (GFAP), connexins (Cx), aquaporin 4 (AQP4), glutamate transporter (GLT) and glutamine synthetase (GS)- in frontolimbic brain areas from depressive people in *postmortem* studies revealed that glial cell disruptions can be implicated in MDD. Moreover studies with animal models and imaging studies of patients with depression have shown that glial dysfunction is implicated in the pathophysiology of MDD and decreased astrocytic function is necessary and sufficient to trigger depressive symptoms (Rial et al. 2016).

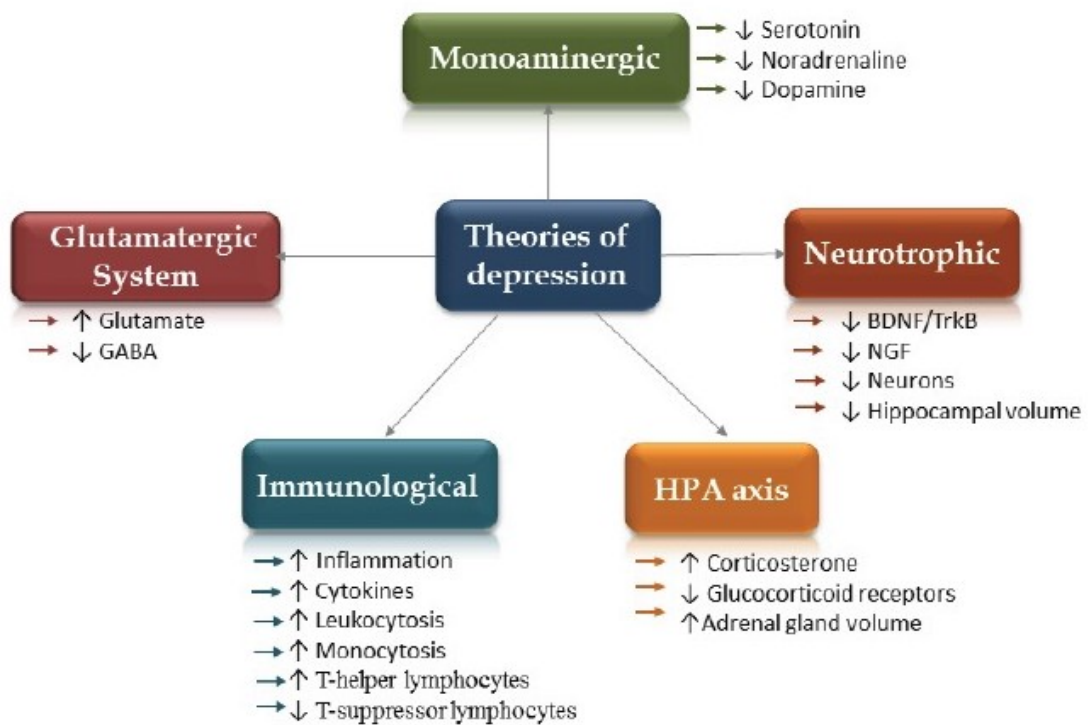


Figure 3. Scheme of some hypothesis of depression. In each plot there is a summary of the most characteristic changes found in samples from MDD samples or animal models (Katarzyna 2015).

1.4 Cellular changes in depressive disorder

Some studies have elucidated the pathophysiology of mood disorders, providing evidence for cell atrophy and loss in relevant limbic brain structures. Some of the cellular changes that have been found in limbic regions in depressive phenotype are the following. Morphological studies that have been made after repeated stress in rodents, and brain imaging and *post-mortem* studies from people suffering MDD demonstrate a reduction in the volume of hippocampus and PFC, and a reduction in the size or loss of neurons and glial cells (Liu and Aghajanian 2008; Duman and Li 2012). The influence of repeated stress on rats has been shown to produce dendritic atrophy pyramidal neurons in the mPFC, in particular decreased apical dendritic branch length and spine density in distal branches (Radley et al., 2005; Liu and Aghajanian, 2008). A retraction in dendritic material in CA3 area of the hippocampus was also found after chronic stress –risk factor for the later development of depression- (Christian et al. 2011). Inhibition of neurogenesis in the adult hippocampus or loss of preexisting hippocampal neurons after neurotoxicity has been described (Sapolsky, 2001). In depressed subjects it has been

observed a hippocampal volume reduction that can be partially explained by dendritic retraction and reduced cell proliferation that has been found in animal models (Czeh et al. 2001).

The impairment of several glial functions are likely to contribute to the pathophysiology of depression. Astrocytes have been found to be modified in frontolimbic regions, and those changes are associated with depression. Most studies analysed *post-mortem* brain samples from adult individuals with major depressive disorder conclude that there is a decreased number of astrocytic-like elements in those areas, an alteration of astrocytic morphology and density of different astrocytic markers, such as GFAP, S100 calcium-binding protein β (S100 β), Cx, AQP4, etc (Rial et al. 2016). Other studies propose that microglia are morphologically altered in frontolimbic regions of depressed patients with hypertrophic cell bodies (Rial et al. 2016). On the other hand, MDD patients do not present prominent astrogliosis or glial scar formation (Dossi, Vasile, and Rouach, 2018). It is still a matter of discussion whether the altered number and morphology of glial cells may be the cause or consequence of glial dysfunction in mood disorders.

1.5 Astrocytes

Astrocytes are defined as a highly heterogeneous class of neural cells of ectodermal, neuroepithelial origin that sustain homeostasis and provides for defence of the central nervous system (Verkhatsky et al. 2017). Astrocytes were first described by Virchow in 1846 and were originally thought to be cells which function to support neurons (Chaboub and Deneen 2012). For many years astrocytes were considered to be passive supporters of neurons but nowadays they are known to play an important role in the brain being an important component of the tripartite synapse. This definition refers to their interaction with neurons and their participation in the regulation of synaptic neurotransmission (Araque et al. 1999). In the human neocortex astrocytes accounts for 20%–40%, oligodendrocytes for 50%–75% and microglia for 5%–10% of the total glial population. The total number of astrocytes in rodents is around 10–20% of total cells in the brain (Verkhatsky et al. 2017). Astrocytes are closely associated with synapses, it is estimated that a single human astrocyte may contact and integrate around 2 million of synapses

residing in their territorial domains, whereas rodent astrocytes cover 20.000–120.000 synaptic contacts (Verkhatsky et al. 2017).

1.5.1 Origin of astrocytes

The embryonic neuroepithelium is composed of a heterogeneous mix of progenitors that produce different neural subtypes within specific spatiotemporal boundaries. During embryonic development, radial glia cells (RG) derived from the neuroepithelium are the primary neural stem cells that produce neurons and glia throughout the brain (**figure 4**). Astrocytes are first detected around embryonic day 16 (E16), however, the vast majority of astrocytes are produced during the first month of postnatal development (Bayraktar et al. 2019).

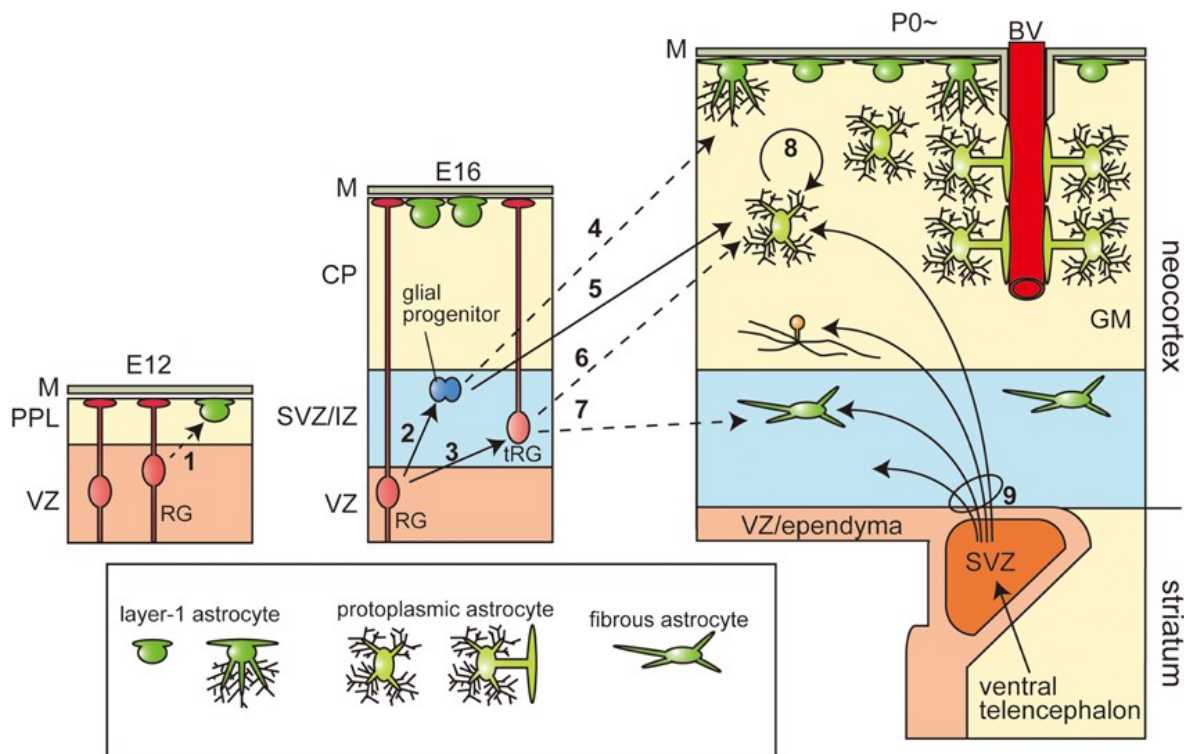


Figure 4. Heterogeneity of astrocytes and their origin. Production and final positioning of the astrocytes during development. Arrows with solid lines indicate the cell lineages confirmed by lineage tracing experiments. Arrows with broken lines show the hypothetical cell lineages by histological investigations. E, embryonic day; P, postnatal day; GM, grey matter; WM, white matter; M, meninges or pia matter; PPL, primordial plexiform layer; VZ, ventricular zone; SVZ, (embryonic or postnatal) subventricular zone; IZ, intermediate zone; CP, cortical plate; BV, blood vessel (Modified from Tabata, 2015)

1.5.2 Neurogenesis, astrogenesis and synaptogenesis

In the cortex neurogenesis is being produced before astrogenesis and synapses only begin to form after astrocytes have been generated, concurrent with neuronal branching and process elaboration. The generation of cortical neurons in mice begins at embryonic day (E10–11). At birth (P0) cortical neurogenesis has finished, but it is not until postnatal day (P7) when the arrangement of neurons into defined cortical layers is completed. Then, the axons of newly generated neurons extend to find their future postsynaptic partners, and dendrites begin to form the protrusions that mark potential postsynaptic sites, after their interaction synapses will be formed (Farhy-Tselnicker and Allen 2018). Astrocytes are generated from the same progenitor cells which gave rise to neurons at birth E18/P0. These progenitors undergo a potency switch from a neurogenic to a gliogenic differentiation program and differentiate into astrocytes (Miller and Gauthier, 2007; Farhy-Tselnicker and Allen 2018). Astrocytes, as they have mitotic properties, continue to expand in number through the end of the first month of life, establishing then a mature morphology (with fine processes that will contact with neuronal synapses). Since then, they are set in particular, non-overlapping domains (Farhy-Tselnicker and Allen 2018). Although neurons send out projections before birth, synapses only begin to form during the first week of postnatal development, concurrent with the appearance of astrocytes, indeed very few synapses are formed in the absence of glial cells and the ones that are present are functionally immature (Ullian et al. 2001). Astrocytes play an important role in promoting synaptogenesis. The formation of chemical synapses begins during the first postnatal week, peaks at P14, and stabilizes at P21 to P28, concurrent with synapse elimination and the refinement of circuits (**figure 5**; Farhy-Tselnicker and Allen, 2018).

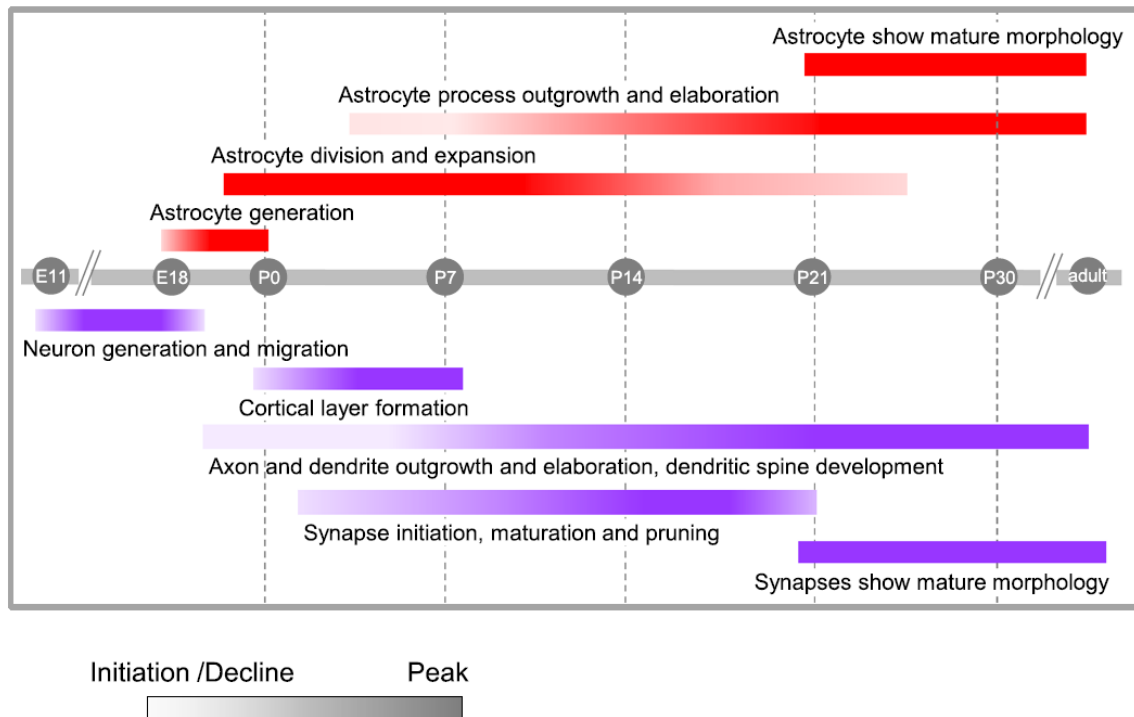


Figure 5. Overview of astrocyte, neuron and synapse generation and development in the rodent cortex. Timeline from neurogenesis, astrogenesis, synaptogenesis, maturation and stabilization of synapses. Timeline for astrocytes is marked red and for neurons in purple (Farhy-Tselnicker and Allen, 2018).

1.5.3 Morphological characterization

Identification and visualization of astrocytes in the nervous tissue relies on the morphological criteria and expression of specific markers (Verkhatsky et al. 2017). Astrocytes have been categorized into two broad morphologies: protoplasmic astrocytes, found in the grey matter, associated with both synapses and endothelial cells and directly participating in the ‘neurovascular unit’. Those protoplasmic astrocytes extend their processes near neurons and are known to be closely associated with synapses being responsible of modulating synaptic functions. The processes of two adjacent protoplasmic astrocytes are mutually exclusive, and occupy non-overlapping domains (Bushong et al. 2002). On the other hand, fibrous astrocytes, located in the white matter express higher levels of GFAP, with short and highly branched extensions, may participate in myelination but their functions need to be further studied (Chaboub and Deneen, 2012).

1.5.4 Astrocytic markers and receptors

A common approach to identify astrocytes is via the expression of diverse markers. Some of the markers include: GFAP, vimentin, S100 β , glutamate transporters (excitatory amino acid transporters 1 and 2 (EAAT-1) and (EAAT-2); known in rodents as GLutamate ASpartate Transporter 1 (GLAST and GLT-1, respectively), GS, inward rectifying Kir4.1 channels, water channels AQP4, Cx30 and Cx43, aldehyde dehydrogenase 1 family member L1 (ALDH1L1), fructose-1, 6-bisphosphate aldolase (or aldolase C), and transcription factor SOX9 (Verkhatsky et al. 2017). Intermediate filaments are a highly dynamic part of the cytoskeleton of cells and their expression is highly cell type specific. Astrocytes express 10 different isoforms of GFAP, together with vimentin, nestin, and synemin (Hol and Pekny, 2015). In the juvenile hippocampus anti-GFAP staining reveals 80% of all astroglia whereas in other regions of the healthy brain only a 10-20% of cells are positive for GFAP (Verkhatsky et al. 2017). On the other hand, GFAP staining reveals only the main processes of astrocytes, with no labelling of perisynaptic and peripheral processes or small endfeet (part of the astrocytic processes that interact with blood vessels). S100 β is another commonly used marker to label astrocytes; it is from the family of calcium binding proteins and usually labels 2–3 times more astroglial compartments than GFAP. None of these markers, however, labels all astrocytes throughout the brain (Verkhatsky et al. 2017). The GLT-1 and GLAST astroglial transporters are glutamate transporters mainly involved in maintaining physiological extracellular glutamate concentrations and protecting neurons against excitotoxicity (Perego et al. 2000). Astrocytes express all receptors of the major neurotransmitters including glutamatergic, GABAergic (γ -aminobutyric acid), adrenergic, purinergic, serotonergic muscarinic and opioid receptors. Other receptors for growth factors, chemokines, and steroids have also been found in astrocytes (Porter and Arthy 1997). Receptors that mediate phagocytosis are also found in astrocytes: Multiple EGF-like-domains 10 (MEGF10) and Proto-oncogene tyrosine-protein kinase MER (MERTK) function as engulfment receptors by recognizing 'eat me signals'. Astrocytes are able to engulf synapses and debris during the development and in the adult mammalian nervous system (Chung et al. 2013).

1.5.5 Functions of astrocytes

Astrocytes have different functions during the development to facilitate the formation of neural networks. Astrocytes are closely associated to neurons and synapses, they form the so called tripartite synapse (Araque et al. 1999). Neural circuits are established through a complex process of synaptogenesis, maturation and synaptic pruning (Bosworth and Allen, 2017).

Astrocytes promote synaptogenesis. The differentiation and maturation of astrocytes occurs at the same time that synaptogenesis. During the second and third postnatal week astrocytes participate in the formation of excitatory synapses by secreting factors as thrombospondins (TSP), glypicans 4 and 6 (Gpc4 and Gpc6), Hevin and secreted protein acidic and rich in cysteine (SPARC), tumor necrosis factor α (TNF- α), transforming growth factor β (TGF- β ; Farhy-Tselnicker and Allen, 2018). TSPs induce ultrastructurally normal synapses that are presynaptically active but postsynaptically silent. Astrocyte conditioned media (ACM) and the presence of astrocytes exhibits the same ability to induce synaptic puncta compared to the presence of neurons alone, furthermore TSP –one of the factors released by astrocytes and present in the ACM- was sufficient to induce synapses (Ullian et al. 2001; Christopherson et al. 2005). Other astrocyte-secreted signals are Gpc4 and Gpc6. Those molecules are sufficient to induce functional synapses between retinal ganglion cell neurons by increasing the clustering and surface level of Glutamate receptor 1 (GluA1) subunit of α -amino-3-hydroxy-5-methyl-4-isoxazolepropionic acid receptor (AMPA) receptor thereby inducing the formation of postsynaptically functioning synapses (Allen et al. 2012). Hevin is sufficient to induce the formation of synapses between cultured retinal ganglion cells (RGCs) and SPARC is unable to induce synapse formation, but strongly inhibits Hevin-induced synapse formation *in vitro* (Kucukdereli et al. 2011). TNF α is produced by glial cells and is able to enhance synaptic efficacy by increasing surface expression of AMPA receptors, participating in the control of synaptic strength at excitatory synapses (Beattie et al. 2002). TGF- β is secreted by glia and is expressed in the embryonic and postnatal brain during the synaptic period and induces the formation of functional synapses involving D-serine (Diniz et al. 2012).

Astrocytes also support excitatory synaptic maturation. During development neural activity and synaptic competition induce the transition of immature filopodia to mature

stubby/mushroom spines. Hevin apart from being a synaptogenic factor, also assembles glutamatergic synapses by bridging neurexin-1 α and neuroligin-1 β , two isoforms that do not interact with each other, this modulation in the adhesion of these proteins is critical for the formation and plasticity of thalamocortical connections in the developing visual cortex (Singh et al. 2016). Astrocytes synthesize cholesterol that contributes to the refinement and maturation of hippocampal synapses by enhancing the efficacy of synaptic transmission at glutamatergic presynaptic terminals (van Deijk et al. 2017). The synthesis of cholesterol is elevated during the peak of synaptogenesis under the control of sterol regulatory element binding proteins (SREBPs). It was seen that diminishing SREBP activity in mouse astrocytes –by deletion of SREBP cleavage-activating protein (SCAP)- resulted in decreased cholesterol and phospholipid secretion by astrocytes. Moreover, SCAP mutant mice showed more immature synapses, lower presynaptic protein SNAP-25 levels as well as reduced numbers of synaptic vesicles, indicating impaired development of the pre-synaptic terminal (van Deijk et al. 2017).

1.6 Phagocytosis and MEGF10 receptor

Astrocytes can contribute to the refinement of neural circuits through synaptic pruning. Astrocytes participate in the eventual elimination of synapses of redundant and nonspecific synaptic contacts in two ways. Astrocytes mediate pruning directly through phagocytosis and indirectly by mediating the neuronal expression of phagocytic markers recognized by microglia. Synapses are eliminated in order to refine neuronal circuits, inappropriate or weaker connections are tagged for elimination (Bosworth and Allen, 2017). The elimination of synapses has been mostly studied in the developing visual system when astrocyte morphogenesis and maturation occur concomitantly with synaptic development. Stevens and colleagues showed that the classical complement cascade, which is part of the innate immune system, participates in synapse elimination. An astrocyte-derived signal triggers complement component 1q (C1q) upregulation in postnatal neurons and it is localized in synapses, following a protease cascade and finally leading to the deposition of the downstream complement component 3 (C3), that can directly activate C3 receptors on macrophages or microglia, thereby triggering elimination by phagocytosis. If C1q or C3 are absent in the brain of mice, those animals

present large sustained defects in central nervous system (CNS) synapse elimination (Stevens et al. 2007).

In the developing and adult brain, astrocytes are able to eliminate synapses through MEGF10 and MERTK pathways. Those molecules play critical role in synapse remodelling underlying neural circuit refinement (Chung et al. 2013). In a transcriptome data analysis for astrocytes, it was found that they are enriched in MEGF10 and MERTK genes, genes for phagocytic pathways in astrocytes, suggesting they are involved in phagocytosis (Cahoy et al. 2008). The phagocytic pathway were first described in *Drosophila* glia cells and *Caenorhabditis elegans* engulfing cells, where the orthologues of MEGF10 –Draper and CED-1 respectively- meditates axon pruning or phagocytosis of apoptotic cells (MacDonald et al. 2006; Zhou, Hartweg, and Horvitz, 2001), suggesting the cellular machinery promoting phagocytosis of corpses of apoptotic cells is well conserved from worms to mammals (**figure 6**). In nematodes, *ced-1* encodes a transmembrane protein similar to human SREC (Scavenger Receptor from Endothelial Cells). The CED-1 protein is localized in the surface of cell membranes that senses cell death signals and recognizes neighbouring cell corpses, possibly by recognizing a phospholipid ligand on their surface. It also clusters at the phagocytic cups and initiates pseudopod extension. (Zhou, Hartweg, and Horvitz 2001). CED-1-dependant phagocytosis involves other CED proteins (such as CED-6 helping to control the delivery of vesicles to phagocytic cups and phagosomes and CED-7 recognizing engulfment signals of cell corpses cognizing engulfment signals of cell corpses; Chen et al. 2009). In the olfactory system of flies, glia upregulate expression of the engulfment receptor Draper and undergo dramatic changes in morphology, and rapidly recruit cellular processes toward severed axons, after axonal injury is produced. In the *draper* mutants, the axons are not cleared properly due to glia fail to respond morphologically to axon injury (MacDonald et al. 2006). To activate Draper some other molecules participates in the pathway. Shark, a non-receptor tyrosine kinase binds Draper through an immunoreceptor tyrosine-based activation motif (ITAM) in the Draper intracellular domain. Moreover, the Src family kinase (SFK) Src42A can markedly increase Draper phosphorylation and is essential for glial phagocytic activity. In order to explain the signalling cascade it was proposed that ligand-dependent Draper receptor activation initiates the Src42A-dependent tyrosine phosphorylation of Draper, the

association of Shark and the final activation of the Draper pathway (MacDonald et al. 2006).

The function of MEGF10 requires other proteins, such as GULP1 (CED-6 ortholog) and ABCA1 (CED-7 ortholog; Chen et al. 2009). ABCA1 is an Adenosine triphosphate (ATP) binding cassette transporter. Hamon and colleagues proposed a model to explain the MEGF10-ABCA1 interactions. At the site of engulfment, ABCA1 molecules are activated, by yet unknown mechanisms, and then enter the catalytic cycle. The binding of ATP induces assembly into complex oligomers containing ABCA1 multimer. ATP hydrolysis at the nucleotide binding domain triggers local remodelling of lipid composition, such as the ABCA1 dependent externalization of phosphatidylserine and disassembly of the oligomeric complexes into individual components. This new membrane configuration could favour the shuttling of the components to MEGF10 in order to help in the engulfment function. Some cytoskeletal scaffolds like dynamin are able to drive MEGF10 along the forming phagosome (Hamon et al. 2006). In other study, the expression of Jedi-1 or MEGF10 in fibroblasts facilitated the engulfment of neuronal corpses, and by knocking-down either protein in glial cells or overexpressing truncated forms inhibited engulfment of apoptotic neurons. This suggest that these receptors may converge on a common pathway or even form a complex (Wu et al. 2009)

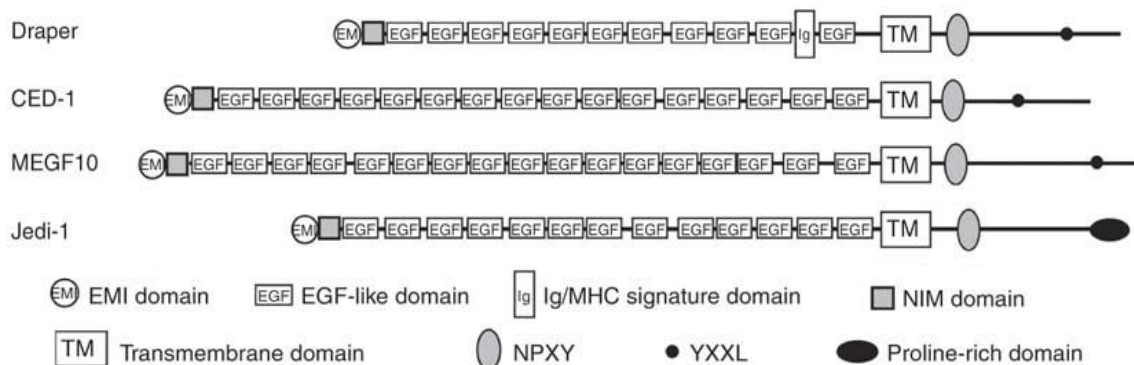


Figure 6. Schematic representation of the modular architecture of Draper, CED-1 and mammalian homologs. Three mammalian proteins, MEGF10, MEGF11 and Jedi-1, were identified as being highly homologous to Draper and CED-1 using BLASTP (National Center for Biotechnology Information). Modified from Wu *et al.*, 2009.

On the other hand, synapse elimination mediated by astrocytes involves an astrocytic $[Ca^{2+}]$ elevation dependent on inositol 1,4,5-trisphosphate receptor (IP3R). The IP3R type 2 knockout (*Itpr2^{-/-}*) mice showed an impaired somatic Ca^{2+} signalling in astrocytes, giving rise to impaired developmental elimination of synapses in the ventral posteromedial nucleus. This impairment was also found in the *P2ry1^{-/-}* mice, where the purinergic receptor was ablated. Even though there was an impairment in pruning in those animals, synapse elimination was still found between P7 and P16 suggesting that there are multiple mechanisms for controlling synapse elimination (Yang et al. 2016).

1.7 Astrocytes heterogeneity

Different regions of the adult brain contain astrocytes with vastly different morphologies. Some studies have tried to underlie the expression pattern of astrocytes from different areas finding that astroglia from each region are molecularly distinct. Those studies were performed with high-density RNA microarray profiling on astrocytes from optic nerve, cerebellum, brainstem, and neocortex during development, it was found that each population contained both common and unique cohorts of genes (Yeh et al. 2009). Astrocytes from different regions demonstrate heterogeneity in their expression of ion channels and coupling molecules. For example, K^+ channel, Kir4.1, is enriched in astrocytes of the ventral horn of the spinal cord compared to those of the dorsal horn (Chaboub and Deneen, 2012). Functional NMDA receptors have been reported in cortical and spinal cord astrocytes and Bergmann glia of the cerebellum but not in other areas as in the hippocampus. Cx43 and 30 are more pronounced in the barrel field of rodents compared to other cortical regions (Chaboub and Deneen, 2012). Glutamate transporters have different cellular dynamics of expression; GLT-1 is expressed mostly in the cortex, grey matter areas of the hippocampus, and spinal cord of mice while GLAST was expressed in the cerebellum, dentate gyrus of the hippocampus, and spinal cord (Regan et al. 2007). All those findings provide molecular evidence for CNS astroglial cell heterogeneity.

During development, synaptogenesis is determined through multiple mechanisms influenced by the astrocyte population, brain region, and neuron type. Here we can see

some examples using *in vitro* approaches. The protein Hevin is necessary for the establishment of thalamocortical synapses in the primary visual cortex, by stabilizing the trans-synaptic connection between presynaptic neuroligin and postsynaptic neuroligin, but has no role in the establishment of intracortical synapses (Singh et al. 2016). In another study, the heterogeneity of the synaptogenic profile of astrocytes from different brain regions was studied by looking at the effect of astrocyte conditioned medium (ACM) from different areas on primary neurons. In summary, they found that different populations of astrocytes have different gene expression profile in some of their synaptogenic factors (e.g Gpc4 is more enriched in the cerebellum while Gpc6 is more abundant in the hippocampus; Hevin is also more expressed in the hippocampus but SPARC present higher expression in cortical astrocytes). This heterogeneity found in the astrocyte population may be relevant for the astrocyte-synapse interactions and might impact neuronal connection events (Buosi et al. 2017). On the other hand, Farmer and colleagues found that astrocytes depend on cues from mature neurons to control their complex molecular profile *in vivo*. They focused on the cerebellar cortex, which contains two specialized astrocyte types, Bergmann glial (BGs) cells -that enwrap Purkinje cell dendrites and synapses- and velate astrocytes (VA) -that surround granule cells and mossy fibers-. Those astrocytes share comparable expression of some genes like GFAP, Sox9 and GLT1 but also display distinct molecular profiles. BGs are enriched in AMPA receptors GluA1 and GluA4, and GLAST, while VAs are known to have low amounts of those genes and large amounts of the AQP4. Sonic hedgehog signal (Shh) that regulate cell specification, axon guidance, and cell proliferation, drives specific molecular and functional changes in BGs but not in VAs. Genetically manipulating an increase in the Shh pathway in VAs allowed those cells to obtain an mRNA profile resembling that of BGs. This is one of the mechanisms that create and maintain differences among astrocytes (Farmer et al. 2016). Another study has related astrocyte subpopulations in healthy brain with analogous populations across a cohort of human tumors. They identified five distinct astrocyte subpopulations present across three brain regions (olfactory bulb, cortex and brainstem) by using an intersectional fluorescence-activated cell sorting (FACS)-based strategy. Moreover, they identified correlative populations in mouse and human glioma, those specific subpopulations emerged during tumor progression corresponded with the onset of seizures and tumor invasion (John Lin et al. 2017). All those results show the

molecular and functional heterogeneity of astrocytes in the nervous system, demonstrating that astrocytes are able to exert particular synaptogenic effects in specific synapses, and revealing that neurons can also control the diversity of astrocytes in the brain.

1.8 Astrocytes in depression

Numerous studies have revealed that MDD is a disorder with prominent pathological astrocytic alterations, which affect density, morphology, protein expression and membrane channel functions of astrocytes as I will describe here. Many of the studies have been performed on *post-mortem* brains and it has been observed prominent decreases in astrocyte number and packing density in MDD subjects compared to non-psychiatric controls. Numerous studies with animals have revealed that a depressive phenotype can be triggered when the astrocyte function is disrupted or diminish. For example, glial ablation in the PFC of adult rat by targeting the astrocytes with L- α -amino adipic acid is sufficient to trigger a depressive-like phenotype similar to chronic stress (Banasr and Duman 2008; Lima et al. 2014). On the other hand, there are some studies in which the functional activity of astrocytes has been inhibited, as a result the animals develop a depressive-like phenotype. ATP is known to be a key factor involved in astrocytic functions, low ATP amounts were found in the brains of mice that were susceptible to chronic social defeat. Likewise, the transgenic blockage of vesicular gliotransmission, by suppression of the expression of the dn-SNARE domain of synaptobrevin 2, induced deficiencies in astrocytic ATP release, causing depressive-like behaviours that could be rescued via the administration of ATP (Cao et al. 2013). Gap junctional channels are composed of connexin proteins. Impaired gap junctional intercellular communication in astrocytes results in altered neuronal function. Animals exposed to chronic unpredictable stress (CUS) and that had behavioural deficits in sucrose preference test and novelty suppressed feeding test exhibited significant decreases in the diffusion of a special channel-permeable dye and expression of Cx43. Moreover, those alterations were reversed and/or blocked by treatment with typical antidepressants (Sun et al. 2012). AQP4 is the main aquaporin isoform expressed by astrocytes in the CNS. Lack of AQP4 exacerbated depressive-like behaviours in chronic

Introduction

corticosterone subcutaneous injection model of depression, this was observed by performing the forced swimming test (FST) and tail suspension test, mice knockout for AQP4 showed longer immobility times compared to WT (Kong et al. 2014). Astrocytes regulate glutamate levels by removing glutamate from the synapse via glutamate transporters. By inhibiting GLT-1 in the PFC, with a particular inhibitor dihydrokainic acid (DHK), was sufficient to produce anhedonia, a core symptom of depression in rats (John et al. 2012).

In human studies, changes in the previous described proteins have been also described. A decrease in Cx43 occurs in the dorsolateral PFC of people who committed suicide and in the locus coeruleus, orbitofrontal cortex and hippocampus of MDD patients (Dossi, Vasile and Rouach 2018). Messenger RNA (mRNA) transcripts involved in glial syncytial function, potassium channel Kir4.1 and AQP4, are downregulated in hippocampus of MDD subjects compared to controls (Medina et al. 2016). The coverage of blood vessels by endfeet of AQP4⁺ astrocytes was reduced by 50% in MDD patients (Rajkowska et al. 2013) This indicates that MDD subjects have an altered K⁺ and water homeostasis. They may have disrupted integrity of the BBB and may not work as effective as in healthy condition. On the other hand, reductions in the mRNA expression of GFAP and S100 β in the locus coeruleus, source of extensive noradrenergic innervation, were found in MDD patients compared to controls (Bernard et al. 2011). In the serum of depressed people higher levels of S100 β were found (Schroeter et al. 2002) which could reflect a leakage from the astrocyte to extracellular compartments (Dossi, Vasile and Rouach, 2018). *Post mortem* samples of patients who had AD treatment have been studied by several groups. Those histopathological studies in humans have also revealed changes in the amount and morphology of glial cells, Rajkowska and colleagues found decreased cortical thickness and reduction of glial densities in the upper and lower layers of the orbito-frontal region, and reduction of density and size in the dorsolateral prefrontal cortex (Rajkowska et al. 1999).

A reduction in the expression of synapse-related genes is another characteristic of this disorder, some of them are classified as regulators of synaptic vesicles -calmodulin 2, synapsin, regulators of dendritic spine formation -Rab3A, Rab4B-, and mediators of axonal outgrowth and regeneration -beta-tubulin 4- are known to be decreased in MDD subjects. CUS models also have a decreased in the expression of synapsin I, calmodulin 2,

Rab3A, and Rab4B, although not beta-tubulin 4 in the PFC (Kang et al. 2012). This data may suggest that the decreased levels of these synapse-related genes in MDD result from chronic stress exposure that could contribute to depressive behaviours (Kang et al. 2012).

1.9 Antidepressants act on the brain, focused on their action in astrocytes and synaptic plasticity

Most ADs have been created based on the monoamine hypothesis of depression. They work increasing the availability of one or more neurotransmitter in the CNS (Schildkraut, 1965). ADs impact these systems through either primary or secondary pharmacological mechanisms. The delay response of some patients to ADs suggest that their secondary actions might involve changes in gene expression and/or synaptic plasticity contributing to their therapeutic mechanisms (Price and Drevets, 2010). The mechanisms of action are the inhibition of the reuptake of norepinephrine (NE) and/or serotonin (5-hydroxytryptamine (5-HT)) into the presynaptic terminal from the synapse (tricyclic ADs (TCAs), selective serotonin (5-HT) reuptake inhibitors (SSRIs) and (5-HT) and norepinephrine (NE) dual-reuptake inhibitors (SNRIs)); the inhibition of the monoamine oxidase, the enzyme that degrades 5-HT, NE, and dopamine (DA) in the presynaptic terminal (MAOIs); and the blockade or stimulation of presynaptic and/or postsynaptic monoamine neurotransmitter receptors (Holtzheimer and Nemeroff, 2008). For this study five different ADs corresponding to the different classes were used: Desipramine (tricyclic AD), Mirtazapine (tetracyclic AD), Fluoxetine (SSRI), Reboxetine (NRI) and Venlafaxine (SNRI).

The negative effects of stress on neuroplasticity contribute to a disease phenotype, treatment with ADs affect then similar mechanism and are predicted to have opposite effect (Pittenger and Duman, 2008). Those ADs also increase synaptic plasticity at several levels. Classical ADs increase the expression of some molecules associated with neuronal plasticity such as BDNF after chronic treatment (Nibuya, Morinobu and Duman, 1995). BDNF in blood is found in platelets and is released upon their activation; serotonin is known to be taken by platelets through the serotonin transporter, although uptake of serotonin to platelets is reduced in depression. Patients have also low levels of BDNF in serum that can be rescued by treatment. Otherwise, BDNF does not pass through the blood-brain barrier, but plasma BDNF could influence brain regions where the blood-

brain barrier is leaky (Castrén and Rantamäki, 2009). In addition to enhancing functional neuroplasticity, ADs enhanced structural plasticity affecting number of synapses, spines and dendrites. ADs have been seen to increase the number of synapses, for instance 5 days treatment with FLX produces a robust increase in pyramidal cell dendritic spine synapse density in the hippocampal CA1, while CA3 areas are required of 14 days to have similar changes (Hajszan, MacLusky and Leranth, 2005). Also in hippocampal areas, the reduction of dendritic complexity caused by stress can be reversed by chronic administration of tianeptine, but not FLX (Magariños, Deslandes and McEwen 1999). Signalling pathways are implicated in the development of mood disorders and can be target of pharmacological treatment (Czéh and Di Benedetto, 2013). The ERK/MAPK pathway, involved in cell survival and plasticity, can be target of ADs, for instance long-term treatment of FLX activates the extracellular signal-regulated-protein kinase (Erk) and p38 mitogen-associated protein (MAP) kinase cascades. Several classes of ADs have been applied to animal or cells. Short term treatments in primary culture of astrocytes showed an up regulation of downstream genes like BDNF and GDNF (Mercier et al. 2004). In the C6 glioma cell line (used as an *in vitro* model to study astrocytes), some antidepressants like RBX and norquetapine activate ERK1 and ERK2 molecules with a consequent increased release of GDNF (Di Benedetto et al. 2012).

ADs also induce transcriptional and translational changes in glial cells. Up- or down-regulation of GFAP, AQP4, vimentin and upregulation of Cx43 in the PFC upon chronic FLX treatment has been seen in the brain of experimental animals (Fatemi et al. 2008). Astrocytes also express serotonergic transporters. The uptake of 5-HT by rat brain astrocytes through a Na⁺-dependent, FLX-sensitive high-affinity transporter has been documented before (Dave and Kimelberg 1994), pointed out that SSRIs inhibit glial serotonin transporters as well. FLX has relatively high affinity for Gq/11 protein-coupled 5-HT₂ receptors and causes an increase in cytosolic calcium concentration ([Ca²⁺]_i) and phosphorylation of ERK1/2 in astrocytes *in vitro* (Li et al. 2008). Regulation of ion homeostasis, such as K⁺ buffering, is an important astroglial function, mediated by Na⁺, K⁺-ATPase. Accumulated K⁺ is released by an inwardly rectifying Kir4.1 channel. This channel is blocked by SSRIs and TCAs. This might alter astrocyte-neuron interactions in K⁺ homeostasis, neuronal excitability and be implicated in the pathophysiology of mood disorders (Ohno et al. 2007; Su et al. 2007). By knocking down AQP4 in mice, the water

homeostasis can be disrupted and the chronic FLX-treatment-induced hippocampal neurogenesis is abolished as well as antidepressant effects (Kong et al. 2009) indicating the proper stability of the BBB is important for AD action. Studies have shown that MDD is accompanied by an activation of the inflammatory response system and an increase in some cytokines like TNF α and IL-6 in depressed subjects compared with control subjects. Those cytokine levels can be normalized after antidepressant treatment (Dowlati et al. 2010). The structural changes found in glial cells in depressive people can play an important role in the progression of the disease but it is not known if they are the cause or consequence of the pathology of depression. In a study, animal models of long-term psychosocial stress were subjected to daily oral administration of FLX. AD treatment prevented the stress-induced numerical decrease of astrocytes. Any AD effect was found in control animals (Czéh et al. 2006). ADs may work by restoring the deleterious effects of stress or influencing cell proliferation by affecting glia cell number. Regarding this effect, Czéh and colleagues have observed enhanced gliogenesis in the PFC of mice subjected to chronic social stress after treatment with FLX (Czéh et al. 2007). Morphological changes can be observed *in vitro* and *in vivo*, cells treated with imipramine exhibited a round-shaped cell body with long, thin processes (Cabras et al. 2010), while in another study treatment with FLX reduced astrocytic somal volumes. Those changes in structural plasticity of astrocytes can reflect functional changes within the glial–neuronal interaction, for instance reduced hippocampal volumes found in depressive phenotype could be related with stress-induced reduction of astroglia size and number (Czéh et al. 2006). Nonetheless the therapeutic response of MDD people to ADs requires still several weeks of treatment that is why new therapeutic-response targets need to be identified to be able to access to more rapid and efficacious treatment (Duman et al. 2016).

In the last years more studies about the action and efficacy of fast acting AD have emerged. Fast acting AD as ketamine can be effective in treating MDD. It is a non-competitive antagonist of N-methyl-D-aspartate (NMDA) receptor, at subanaesthetic dose can produce a rapid response that is sustained about 1 week, even in patients considered treatment-resistant. Ketamine induces a rapid and transient increase of glutamate release, which stimulates presynaptic metabotropic glutamate receptors (mGluRs). The activation of mGluRs induces a long-lasting decrease of glutamate release that possibly compensates the impaired astrocytic glutamate clearance in MDD

(Sanacora, Treccani, and Popoli 2012). Ketamine activates mTOR pathway, leading to increased synaptic signalling proteins and increased number and function of new spine synapses in the prefrontal cortex of rats (Li et al. 2010).

Electroconvulsive therapy (ECT) is another antidepressant therapy currently used that result and effective therapy for some treatment-resistant depressed patients. This therapy induces normalization of aberrant hippocampal connectivity and increased hippocampal volumes in as a clinical response. It has a slightly faster onset of action than typical ADs medications (Duman and Li, 2012; Abbott et al. 2014).

The exact cellular mechanism by which ADs exerts their therapeutic effect is not fully understood; apart from their capacity to inhibit the neuronal reuptake of serotonin. As it has been previously described we should not forget how ADs have a direct effect on astrocytes as well, with consequences for the plasticity of the whole brain.

1.10 Animal models of depression

Animal models have been developed based on evidences that link stressful events with depressive phenotype. Animal models of psychiatric disorders are usually discussed with regard to three criteria first proposed by Willner in 1984. It is important to validate an animal model and see how well the symptoms observed in animals resemble to the ones in patients suffering the disease. The presence of a similar pathophysiology is known as face validity. How well animals respond to any kind of treatment -as antidepressive treatment- compare to how humans would do it, is known as predictive validity. How well the mechanism used to induce the disease phenotype in animals reflects a similar biological dysfunctions/etiology between the human and animal model is known as construct validity. Those criterions that relies on etiological and symptomatic aspects and have a pharmacological correlation should be fulfilled by the animal model in order to be considered relevant for human pathology (Belzung and Lemoine, 2011). Some models of depression are based on the exposure to various types of acute or chronic stressors (Czeh et al. 2001). To understand the neurobiology of depression, valid animal models have been studied: learned helplessness model, chronic stress model, social defeat stress and early life stress models are among the most important ones. The *learned helplessness model*, those animals develop a state of helplessness after being exposed to direct acute

stress, like inescapable electric shocks, resulting in increased escape latency or failure to escape. *Chronic mild stress*, this paradigm involves the application of a variety of intermittent physical stresses over a prolonged time period (Krishnan and Nestler, 2011). *Social defeat stress*, this model is obtained after a prolonged social stress. The chronic social defeat stress model repeatedly exposes young adult male mice to a series of antagonistic encounters with an older and more aggressive male mouse, resulting in a range of depression-like phenotypes in the young mice (Heshmati and Russo, 2015). *Early life stress models*, typically applied in the form of maternal separation during early postnatal developmental periods give rise to cognitive and emotional changes that persist through adulthood (Krishnan and Nestler, 2011).

For this study rats with an endogenous depressive phenotype have been used. The *High Anxiety-like Behaviour (HAB)* rat breeding line is a type of Wistar rats bred for high anxiety-related behaviour after their performance on the elevated plus-maze. Those rats, extremes in anxiety, should spend less than 5% of the time on the open arms of the maze to be classified inside this group and be used for further breeding and less than 10% to be used for experimental purposes. This test is a well-established test that creates a conflict between the natural animal's curiosity to explore the territory surrounding him and the avoidance of open and brightly spaces (Neumann et al. 2011). HAB rats also show a depressive phenotype in the FST, where they display a more passive coping style predominant with higher immobility and less struggling. This test probes the coping mechanism of rodents under a complex situation, i.e. the animal cannot escape from a water-filled cylinder, he starts moving with active movements, then swimming-struggling as a scape behaviour, and a final immobile posture that indicates a behavioural loss of hoping. This change to immobility is believed to reflect behavioural despair due to a failure to a directed behaviour to keep escaping or a passive behaviour to cease active forms of coping to the stressful stimuli. The acute administration of ADs in this test increase the time that rodents spend in escape-directed behaviour (Slattery and Cryan, 2014). These animals have been also tested in a broad variety of test for anxiety-related behaviour such as open field, light-dark box, holeboard and fear conditioning, where a highly anxious phenotype has been described (Neumann et al. 2011). With respect to the neuroendocrine system, the HPA axis is one of the major stress systems. It is regulated by the release of CRH and AVP from the PVN into the pituitary, which stimulates the

secretion of ACTH into the bloodstream. ACTH, in turn, triggers the adrenal release of glucocorticoids which facilitate physiological and behavioural adaptations to a stressor at multiple peripheral and brain levels. As we have seen before, the dysregulation of the HPA axis has been linked to anxiety- and depression-related disorders. This line share an elevated HPA axis responsiveness, when exposed to a non-social stressor, e.g. a novel environment, HAB rats show a more pronounced ACTH and corticosterone secretory response and elevated neuronal responsiveness in the PVN, the medial preoptic area and the locus coeruleus (Neumann, Veenema and Beiderbeck, 2010). In terms of gene expression, AVP and CRH mRNA expression from hypothalamus and PVN respectively are upregulated in HAB rats (Neumann et al. 2011). Chronic treatment with paroxetine -SSRI AD- or infusion of an AVP receptor antagonist directly into the PVN has been shown to successfully reverse the passive stress-coping style in HAB males accompanied by a reduction in hypothalamic AVP expression (Slattery and Neumann, 2010; Neumann et al. 2011). At the cellular levels, previous work from our laboratory described a reduction of coverage of blood vessels in the adult PFC of HAB rats by analysing AQP4-immunoreactive astrocyte processes, confirming the data found within the PFC of MDD patients, indicating that the integrity of the BBB could be perturbed (Di Benedetto et al. 2016). Previous studies from our group validated HAB rats at the cellular level as a model to study MDD. A significant decrease in astrocyte density was found in HAB rats when compared to normal anxiety-related behaviour (NAB) rats. These alterations are consistent with the observed reduction of glia cells, especially astrocytes, in *post-mortem* fronto-limbic brain regions of MDD patients (Rajkowska and Miguel-Hidalgo, 2007). Furthermore, an increase in global abundance of H3K4me3 (tri-methylation at the 4th lysine residue of the histone H3) was found in HAB rats, when compared to NAB, particularly, a specific cell-type was affected, the astrocytes. H3K4me3 is necessary for packaging DNA in eukaryotic cells by increasing the accessibility of DNA. Thus, changes in abundance of these methylation markers strongly affects accessibility of genomic regions for the initiation of transcription. A similar alteration of H3K4me3 has seen in HAB rats, and in depressive patients (Cruceanu et al. 2013). In conclusion, HAB is a well-established animal model with robust behavioural and cellular phenotype that mimics many symptoms of human anxiety and depression related disorders.

The *Wistar–Kyoto* (WKY) rat strain has been proposed as an animal model of endogenous depression. They show hyperresponsive behavioural and endocrine responses to stress that exceed normal controls, distinct neurochemical profiles and enhanced depressive-like behaviours in a variety of tests (Gosselin et al. 2009). In the second day of the FST, WKY rats were more immobile compared to controls, indicating a passive behaviour and reflecting two functional characteristics related to depression—greater psychomotor retardation as well as enhanced learned helplessness. In the social interaction assessment, WKYs also showed greater social avoidance, avoiding both male and female stimulus rats. Interestingly, WKYs did not avoid novel objects in this paradigm. They have enlarged adrenal glands and hearts relative to other strains (Nam et al. 2014). WKY rats exhibit a delayed activation of the HPA axis, followed by an over stimulation, and altered neuroendocrine stress responses, including increased plasma corticosterone and ACTH levels (Rittenhouse et al. 2002). Treatment with different AD drugs attenuated depressive-like behaviour in those animals. This was seen by decreasing immobility and increasing swim time in the FST (Tejani-Butt, Kluczynski and Paré 2003). Glial cell characteristics have been studied in the context of depressive phenotype. Specific astrocytic deficits in GFAP expression have been found in cortico-limbic areas (PFC, basolateral amygdala and CA3 and dentate gyrus from hippocampus) in WKY rat brain. This data may be a general correlate of depressive-like behaviour in animal models (Gosselin et al. 2009).

1.11 Aim

Major Depressive Disorder (MDD) has become the leading cause of disability worldwide. Although several treatment options exist, the late onset of beneficial effects and a high rate of non-responder patients still represent a huge problem. To date, the molecular underpinnings of MDD are not completely understood. Therefore, it is important to identify new targets to treat this disease.

I have focused my study in the interaction of astrocytes with neurons and synapses after AD treatment. Both cell types have been described to be implicated in depression. The importance of balanced synaptic function and plasticity becomes evident when considering that synaptic dysfunctions have been ascribed to various psychiatric brain disorders. Therefore, some hypothesis have proposed a disrupted interaction between astrocytes with the synapse as the underlying cause of those disorders.

For this project, I have investigated other pharmacological targets of antidepressants (ADs). I could observe that ADs were able to target specific synapses in an early time point and only in the presence of cortical astrocytes. For this reason, my focus was on the study of astrocytic molecules that were highly related with the synapse. The molecule I investigated was MEGF10, a membrane bound protein which participates in synaptic pruning, being therefore a promising candidate responsible for the reduction in excitatory synaptic densities observed after acute AD treatment.

Those studies were performed in naïve animals in order to not interfere with other physiological changes produced by the disease itself. Furthermore, ongoing experiments are focused on the study of synapses and the MEGF10 receptor in animal models of depression. I hypothesize that changes in the MEGF10 pathway, probably during development, may have a negative influence on neuronal circuits. If this is true an improper remodelling of neuronal circuits takes place during early development, and could be the cause of neuropathologies in adulthood.

2 Materials and Methods

2.1 Animals

All animal experiments were approved by the government of the Oberpfalz (Germany). For the next study, all animals were kept under standard housing conditions (RT 22-24°C, humidity 55%, 12h light/dark cycle with lights on at 6:00 a.m., water and pellet food *ad libitum*). For the experiments in which cells from pups were required, animals at E18 stage and pups at P0-4 were used. The mothers were purchased from Charles River.

For experiments with adult animals, adult male Wistar rats (Charles River, Sulzfeld, Germany, 310 – 340 g body weight) were housed under standard laboratory conditions in groups of 3. After one week of habituation they were injected intraperitoneally (i.p.) with fluoxetine or saline for 48h. Fluoxetine was prepared fresh every day and diluted in water. Rats received an i.p. injection of either saline or 10 mg/kg in 0.5 ml twice per day for two days. On day 3, animals were anaesthetized with CO₂ and perfused with 4% paraformaldehyde (PFA, Sigma Aldrich) in phosphate buffered saline (PBS). Brains were removed and post-fixed overnight (O/N) at 4°C, cryoprotected in 25% sucrose in PBS and cut coronally at 40 µm on a cryostat. Sections were preserved in a solution with 25% ethylene glycol, 25% glycerol in PBS at -20°C until further processed for immunofluorescence-immunohistochemistry (IF-IHC).

The experiments were approved by the government of the Oberpfalz, Germany, and performed in accordance with the Guide for the Care and Use of Laboratory Animals of the Government of Oberpfalz, and recommendations from the NIH. All efforts were made to minimize the number of animals used and their suffering.

2.2 Drugs

Desipramine (DMI), Mirtarapine (MTZ) (#M0443), Fluoxetine (FLX) (#132) and Venlafaxine (VLX) (#V7264) were purchased from Sigma, Reboxetine (RBX) (#Cay15038) from Biomol. For stock solutions DMI, MTZ and RBX were dissolved in 100 % DMSO, FLX and VLX in H₂O. U0126 (Promega, Madison, MI, #V1121) was dissolved in 100% DMSO.

2.3 Preparation of neurons

Primary cortical neurons of Wistar Rat were isolated on E18. In brief, the dam was euthanize/sacrificed using CO₂, and the embryos were removed from the embryonic sack. The embryos were then decapitated and the skull was opened. The meninges were carefully removed from the brain, and the cortex, our area of interest, was dissected. Dissected cortex was placed in ice-cold HBSS (Hanks' balanced salt solution by Thermo Fischer #192109) and then fragmented into small pieces. The cortex was washed with Neurobasal media, mixed with Trypsin-EDTA for 20 minutes at 37°C for proper digestion and finally after washing again with Neurobasal media, the cortex was homogenized using fire- polished Pasteur pipette. Last step of the procedure is the centrifugation of the dissociated cells 5 minutes at 900 rpm. Supernatant was aspirated and cells were resuspended in neuron-specific medium (Neurobasal A medium-Thermofisher, #10888022, supplemented with B27 #17504-044 and Glutamine #25030024). Before seeding, CultureOne supplement (Thermofisher, #A33202-01) was added to avoid the growing of glial cells. Cells were seeded in on laminin-coated (Sigma, #L-2020) over 24-well plates at a density of 40.000 cells/well. Pure neuronal cultures were allowed to grow for 3 weeks. Half of the medium per well was change every 7 days.

2.4 Preparation of astrocytes

Primary cortical astrocytes were isolated between P0-P4 from cortical areas from NAB rat brains. Astrocytes were taken from cortical areas following the same protocol than for neurons (see 2.3). In the last step, cells were resuspended in warm astrocyte growth

medium DMEM, supplemented with 10% fetal calf serum, 1% antibiotic-antimycotic, 15 sodium pyruvate, 1%HEPES 1M, 1% MEM non-essential amino acids. Cells homogenates were plated on poly-D-lysine coated T75 cm² flasks.

2.5 Preparation of co-cultures

Primary cortical astrocyte derived from NAB rats were used. Cells were seeded on PDL-Coated cover glasses in astrocyte-growth medium. Astrocytes were allowed to growth for 4 days *in vitro* (DIV), and then medium was changed to neuron-specific medium shortly before isolated neurons were plated on top of these astrocytes. The co-cultures were allowed to growth for 14 DIV. Half of the neuron specific medium was changed once per week. The absence of unwanted cells such as microglia was analyzed by terms of immunofluorescence in every preparation.

2.6 Antidepressant treatment

The different five ADs were added to the cells in co-culture to a concentration of 10 µM for the experiments of the analysis of the synaptic densities. U0126 was administered 30 minutes before the respective co-treatments at a final concentration of 20 µM which elicits the maximal inhibitory effect. At 14 DIV, co-cultures were treated with the antidepressants (DMI, MTZ, FLX, RBX and VLX) for 48 hours (h)-with the presence or absence of U0126- or for 120h.

2.7 Harvesting astrocytes for western blot

When finishing the treatment, medium containing ADs was discarded, single cultures were washed with ice-cold PBS, 100 µl of lysis buffer was added to the different wells and the samples were placed on eppendorfs and stored at -80° until further processing.

2.8 Western blot experiments

For western blot experiments primary cortical neurons were seeded in 24 well-plates at a concentration of 40.000-50.000 cells/well (medium changed one per week) until DIV 18-21. After treatment with ADs (25 μ M) cells were harvested, as described before. Cells in lysis buffer were stored in -80 or -20°C. BCA protein concentration estimation (Thermo, #23227) was performed on all protein samples (**figure 7**).

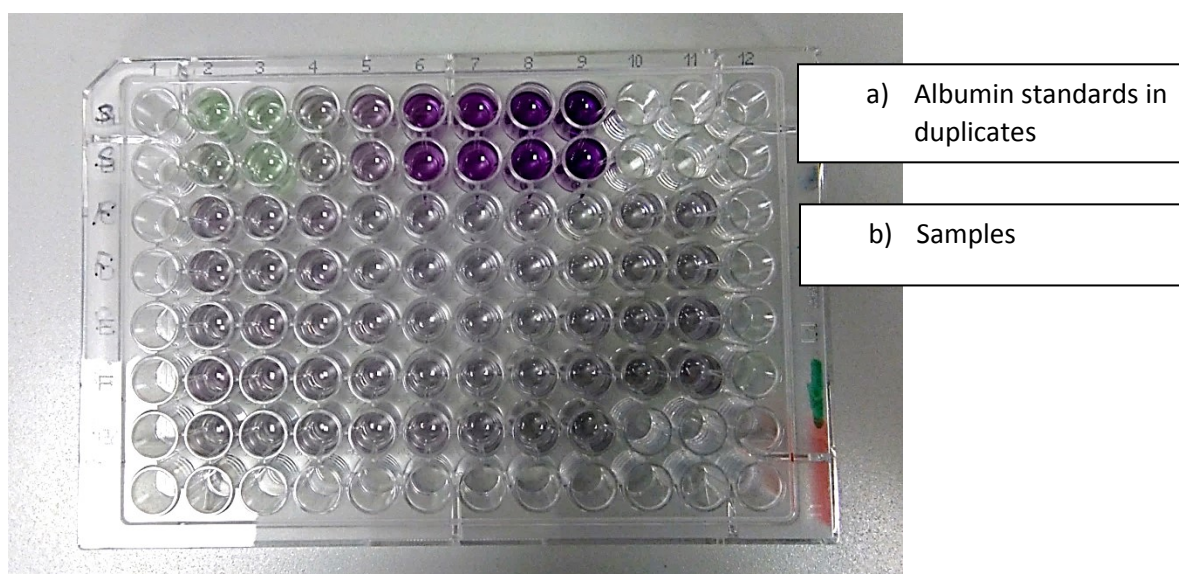


Figure 7. BCA test in a 96 well plate. a) Diluted albumin standards in duplicates. The gradient of colors, from green to purple, indicate a lower and higher amount of proteins, essential for the preparation of the standard curve. The BSA concentration goes from 0 to 2000 μ g/ml. **b)** Samples with 200 μ g of protein/ml approximately.

According to the concentrations, specific amounts of Laemmli buffer was added to them. 10 mg of total proteins/sample were denatured at 99°C for 4 min, quickly spun down and loaded on a SDS-acrylamide gel at 10% or 12%. Gel run was performed for 1.5h, 90V at RT in running buffer (25mM Tris, 190mM Glycine (Sigma, #G8898) and 0.1% SDS in distilled water pH 8.3). After full separation of all the proteins, the gel was transferred to a blotting chamber. Polyvinylidene fluoride (PVDF) membranes (Merck, #IPVH00010) were used for the transfer. Proteins were blotted for 2h, 90V at 4°C. To maintain a stable temperature environment the transfer buffer (20mM Tris, 140mM Glycine, 20% Methanol (Merck, #M79090) in distilled water, pH 8.3) was pre-cooled at 4°C. Membrane

was blocked in bovine serum albumin (BSA, Roth, #8076.4) for 1h and then incubated with the next primary antibodies (see **table 1**) in 5% BSA in 1x T-BST for 24h. To enable chemiluminiscencent anylisis, secondary antibodies were used. Membranes were incubated with secondary antibody in 5% BSA in T-BST at RT rotating for 2h. Membrane were washed 3x 10min in TBST and incubated with SuperSignal West Pico Chemiluminiscent Substrate (ThermoScientific #RE232696) for 1-2min. Chemiluminiscent reaction was visualized with ImageQuant LAS4000 (GE Healthcare Life Sciences, Freiburg, Germany).

MEGF10 experiments

Antibody and company	Concentration	Corresponding secondary AB	Concentration
Rabbit anti-MEGF10 (ThermoFisher #PA5-76556)	1:500	Goat-anti-rabbit	1:1000
Mouse anti β -Actin (Cell Signalling #3700)	1:200	anti-mouse	1:3000

Pre and post-synaptic experiments

Antibody and company	Concentration	Corresponding secondary AB	Concentration
Mouse anti-PSD95 (Sigma #MAB1596)	1:2500	anti-rabbit	1:2500
Mouse anti β -Actin (Cell Signalling #3700)	1:4000	anti-mouse	1:4000

Antibody and company	Concentration	Corresponding secondary AB	Concentration
Rabbit anti-Synaptophysin (Abcam #ab52636)	1:5000	anti-rabbit	1:1000
Rabbit anti Cofilin (Cell Signalling #5175S)	1:1000	anti-mouse	1:1000

Table 1. Primary and secondary antibodies for western blot analysis

2.9 Protein expression quantification

For the analysis, Fiji ImageJ was used. Gels files were imported in ImageJ via drag'n'drop. The region of interest (ROI) was selected with the rectangle and consecutive lines/ROIs were selected in the option Analyze → Gels → Select next line (**figure 8**).

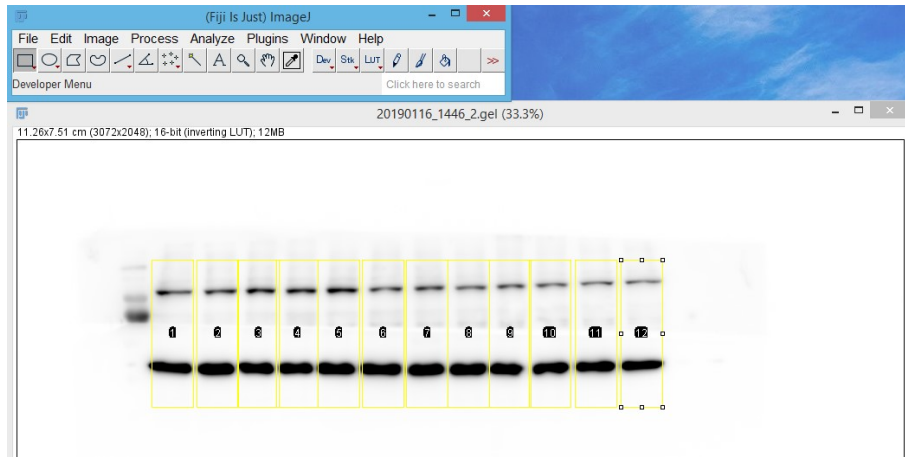


Figure 8. Analysis of the bands from western blot.

After that, the Plot line option was chosen in order to have the plots from all the lines (**figure 9**).

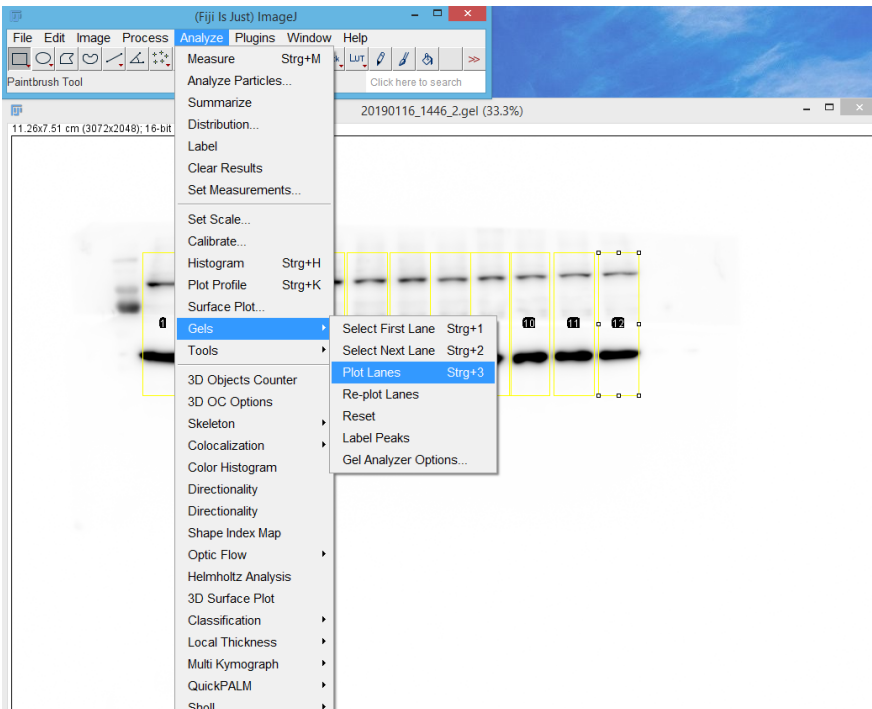


Figure 9. Analysis of the bands western blot. Gel option was chosen in order to get the plot lanes.

From every plot, their area was closed using the straight line and then selected using the wand tool (**figure 10**).

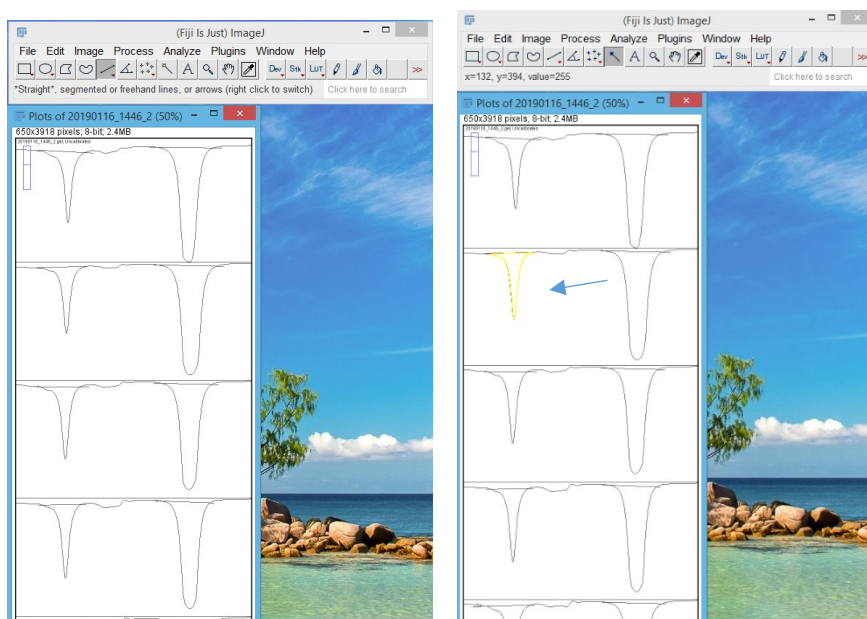


Figure 10. Selection of region of interest (ROI) referring to the area of a particular band.

After selecting the area, data from the area and percentage was obtained and used for the analysis. All lines were normalized to the corresponding total amount of housekeeper protein (protein of interest/housekeeper protein= normalized results). First, the mean of all controls was calculated in % (results normalized x 100/ mean of controls). Then the value of the different conditions was calculated accordingly.

2.10 Immunofluorescence procedure and analysis

Immunofluorescence of excitatory synapses. To terminate the treatment, single and co-cultures were washed with ice-cold PBS and fixed with 4% paraformaldehyde (PFA, Roth, #0335.2) in PBS for 20 mins, then washed 3 times every 5 mins with cold PBS. For the immunostaining of synapses, the cells were washed thoroughly in PBS (3x 10 min), the day of the immunostaining procedure and blocked in 2% NGS (Linaris, #S1000), supplemented with 0.1% Triton-X-100 in PBS, for 20 min at RT. After washing, staining was performed by incubating the cells with different combinations of primary antibodies, O/N at 4°C, diluted in the aforementioned solution with gentle shaking (**table 2**). On the

Materials and methods

second day, cells were washed (3x 10 min in PBS) to get rid of unbound primary antibody and incubated for 1h with the corresponding secondary and tertiary antibodies.

Antibody and company	Specificity	Concentration	Corresponding secondary AB	Concentration	Corresponding tertiary AB	Concentration
Rabbit anti synaptophysin (Abcam #ab52636)	Excitatory pre-synaptic marker	1:500	Biotin-SP- goat anti-rabbit IgG (Dianova #111-065-003)	1:500	Streptavidin AF647 (Invitrogen #S21374)	1:1000
Mouse anti PSD95 (Biolegend MMS-5182)	Excitatory post-synaptic marker	1:500	Anti-mouse Cy3 (Sigma #C2181)	1:500		
Chicken anti MAP2 (Acris #CH22103)	Microtubule-associated protein 2. Neuron marker	1:1000	Anti-chicken AF488 (Invitrogen #A-11039)	1:1000		

Table 2. Primary and secondary antibodies for immunofluorescence.

To label nuclei in all IF-experiments DAPI (1:1000, Sigma, #32670) was used. At the end of the procedure, cells were washed (3x 10 min in PBS) and mounted on specimen slices using aqueous mounting medium (Abcam, #ab128982) for confocal analysis.

Immunofluorescence of inhibitory synapses. The same protocol as *Immunofluorescence of excitatory synaptic densities* was used with the following antibodies (**table 3**).

Antibody and company	Specificity	Concentration	Corresponding secondary AB	Concentration	Corresponding tertiary AB	Concentration
Rabbit anti VGAT (Synaptic System #197 863)	Inhibitory pre-synaptic marker	1:1500	Biotin-SP- goat anti-rabbit IgG (Dianova #111-065-003)	1:500	Streptavidin AF647 (Invitrogen #S21374)	1:1000
Mouse Anti Gephyrin (Synaptic System #197 862)	Inhibitory post-synaptic marker	1:1000	Anti-mouse Cy3 (Sigma #C2181)	1:500		
Chicken anti MAP2 (Acris #CH22103)	Microtubule-associated protein 2. Neuron marker	1:1000	Anti-chicken AF488 (Invitrogen #A-11039)	1:1000		

Table 3. Primary and secondary antibodies for immunofluorescence.

synphys⁺/LAMP1⁺ in astrocytes. The same protocol as *Immunofluorescence of excitatory synaptic densities* was used with the following antibodies (**table 4**) and DAPI for DNA staining (nuclei).

Antibody and company	Specificity	Concentration	Corresponding secondary AB	Concentration	Corresponding tertiary AB	Concentration
Rabbit anti LAMP1 (Abcam #Ab24170)	Lysosomal-associated membrane protein 1	1:100	Biotin-SP- goat anti-rabbit IgG (Dianova #111-065-003)	1:500	Streptavidin AF647 (Invitrogen #S21374)	1:1000
Mouse anti S100 β (Abcam # ab11178)	Calcium binding protein. Astrocytic marker	1:1000	Anti-mouse Cy3 (Sigma #C2181)	1:400		
Mouse anti GFAP (Sigma #G3893)	Glial fibrillary acidic protein. Astroglia marker	1:400				
Chicken anti synaptophysin (sysis #101006)	Excitatory pre-synaptic marker	1:500	Anti-chicken AF488	1:500		

Table 4. Primary and secondary antibodies for immunofluorescence.

Immunofluorescence microglia. The presence of microglia was examined in co-cultures of astrocytes and neurons. The same protocol as *immunofluorescent of synaptic densities* was used with the following primary and secondary antibodies (**table 5**) and DAPI (1:1000) as tertiary.

Antibody and company	Specificity	Concentration	Corresponding secondary AB	Concentration
Rabbit anti Iba 1 (Wako #019-19741)	Ionized calcium binding adaptor molecule 1. Microglia/macrophage-specific protein	1:1000	Anti-rabbit AF488 (Invitrogen #A-11008)	1:300
Mouse anti S100 β (Abcam # ab11178)	Calcium binding protein. Astrocytic marker	1:1000	Anti-mouse Cy3 (Sigma #C2181)	1:400
Mouse anti GFAP (Sigma #G3893)	Glial fibrillary acidic protein. Astroglia marker	1:400		

Table 5. Primary and secondary antibodies for immunofluorescence.

2.11 Confocal microscopy

To analyze immunofluorescence-immunocytochemistry (IF-ICC), micrographs were taken using a Leica SP8 confocal microscope (Leica, Wetzlar, Germany). The appropriate lasers for detection of the fluorochromes were selected and settings were adjusted based on the highest fluorescent signal. The following settings were adjusted and kept constant throughout the experiments: objective and digital zoom, range of wavelengths, pinhole, gain/offset, line average and number of pixels per picture (512x512). To ensure an appropriate recording of entire sections Z-stack acquisition was used and the sequential acquisition mode was used in order to avoid bleed-through between different channels. The beginning and the end point were defined before taking the picture. For the quantification of synapses, MAP2 was used as a reference to identify secondary branches. For both IF-ICC excitatory and inhibitory synapses, 10-12 cells per coverslip, using a 60x oil immersion objective and at 10x zoom, were analyzed in any of the 3-4 independent experiments.

2.12 Quantitative analysis

Acquired images were saved by the confocal microscope software as .lif, then this file was open by the Bio-Format-Importer plugin in Fiji. To open the images, the next options were chosen: stack viewing: hyperstack; metadata viewing: display metadata; color options: default color mode and autoscale. For the quantification of synaptic densities single presynaptic (synaptophysin+) and single postsynaptic (PSD95+) or single VGAT⁺ and gephyrin⁺ and colocalizing puncta were counted with the extra plugin Cell Counter. For quantification synaptophysin/LAMP1 the plugin Spots colocalization (ComDet) was used in ImageJ.

Quantification of excitatory and inhibitory markers:

Acquired images were saved by .lif files, which contained the relevant metadata. The .lif file was opened via drag'n'drop. To open every single image, the appropriate import option in Bio-Format Import Option was chosen. By choosing to open all the series of images at once, the single stacks of every picture are open individually. Single channels could be selected by using the C slider and to go through the stack of images, the Z slider was used. Every single image was merged by binding the Z-stack. All the channels can be seen in the same image by choosing the Image → Channel tool → Color → Composite option. A ROI of 10µm of dendrite was cut in the picture.

For the analysis of the single channels, one channel at a time was selected. The plugin Cell Counter → Cell Counted, allows you to count the ROIs of every channel (**figure 11 and 12**).

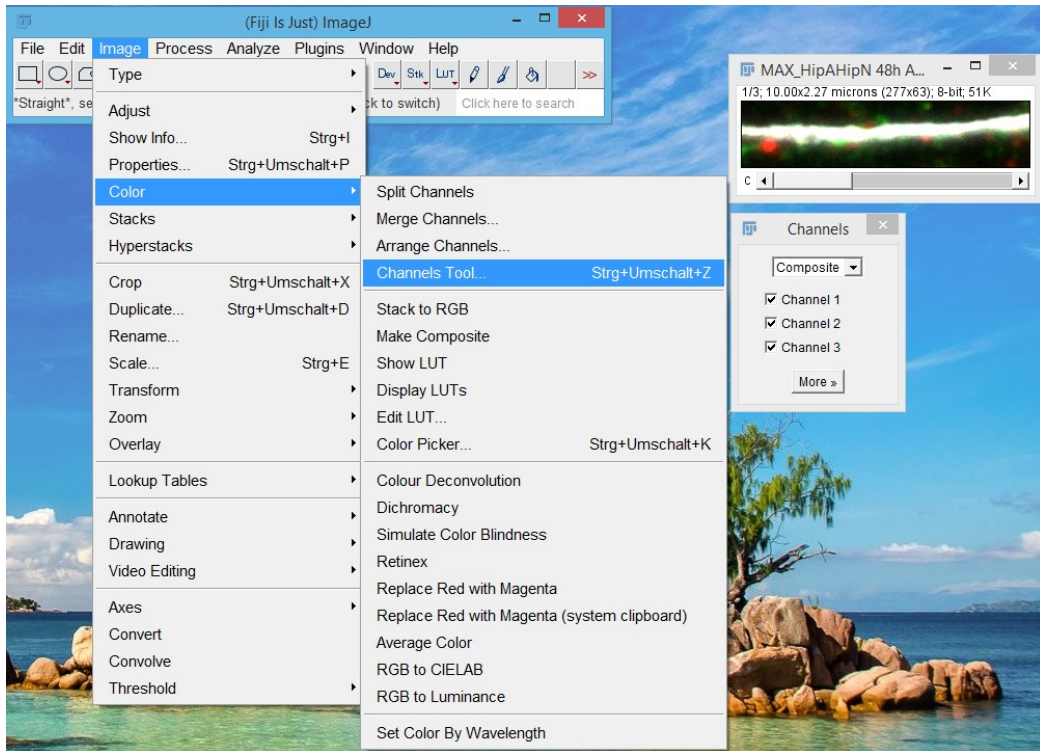


Figure 11. Cell counter plugin.

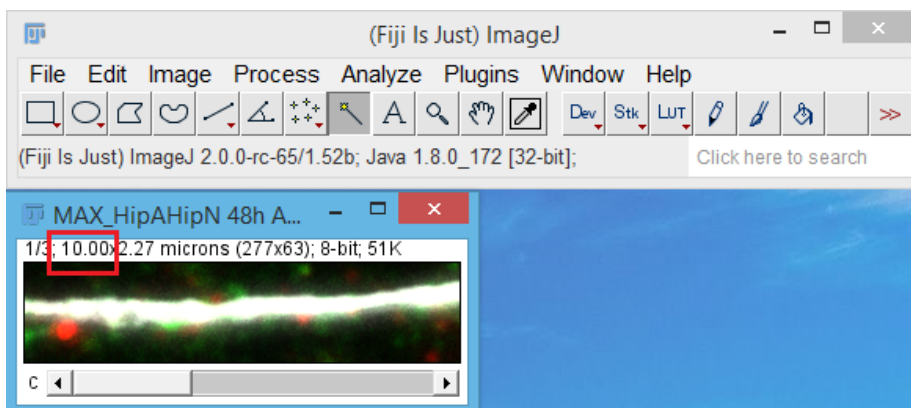


Figure 12. Analysis in 10 μm of dendrite.

I choose different counter types to analyze every single channel individually. Synapthopsin⁺ and PSD95⁺ puncta on the dendrites were quantified with counter 1 and 3 respectively (**figure 13**). Furthermore, for the analysis of the merged channels, three channels at a time were selected and the colocalization of the two puncta in the dendrite was quantified with the counter 5.

Materials and methods

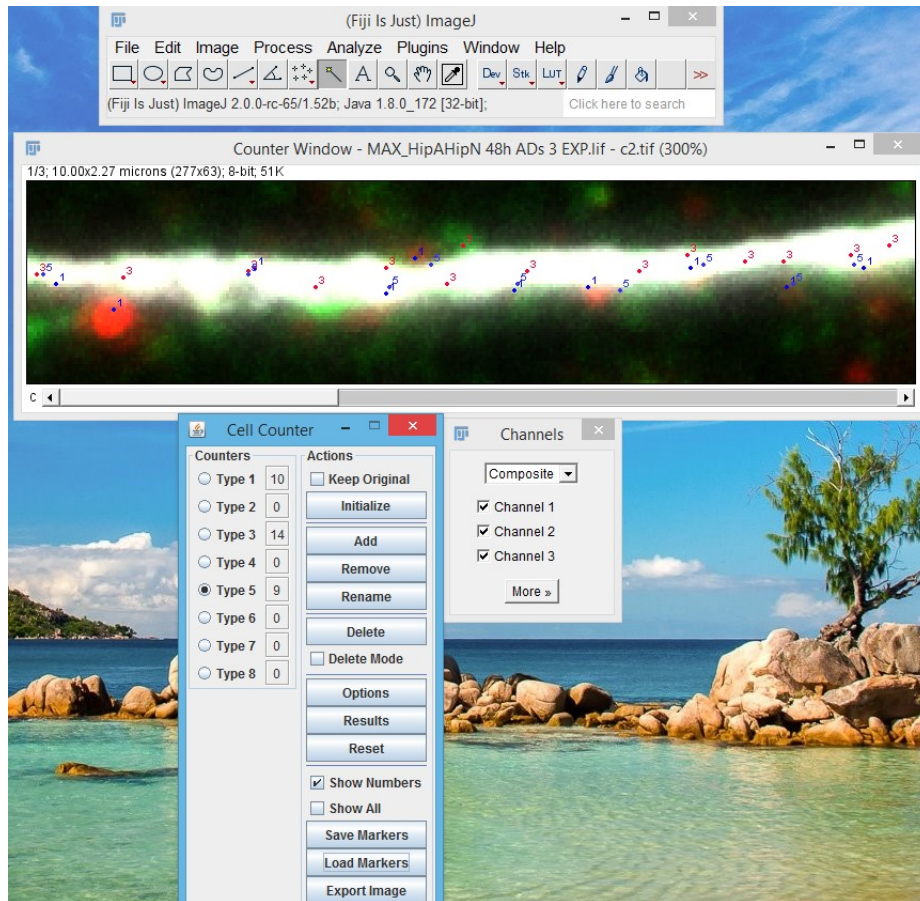


Figure 13. Quantification of pre and post-synaptic markers using cell counter plugin in 10 μm dendrite.

Similar analysis was performed in 20 μm of dendrite for the inhibitory markers VGAT+ and gephyrin+.

Quantification of synaptophysin⁺/LAMP1⁺:

Acquired images were saved by .lif files, which contained the relevant metadata. The .lif file was opened via drag'n'drop. After single stacks of every picture were open individually, z-stacks were made to select the ROI and size of the astrocytes (S100 β -GFAP/LAMP1/synphys) and to quantify lysosomes and synaptic markers and their colocalization (LAMP1⁺/synphys⁺). A reduced number of z-stack was chosen to avoid synphys⁺ particles in dendrites on top of some astrocytes. With the plugin Spots colocalization (ComDet), particles were selected by size and intensity threshold (channel 1: synphys⁺; channel 2: LAMP1⁺). For the colocalization the distance between spots' centers was defined by 1 pixel (**figure 14**).

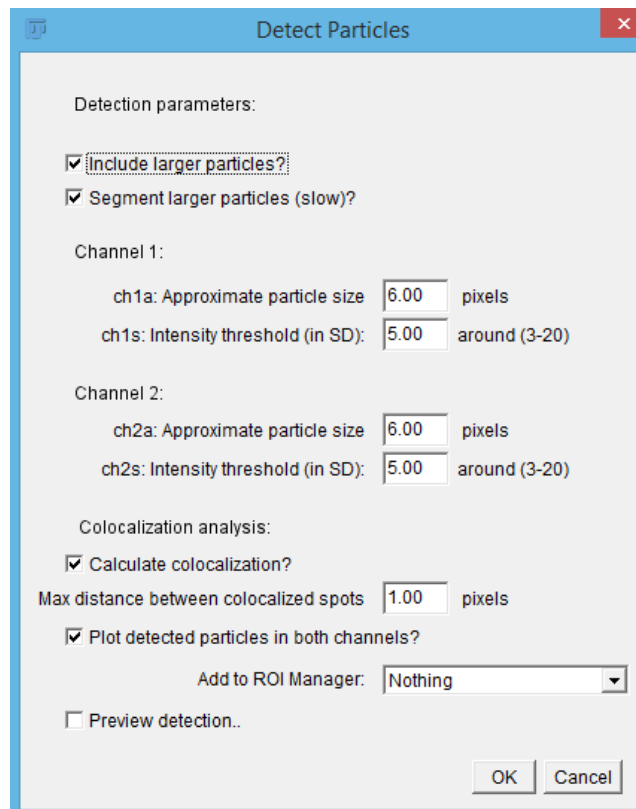


Figure 14. Selected setting for the plugin Spots colocalization (ComDet). Particles were quantified attending to a 6 pixels size and certain intensity of the signal. The markers were considered to be colocalized when the maximum distance between spots was 1 pixel.

2.13 Sholl analysis

Following two weeks of culture, cells were fixed in 4% PFA for 20 min. IF-ICC was performed as previously described with chicken anti-MAP2 as primary antibody, goat anti-chicken IgG-Alexa 488 as secondary antibody and DAPI. Up to 14 cells from one coverslip were randomly chosen using a confocal microscope (~8 optical sections, 0.4 μm step size, zoom 1). Images of labelled cells were imported into Fiji and a z-projection of the stack with maximum intensity was performed. The channels were split and the image showing the stained neuron MAP2⁺ was saved as 8-bit file. Neurites were traced using the semi-automated plugin Simple Neurite Tracer Version 3.1.6 (Longair et al. 2011). The common starting point of all paths was defined as soma center. Path length and distribution of dendritic branches over increasing distances from the soma were revealed by Sholl analysis from the same plugin (Ferreira et al. 2014).

2.14 Short interfering RNAs (siRNAs) for the downregulation of MEGF10

I designed siRNAs complementary to the mRNA sequence of MEGF10 in rat (NCBI Reference Sequence: NM_001100657.1) using the siDesign Center (Dharmacon Research, Lafayette, Co, USA). Four different siRNA were chosen and synthesized, taken into account the next parameters: lower content of GC islands, higher score, not required sense modifications and different start positions in the sequence (**table 6**). The sequences were also submitted to a BLAST search in order to verify the specific targeting of the siRNAs to MEGF10 in rat, or the lack of targeting for any sequence for the Scr (Scramble) sequence.

Name	Sense sequence 5'-3'	%GC	Starting position
siRNA1	GGACUGUACUGUAAUGAAAUU	37	1194
siRNA2	GGAAGAAUUCUGAGUACAAUU	37	3049
siRNA3	GGUUAUCA AUGCAGACUAUUU	37	2717
siRNA4	CCAACAGGAAUGUCUAUGAUU	42	3226

Table 6. Sequences for siRNA.

A non-targeting Scr sequence (5'-CCUAAGGUUAAGUCGCCCUUU-3') was used as a negative control. The siRNA was resuspended in nuclease-free water for a final concentration of 100 μ M.

Transfection of primary rat astrocytes was performed using Lipofectamine 2000 (Thermofisher, #11668027) according to the manufacturer's instructions. 24h before the transfection, the medium was change to medium without antibiotics. The appropriate amount of siRNA was diluted in Opti-MEM I Reduced Serum (Thermofisher, #31985070) to work with a final concentration of 50nM or 100nM siRNA (**figure 15**). Lipofectamine 2000 was diluted in Opti-MEM I Reduced Serum and incubated at room temperature (RT) for 5 minutes. Afterwards, the mix of Lipofectamine and siRNA was incubated at RT for 20 min and added to the cells. Astrocytes were allowed to growth for 3 or 5 additional

days. Afterwards, cells were washed with cold PBS and harvested in Eppendorf tubes until they were used for Western Blot.

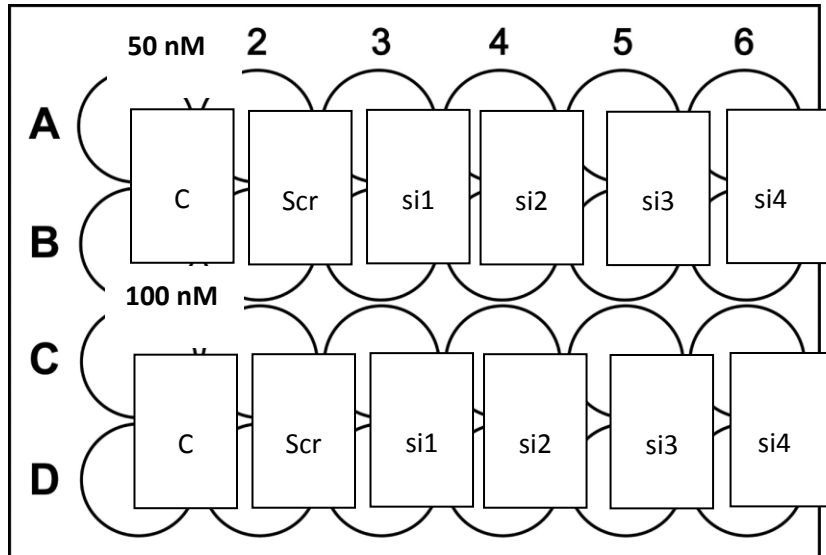


Figure 15. Layout of primary astrocytes culture for the transfection with siRNA.

As we were interested in longer- term MEGF10 reduction, most efficient siRNA sequences + Lipofectamine were added to NAB cortical astrocytes in order analyzed the interaction of the transfected astrocytes together with cortical neurons after 14DIV. In the end of this incubation, cells were treated with 10 μ M FLX (**figure 16**).

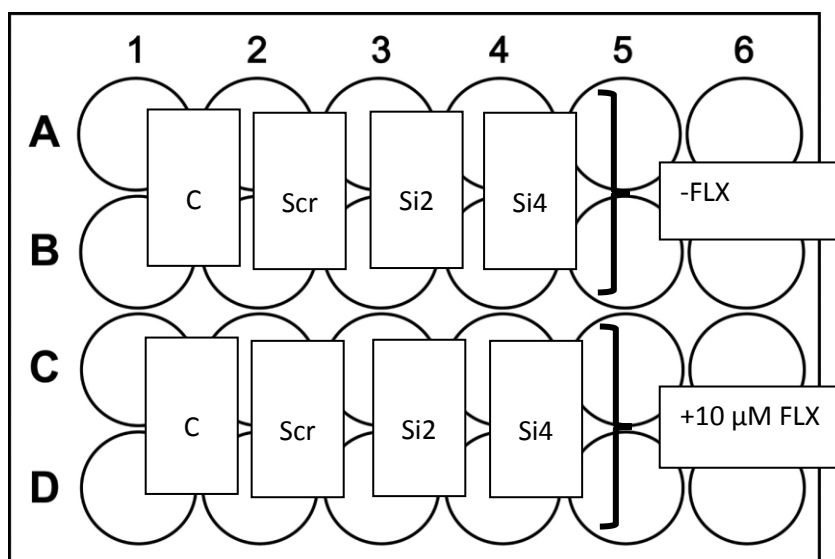


Figure 16. Layout of co-cultures neurons growing on astrocytes after the transfection with siRNA and the following FLX treatment.

2.15 RNA isolation, reverse transcription and qPCR

Isolation of RNA from single-cultured astrocytes (DIV 7) grown on six well plates was performed based on the suggested protocol from Merck. Briefly, 1 ml of TRI Reagent (Sigma, T9424-100ml) was added to each well. After a short incubation for 5 min at room temperature, the solution containing the lysed cells was transferred to 1.5 ml reaction tubes, 200 μ l of chloroform was added and the sample was mixed thoroughly for 15 sec to ensure phase separation during the subsequent 15 min centrifugation step with 12 000 xg at 4°C (Centrifuge: Eppendorf 5415R, Rotor: F45- 24-11). The aqueous phase, containing RNA, was transferred into a new reaction tube and mixed with 500 μ l isopropanol. RNA was precipitated overnight at -20°C. The next day, after aspirating the supernatant, pelleted RNA (30 min, 12 000 xg, 4°C) was washed with 80% ice-cold ethanol by centrifuging for 30 min (12 000 xg, 4°C). Afterwards, the liquid was removed, and the pellet was air dried and then resuspended in an appropriate amount of RNase-free water and stored at -80°C.

For reverse transcription the following kits were used: QuantTech Reverse Transcription Kit, Qiagen, Cat. Nr. 205311. QuantiTect SYBR Green PCR Kit, Qiagen, Cat. Nr. 204143.

Genomic DNA elimination was conducted for 2 min at 42°C using following mix of reagents (**table 7**).

Reagents	Volume/Reaction
gDNA Wipeout Buffer (7x)	2 μ l
template RNA	Up to 1 μ g
RNase – free water	Up to final volume
Total	14 μ l

Table 7. Reagents required for genomic DNA elimination.

Then, 1 μ g of isolated RNA was mixed with random hexamer primer for the cDNA synthesis (**table 8**).

Reagents	Volume/Reaction
Quantitative reverse Transcriptase	1 μ l
Quantitative RT Buffer(5x)	4 μ l
RT primer mix (final concentration: 1 μ M)	1 μ l
Total	6 μ l

Name of primers	Sequence 5' \rightarrow 3'
rMEGF10 – 90 F	GGG CTG GAC AGA AGC TAC AT
rMEGF10 – 90 R	CGA GCT GCT TAG GGA ACA AG
rHPRT1 – 115 F	CAG GCC AGA CTT TGT TGG AT
rHPRT1 – 115 R	TCC ACT TTC GCT GAT GAC AC

Table 8. Reagents and primers (from Metabion) required for cDNA synthesis.

For reverse transcription the sample was incubated for 30 min at 42°C, then the reaction was stopped by heat inactivation at 95°C for 3 min. Complementary DNA (cDNA) was stored at -20°C.

Primer were designed as intron spanning, in that way ensuring cDNA sequence specificity. The amplicon length of the target gene was 90 bp. Reactions were prepared as following in 10 μ l tubes (**table 9**).

Reagents	Volume/Reaction
2x Rotor gene SYBR Green PCR MM	5 μ l
1 μ M Primer forward	1 μ l
1 μ M Primer reverse	1 μ l
RNase – free water	2 μ l
cDNA (50 μ g)	1 μ l

Table 9. Reagents for Quantitative Real Time Polymerase Chain Reaction.

A mixture without cDNA was used as non-template control for each primer. Qiagen cyclor Rotor-Gene Q was programmed as below (Activation/Denaturation 45 cycles; **table 10**).

Materials and methods

Activation	95 °C	5 min
Denaturation	95 °C	15 sec
Primer annealing and elongation	60°C	30 sec

Table 10. Program in Qiagen cyclor Rotor-Gene Q.

Cycle threshold (Ct) -value was manually set in the linear phase of the amplification curve. Ct-values of the analysed target gene were normalized to reference gene HPRT, using subsequent formula: $(\text{Efficiency (HPRT)}^{\text{ct(HPRT)}})/(\text{Efficiency target gene}^{\text{ct(target gene)}})$. All efficiencies were assumed as 2.

2.16 Statistical analysis

For selection of the appropriate statistical test, the D'Agostino and Pearson omnibus normality test was performed for each data set. Data are plotted as mean \pm Standard error of the mean (SEM). Two-tailed Students t-test was used when comparing two groups. One-way ANOVA, followed by Dunnett's or Tukey's comparison post hoc test or two-way ANOVA were used when comparing more than two groups. Differences were considered to be significant, when the p-value was equal or less than 5% ($p < 0.05$ *), 1% ($p < 0.01$ **), 0.1% ($p < 0.001$ ***), 0.01% ($p < 0.0001$ ****). All graphs were obtained and data analyzed in GraphPad Prism version 8.0.1 for Windows, GraphPad Software, San Diego, California, USA.

3 Results

3.1 Astrocytes as targets of antidepressant (AD) drugs

3.1.1 pERK protein expression in primary astrocytes

Some studies perform gain or loss of function mutations by genetic tools, pharmacology, chemogenetic and optogenetic experiments to get some insights in the role of some genes, proteins or molecules in diseases. Previous work from our laboratory described that norepinephrine, a reuptake inhibitor activates both ERK1/2 (pERK1/2) in C6 cells. Those cells belongs to a cell line which shares similar ERK activation patterns with astrocytes in response to ADs and might therefore be used as astrocytic model to analyse an AD-dependent modulation of ERK activation (Di Benedetto et al. 2012). In other study with C6 cells, it was seen that treatment of amitriptyline, a tricyclic antidepressant, rapidly increased extracellular signal-regulated kinase (ERK) activity (Hisaoaka et al. 2007). Therefore, the activation of ERK1/2 in astrocytes with other ADs treatment was analysed. We found that ADs of different classes induced an early and sustained ($\geq 25\%$ increase) in pERK activity in astrocytes (**figure 17**). This indicated that the activation of ERK1/2 in astrocytes is specific for all the analysed ADs.

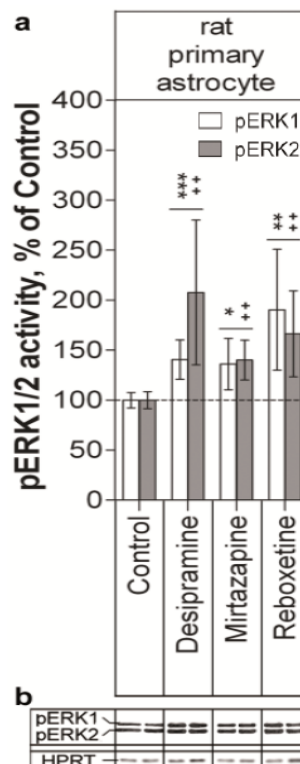


Figure 17. Specific pERK1/2 modulation in astrocytes upon AD treatment. **a)** Astrocytes were treated with different antidepressants drugs showing an activation of both ERK1/ERK2 only after AD administration. (N=3-4: ERK1: * $p < 0.05$, ** $p < 0.01$, *** $p < 0.001$; ERK2: ++ $p < 0.01$). Values are plotted as means \pm 95% CI (Confidence Interval at 95%). **b)** Representative Western blots show changes in relative amounts of pERK1/2 with respect to an internal control protein (HPRT) and to their respective control samples. Data provided by Di Benedetto's lab.

3.2 Synaptic remodelling

3.2.1 Analysis of synaptic densities *in vitro* and *in vivo*

A synapse assay may be useful to determine the effect of either astrocyte-secreted molecule or membrane bound proteins on synapse formation and remodelling. The distribution of glutamatergic and GABAergic synapses around neuronal dendrite or whole neuron can be visualized by using a combination of presynaptic and postsynaptic marker proteins. Within this analysis, the colocalization of presynaptic and postsynaptic puncta reveals structurally accomplished - true synapses, which likely contribute to network connectivity (Ippolito and Eroglu, 2010). For the next analysis synaptophysin (synphys⁺) and postsynaptic density protein 95 (PSD95⁺) were used to visualize excitatory pre- and post-synaptic terminals while vesicular GABAergic transporter (VGAT⁺) and gephyrin (gephyrin⁺) were used to see inhibitory synaptic terminals. Synapses are indeed miniature structures, with a typical size range of 200 - 500 nm in diameter, based on electron microscopy data (Dzyubenko et al. 2016). Here we quantified synaptic densities in a total of 10-12 secondary and tertiary branches from different neurons from each condition.

3.2.2 Excitatory synaptic densities in a monoculture model

In the MAPK/ERK pathway, the phosphorylation of pERK1/2 molecules will activate transcription factors that control the expression of genes that are required for cell growth, differentiation and survival (Kim and Bar-Sagi 2004). ERK1/2 also regulates astrocyte morphology (Rossi et al. 2011; Fields et al. 2013). Due to astrocytes are modulators of synapses, it is proposed that changes in their plasticity and interaction could further affect the number and density of synapses. For that reason, it was examined whether 48h ADs treatment was accompanied by any change in neuronal synaptic

densities. First, experiments were conducted in single primary neuron to see the direct and acute effect of ADs on those cells. Primary cortical neurons from NAB rats grew for three weeks and were treated with five different ADs (DMI, MTZ, FLX, RBX and VLX). After treatments with 10 μ M ADs for 48h, immunocytochemistry staining with specific antibodies for the pre- and post-synaptic marker were used. To assess synapse density, the number of pre- and postsynaptic puncta of mature excitatory synapses, synphys⁺ and PSD95⁺ respectively, as well as co-localisation of both markers was analysed. Co-localization of both markers reflects a true synapse as it has been described with these and other markers. Synapses were quantified in secondary or tertiary branches from different dendrites, specifically on 10 μ m of dendrite. However, no differences in the number of excitatory synaptic densities after 48h ADs were found in single cortical neurons (**figure 18: Synphys⁺**: C: n=3, 9.25 \pm 0.30; DMI: n=3, 8.10 \pm 0.51; MTZ: n=3, 8.62 \pm 0.08; FLX: n=3, 8.17 \pm 0.44; RBX: n=3, 8.53 \pm 0.35; VLX: n=3, 8.27 \pm 0.45. **Synphys⁺/PSD95⁺**: C: n=3, 5.71 \pm 0.14; DMI: n=3, 5.03 \pm 0.44; MTZ: n=3, 5.42 \pm 0.36; FLX: n=3, 5.49 \pm 0.32; RBX: n=3, 5.50 \pm 0.28; VLX: n=3, 5.37 \pm 0.42. **PSD95⁺**: C: n=3, 10.59 \pm 0.69; DMI: n=3, 9.90 \pm 0.69; MTZ: n=3, 9.58 \pm 0.40; FLX: n=3, 9.16 \pm 0.16; RBX: n=3, 8.98 \pm 0.60; VLX: n=3, 8.60 \pm 0.80. Ordinary one-way ANOVA followed by Dunnett's multiple comparisons test).

Results

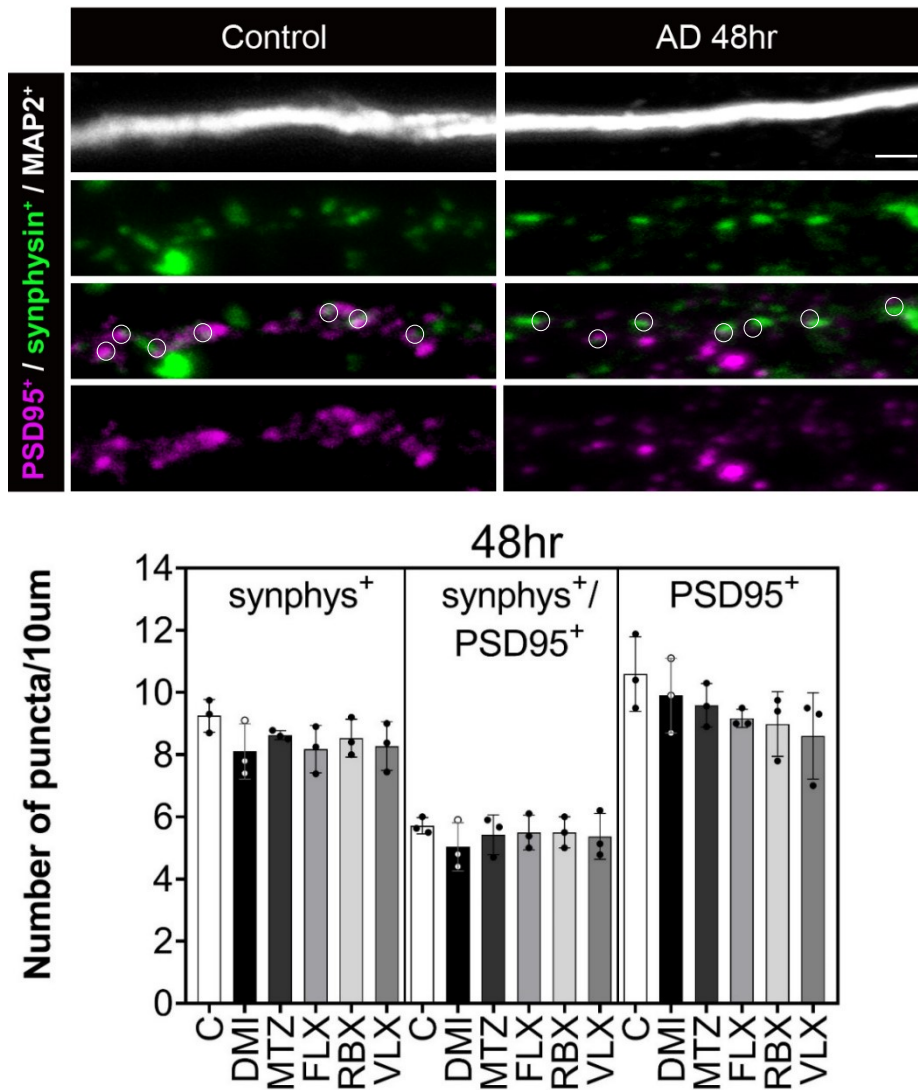


Figure 18. Synaptic densities are not affected by any AD treatment in neurons alone. Quantitative analysis of presynaptic puncta synphys⁺, postsynaptic puncta PSD95⁺ and their co-localization synphys⁺/PSD95⁺ representing true excitatory synapses (white dots and circles). Scale bar 1µm. n=3 (10-12 dendrites per treatment group). All data are represented as mean ± SEM. Ordinary one-way ANOVA with by Dunnett's multiple comparisons *post hoc test*.

Statistics:

Parameter	ADs effects
C vs. treatment for synphys ⁺	F (5, 12) = 1.212, p=0.3611
C vs. treatment for synphys ⁺ /PSD95 ⁺	F (5, 12) = 0.4083, p=0.8341
C vs. treatment for PSD95 ⁺	F (5, 12) = 1.417, p=0.2866

3.2.3 Inhibitory synaptic densities in a monoculture model

Inhibitory synaptic densities were analysed in primary cortical neurons in order to see whether they could be also affected by AD treatment. VGAT⁺ and Gephyrin⁺ puncta, corresponding to inhibitory markers in the pre-synaptic bottom or post-synaptic terminal were analysed. The quantification was made on 20 μm of the dendrite. No differences were found between the control and different treatments after 48h ADs (**figure 19**, **VGAT⁺**: C: n=3, 12.66 ± 1.52 ; DMI: n=3, 12.51 ± 0.50 ; MTZ: n=3, 11.86 ± 1.43 ; FLX: n=3, 11.01 ± 0.79 ; RBX: n=3, 11.63 ± 0.87 ; VLX: n=3, 12.89 ± 1.09 . **VGAT⁺/Gephyrin⁺**: C: n=3, 8.34 ± 1.56 ; DMI: n=3, 8.40 ± 0.14 ; MTZ: n=3, 8.26 ± 0.93 ; FLX: n=3, 5.49 ± 0.23 ; RBX: n=3, 7.21 ± 0.39 ; VLX: n=3, 8.54 ± 0.34 . **Gephyrin⁺**: C: n=3, 16.84 ± 1.59 ; DMI: n=3, 16.57 ± 0.21 ; MTZ: n=3, 15.90 ± 0.95 ; FLX: n=3, 13.55 ± 1.17 ; RBX: n=3, 14.95 ± 0.98 ; VLX: n=3, 16.79 ± 1.49 . Ordinary one-way ANOVA followed by Dunnett's multiple comparisons test).

Results

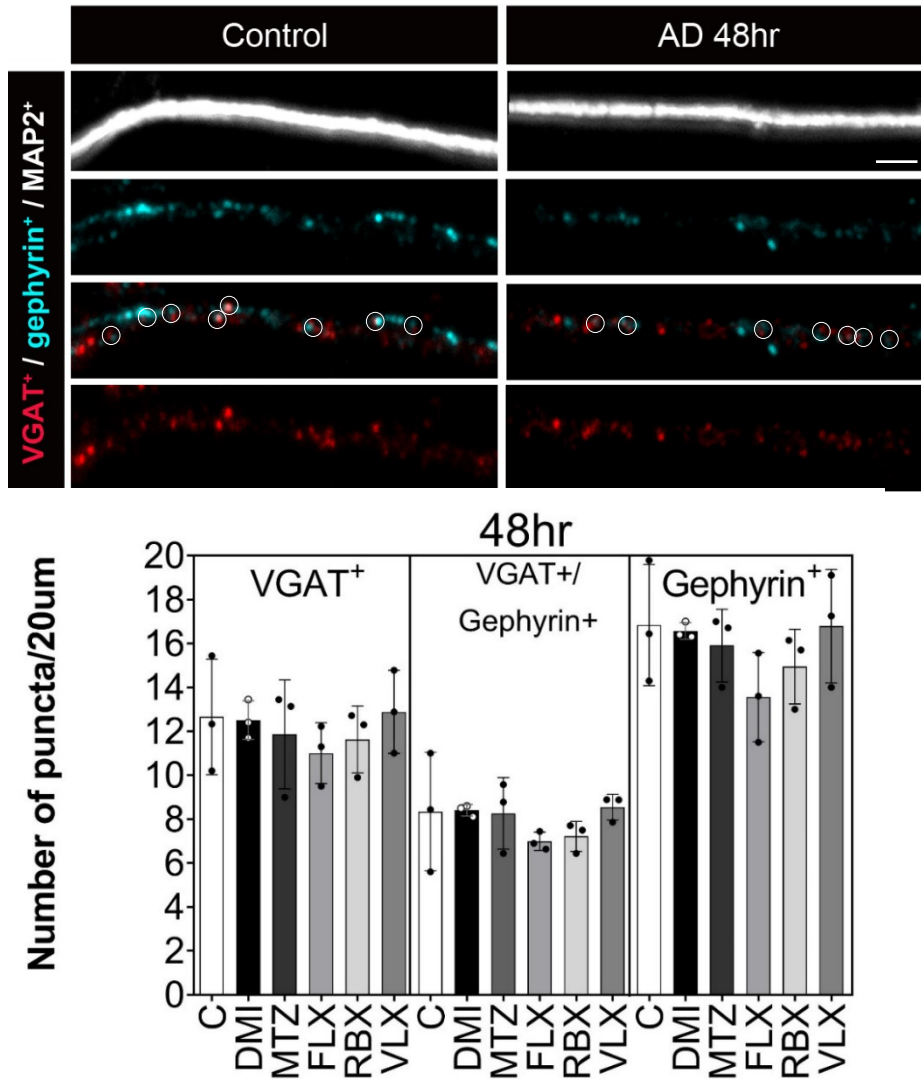


Figure 19. Number of inhibitory synapses is kept after ADs treatment in a monoculture of cortical neurons. Quantitative analysis of VGAT⁺ and Gephyrin⁺ -presynaptic and postsynaptic elements respectively- and their colocalization representing true inhibitory synapses (white circles). Scale bar 2µm. n=4, 10-12 dendrites per treatment group. All data are represented as mean ± SEM. Ordinary one-way ANOVA with by Dunnett’s multiple comparisons *post hoc test*.

Statistics:

Parameter	ADs effects
C vs. treatment for VGAT ⁺	F (5, 12) = 0.4268, p=0.8214
C vs. treatment for VGAT ⁺ /gephyrin ⁺	F (5, 12) = 0.7437, p=0.6057
C vs. treatment for VGAT ⁺	F (5, 12) = 1.252, p=0.3450

3.2.4 Excitatory synaptic densities in a co-culture model after 48h and 120h continuous AD treatment

Neurons interact with a number of glial cells in the brain. Our particular interest was to study the interaction of cortical astrocytes on neurons *in vitro*, and see how AD treatment could affect this interaction. Interactions between cortical neurons co-culture with primary cortical astrocytes were analysed. These cells in co-culture grew for two weeks. After this time point, they were treated with 10 μ M ADs for continuous 48h and 120h. Immunofluorescent- immunocytochemical staining of excitatory synaptic markers was performed. Interestingly in this case, a reduction in synaptic densities after 48h continuous ADs treatment was observed. The significant difference was found with the five different ADs, in terms of the pre-synaptic and post-synaptic marker but what is more important in the number of true synapses (**figure 20, Synphys⁺**: C: n=4, 10.98 ± 0.87 ; DMI: n=4, 7.89 ± 0.38 ; MTZ: n=4, 8.07 ± 0.82 ; FLX: n=4, 7.44 ± 0.86 ; RBX: n=4, 7.24 ± 0.58 ; VLX: n=4, 7.12 ± 0.36 . **Synphys⁺/PSD95⁺**: C: n=4, 7.34 ± 0.53 ; DMI: n=4, 4.8 ± 0.47 ; MTZ: n=4, 5.01 ± 0.23 ; FLX: n=4, 4.43 ± 0.45 ; RBX: n=4, 4.34 ± 0.23 ; VLX: n=4, 4.67 ± 0.33 . **PSD95⁺**: C: n=4, 10.94 ± 0.30 ; DMI: n=4, 8.47 ± 0.81 ; MTZ: n=4, 8.33 ± 0.56 ; FLX: n=4, 8.32 ± 0.33 ; RBX: n=4, 8.27 ± 0.41 ; VLX: n=4, 8.28 ± 0.52 . Ordinary one-way ANOVA followed by Dunnett's multiple comparisons test).

Contrarily to 48h treatment of ADs, 120h continuous AD treatment did not exert any effect on excitatory synaptic densities. Indeed the number of excitatory synapses after 120h ADs went back to baseline levels (**figure 21, Synphys⁺**: C: n=3, 10.28 ± 0.28 ; DMI: n=3, 10.72 ± 0.69 ; MTZ: n=3, 10.19 ± 0.64 ; FLX: n=3, 9.76 ± 0.49 ; RBX: n=3, 10.18 ± 0.55 ; VLX: n=3, 9.82 ± 0.35 . **Synphys⁺/PSD95⁺**: C: n=3, 6.99 ± 0.15 ; DMI: n=3, 6.95 ± 0.86 ; MTZ: n=3, 6.49 ± 0.50 ; FLX: n=3, 5.59 ± 0.09 ; RBX: n=3, 6.15 ± 0.23 ; VLX: n=3, 6.38 ± 0.22 . **PSD95⁺**: C: n=3, 9.91 ± 0.41 ; DMI: n=3, 10.77 ± 0.40 ; MTZ: n=3, 10.13 ± 0.68 ; FLX: n=3, 9.62 ± 0.11 ; RBX: n=3, 9.78 ± 0.32 ; VLX: n=3, 9.48 ± 0.46 . Ordinary one-way ANOVA followed by Dunnett's multiple comparisons test).

Results

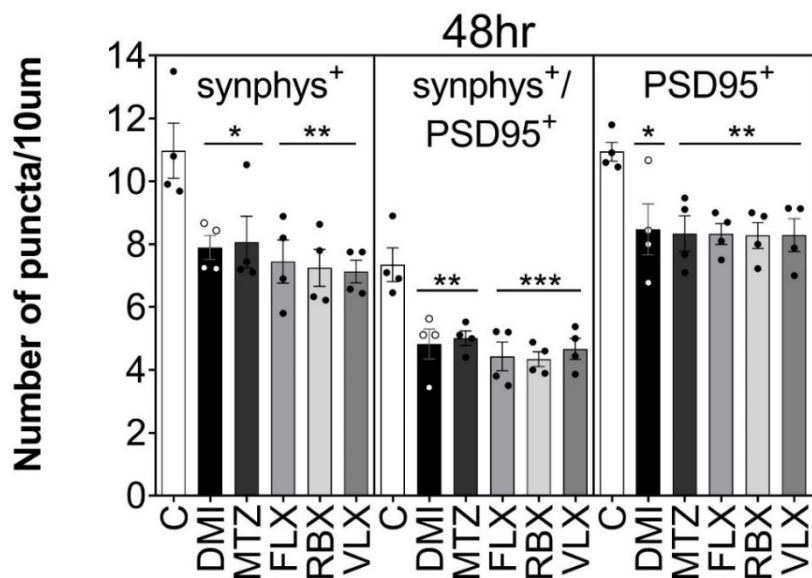
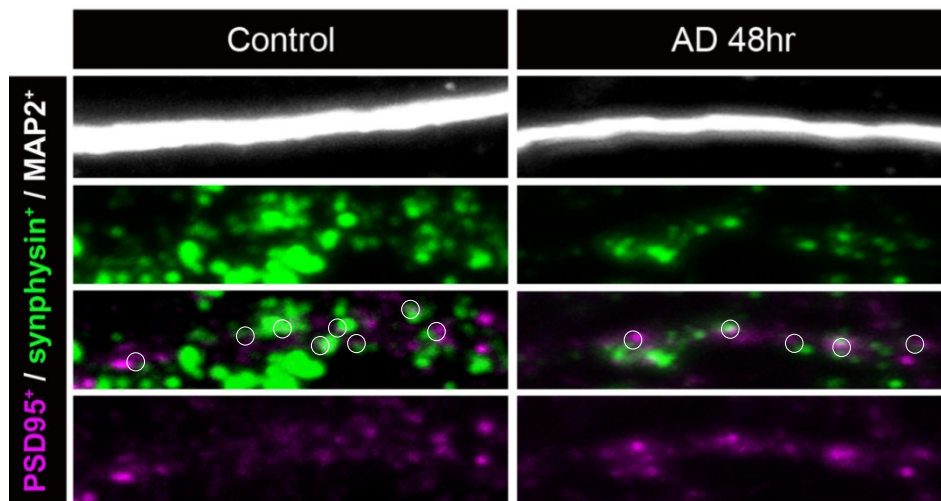


Figure 20. Reduction of excitatory synaptic densities in cortical neurons growing with cortical astrocytes. Quantitative analysis of presynaptic puncta synphysin⁺, postsynaptic puncta PSD95⁺ and their co-localization synphysin⁺/PSD95⁺, representing true excitatory synapses (white dots and circles) in 10 μ m of dendrite from cortical neurons growing with cortical astrocytes. n=3, 10-12 dendrites per treatment group. All data are represented as mean \pm SEM. * p<0.05; ** p<0.01; *** p<0.001. Ordinary one-way ANOVA with by Dunnett's multiple comparisons *post hoc* test.

Statistics

Parameter	ADs effects
C vs. treatment for synphysin ⁺	F (5, 18) = 4.926, p=0.0051**
C vs. treatment for synphysin ⁺ /PSD95 ⁺	F (5, 18) = 8.049, p=0.0004***
C vs. treatment for PSD95 ⁺	F (5, 18) = 4.177, p=0.0107*

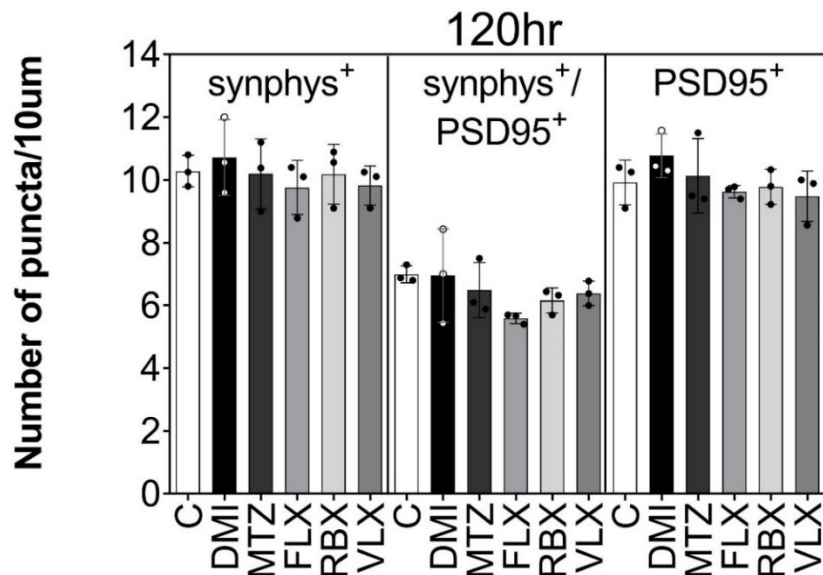
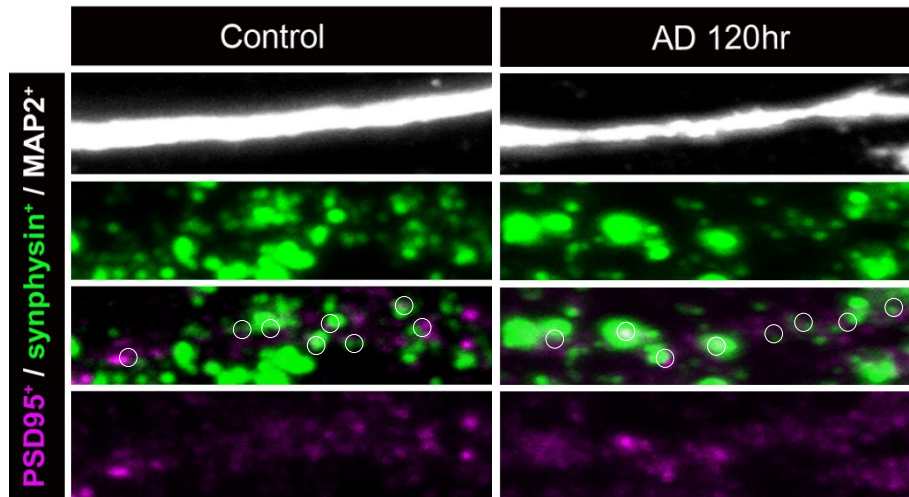


Figure 21. No effects in excitatory synaptic densities in cortical neurons growing with cortical astrocytes after 120h continuous AD treatment. Quantitative analysis of presynaptic puncta synphys⁺, postsynaptic puncta PSD95⁺ and their colocalization synphys⁺/PSD95⁺, representing true excitatory synapses (white dots) in 10 μ m of dendrite from cortical neurons growing with cortical astrocytes. n=3, 10-12 dendrites per treatment group. All data are represented as mean \pm SEM. Ordinary one-way ANOVA with by Dunnett's multiple comparisons post hoc test.

Statistics:

Parameter	ADs effects
C vs. treatment for synphys ⁺	F (5, 12) = 0.436, p=0.8150
C vs. treatment for synphys ⁺ /PSD95 ⁺	F (5, 12) = 1.454, p=0.2750
C vs. treatment for PSD95 ⁺	F (5, 12) = 1.124, p=0.3986

3.2.5 Analysis of inhibitory synaptic densities in co-culture model

An alteration in the balance between excitatory and inhibitory neurotransmission could be one of the reasons behind the development of psychiatric disorders (Rubenstein and Merzenich, 2003; Selten, van Bokhoven and Nadif Kasri, 2018). For that reason and in order to see which type of synapses are target of AD treatment, inhibitory synapses were quantified in the co-culture model. Neither VGAT⁺/Gephyrin⁺ co-localization nor analysis of single markers reflected any change after AD treatment (**figure 22, VGAT⁺**: C: n=3, 9.31 ± 0.50; DMI: n=2, 7.85 ± 0.47; MTZ: n=3, 10.54 ± 1.48; FLX: n=3, 8.15 ± 1.36; RBX: n=3, 9.66 ± 0.74; VLX: n=3, 9.18 ± 0.78. **VGAT⁺/Gephyrin⁺**: C: n=3, 4.12 ± 0.42; DMI: n=2, 4.13 ± 0.24; MTZ: n=3, 4.63 ± 0.76; FLX: n=3, 3.52 ± 0.52; RBX: n=3, 4.01 ± 0.15; VLX: n=3, 3.67 ± 0.53. **Gephyrin⁺**: C: n=3, 13.30 ± 0.31; DMI: n=2, 12.49 ± 0.73; MTZ: n=3, 12.25 ± 0.31; FLX: n=3, 11.37 ± 1.62; RBX: n=3, 11.14 ± 1.42; VLX: n=3, 11.53 ± 1.12. Ordinary one-way ANOVA followed by Dunnett's multiple comparisons test).

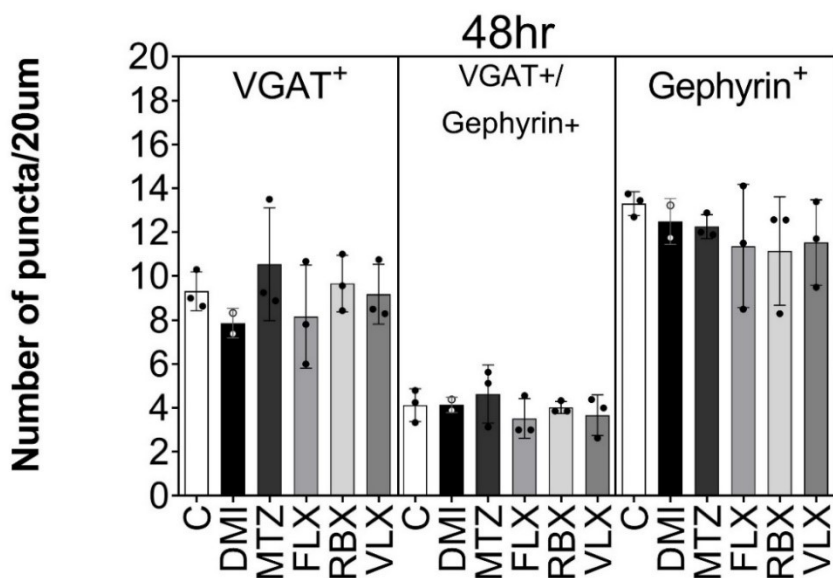
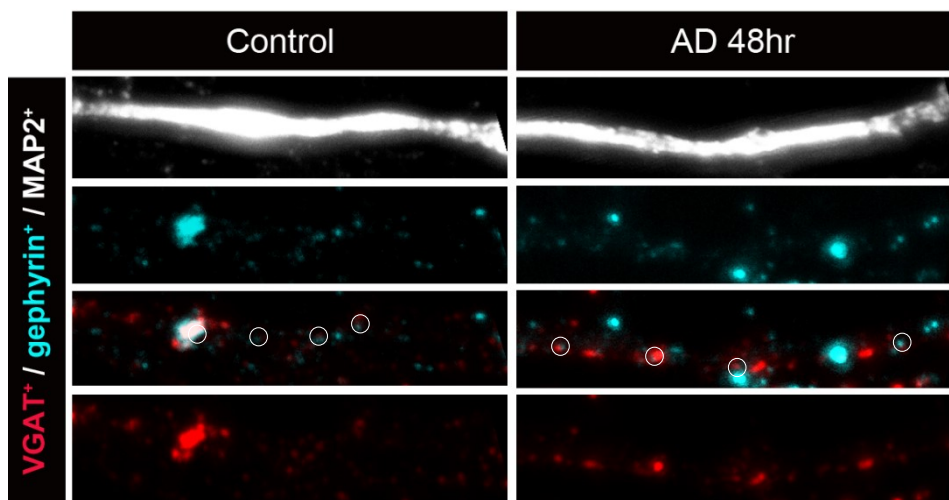


Figure 22. Number of inhibitory synapses is not changed after ADs treatment in the presence of cortical astrocytes. Quantitative analysis of VGAT⁺ and Gephyrin⁺, presynaptic and postsynaptic elements respectively and their co-localization representing true inhibitory synapses on 20 μ m of cortical neurons growing with cortical astrocytes. n=3, 10-12 dendrites per treatment group. All data are represented as mean \pm SEM. Ordinary one-way ANOVA with by Dunnett's multiple comparisons *post hoc* test.

Statistics:

Parameter	ADs effects
C vs. treatment for VGAT ⁺	F (5, 11) = 0.8573, p=0.5384
C vs. treatment for VGAT ⁺ /gephyrin ⁺	F (5, 11) = 0.6160, p=0.6906
C vs. treatment for gephyrin ⁺	F (5, 11) = 0.5692, p=0.7225

3.2.6 Examination amount of microglia in co-cultures

Microglial cells are the brain-resident macrophages. The presence of those cells in our co-culture model could influence the results and interpretation of the data due to microglia are able to phagocyte debris and synapses. For this reason, microglial cells were quantified in areas obtained at 20x magnification to get a larger approach, and 63x as it is the same magnification as the analysis of synaptic densities was made (**figure 23**). The proportion microglia varies from 5% to 12% in different areas of the brain (Lawson et al. 1990). In our co-culture a 2% of cells was quantified to be Iba1⁺, a microglial marker.

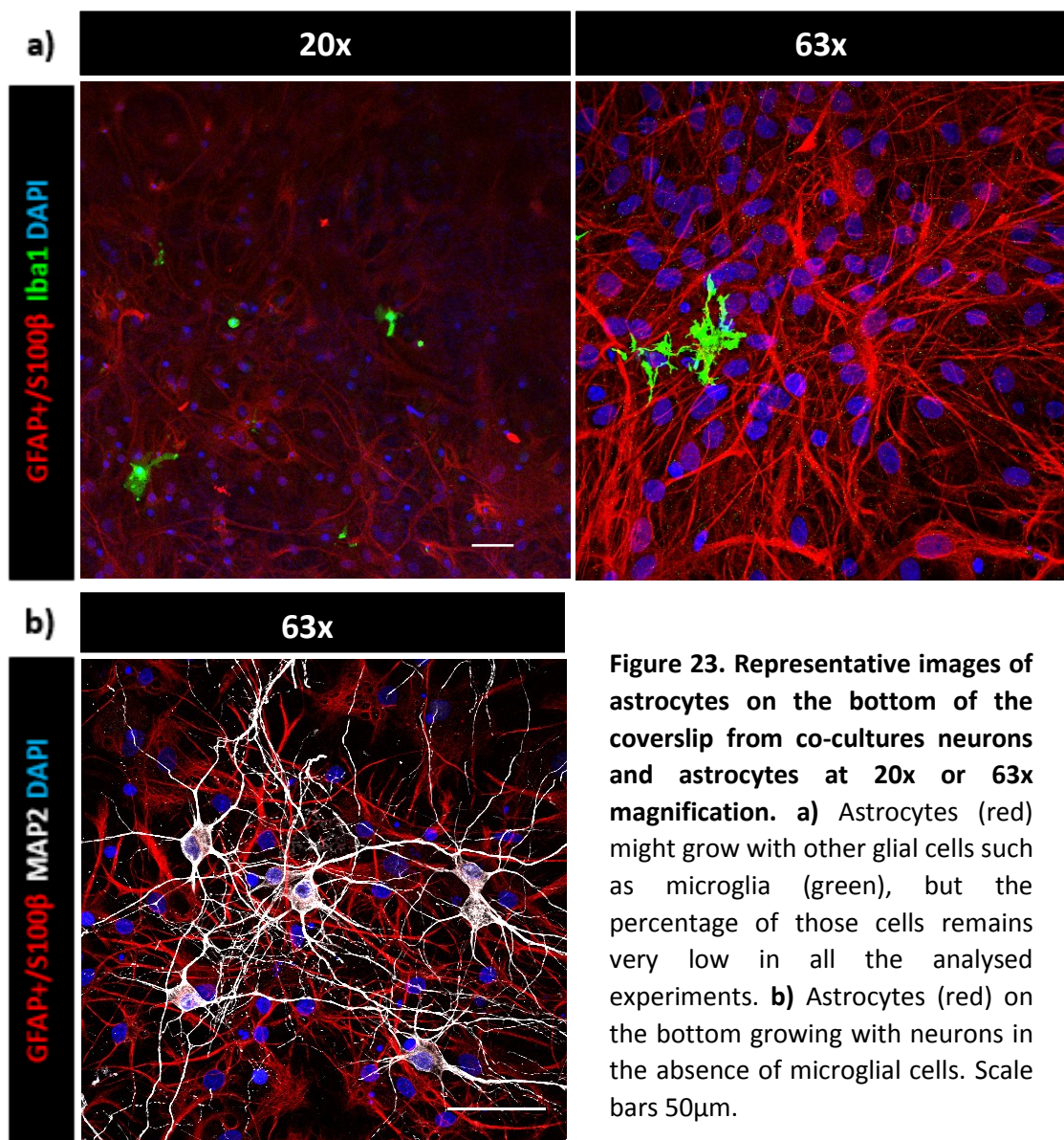


Figure 23. Representative images of astrocytes on the bottom of the coverslip from co-cultures neurons and astrocytes at 20x or 63x magnification. **a)** Astrocytes (red) might grow with other glial cells such as microglia (green), but the percentage of those cells remains very low in all the analysed experiments. **b)** Astrocytes (red) on the bottom growing with neurons in the absence of microglial cells. Scale bars 50µm.

3.2.7 Excitatory synaptic densities in a monoculture model in the presence of Astrocyte Neuron Condition Media (ANCM)

Factors released from astrocytes or neurons (i.e. TSP, glypicans) may influence synaptogenesis or synapse refinement and may mediate AD efficacy (Christopherson *et al.*, 2005; Allen *et al.*, 2012). For that reason, it was examined whether administration of astrocyte-neuron AD-conditioned media (ANCM) to neurons alone would be sufficient to induce the reduction in the excitatory synaptic density. ANCM + ADs were extracted from co-cultures and added to neurons alone. No differences were found after AD treatment compared to control when the ANCM was added for short term (48h; **figure 24a**, **Synphys⁺**: C: n=3, 9.89 ± 0.93 ; DMI: n=3, 9.75 ± 0.77 ; MTZ: n=3, 9.26 ± 1.43 ; FLX: n=3, 8.72 ± 0.71 ; RBX: n=3, 9.25 ± 0.38 ; VLX: n=3, 9.22 ± 0.26 . **Synphys⁺/PSD95⁺**: C: n=3, 6.50 ± 0.87 ; DMI: n=3, 6.23 ± 0.54 ; MTZ: n=3, 6.39 ± 0.25 ; FLX: n=3, 5.66 ± 0.56 ; RBX: n=3, 6.20 ± 0.49 ; VLX: n=3, 6.07 ± 0.46 . **PSD95⁺**: C: n=3, 11.14 ± 1.00 ; DMI: n=3, 11.17 ± 0.96 ; MTZ: n=3, 11.38 ± 1.03 ; FLX: n=3, 10.39 ± 1.20 ; RBX: n=3, 10.81 ± 0.66 ; VLX: n=3, 11.90 ± 0.92). No differences were found in the presence of ANCM and after longer term treatments (120h; **figure 24b**, **Synphys⁺**: C: n=3, 11.20 ± 0.52 ; DMI: n=3, 10.81 ± 0.42 ; MTZ: n=3, 11.61 ± 0.38 ; FLX: n=3, 10.78 ± 0.33 ; RBX: n=3, 10.44 ± 0.55 ; VLX: n=3, 10.70 ± 0.53 . **Synphys⁺/PSD95⁺**: C: n=3, 7.80 ± 0.20 ; DMI: n=3, 7.57 ± 0.29 ; MTZ: n=3, 7.96 ± 0.26 ; FLX: n=3, 7.33 ± 0.08 ; RBX: n=3, 7.58 ± 0.56 ; VLX: n=3, 7.92 ± 0.52 . $p=0.9232$. **PSD95⁺**: C: n=3, 12.63 ± 0.70 ; DMI: n=3, 12.03 ± 0.97 ; MTZ: n=3, 12.32 ± 0.26 ; FLX: n=3, 11.48 ± 0.58 ; RBX: n=3, 11.37 ± 0.55 ; VLX: n=3, 13.14 ± 0.66 . Ordinary one-way ANOVA followed by Dunnett's multiple comparisons test). In the absence of astrocytes, there is no reduction in the number of synaptic densities after 48h continuous ADs treatment. These results indicate that a membrane-bound protein may be mediating those effects after AD treatment.

Results

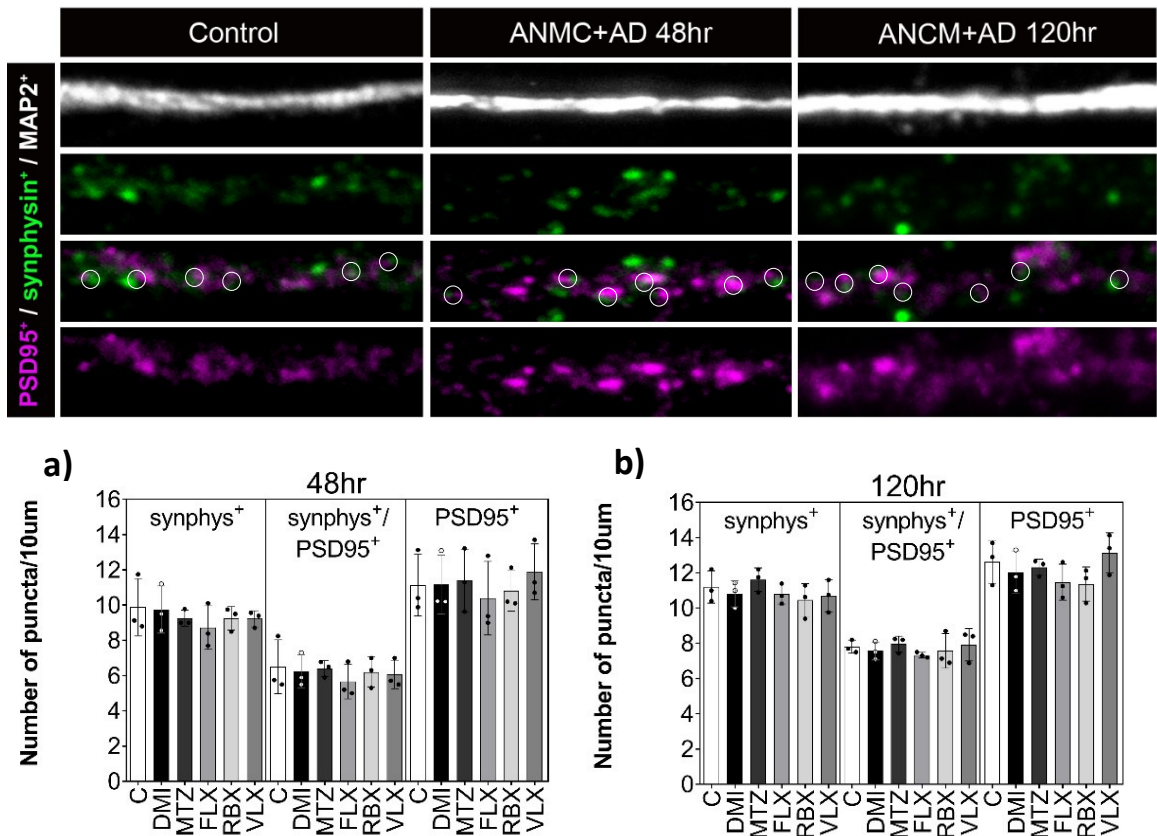


Figure 24. Factors found in ANCM are not sufficient to reduce the number of synaptic densities in a primary culture of neurons. Quantitative analysis of synphys⁺ and PSD95⁺, presynaptic and postsynaptic puncta respectively, and their co-localization representing true excitatory synapses on 10 µm of dendrite. Neurons grew alone until reaching a mature state and ANCM+ADs were added for short (48h) or long time points (120h). n=3, 10-12 dendrites per treatment group. Data are represented as mean ± SEM. Ordinary one-way ANOVA with by Dunnett's multiple comparisons *post hoc* test.

Statistics:

Parameter	ANCM+ADs for 48h	ANCM+ADs for 120h
C vs. treatment for synphys ⁺	F (5, 12) = 0.4670, p=0.7937	F (5, 12) = 0.7927, p=0.5750
C vs. treatment for synphys ⁺ /PSD95 ⁺	F (5, 12) = 0.2658, p=0.9232	F (5, 12) = 0.4421, p=0.8110
C vs. treatment for PSD95 ⁺	F (5, 12) = 0.2715, p=0.9201	F (5, 12) = 1.302, p=0.3264

3.2.8 Analysis synaptic densities ex vivo in the rat PFC : synaptic signal intensity

Next step was to analyse what happens with synaptic densities after AD treatment in the brain of rats, in which the effects of ADs in the brain can be related to more real conditions. As it has been previously described by our group, ADs inhibit neuronal pERK1/2 in the prefrontal cortex (PFC) of adult mice shortly after drug treatment (Di Benedetto et al. 2013). Next it was evaluated whether ADs induced synaptic remodelling in adult rat brains, as in our co-culture experiments. NAB rats were injected i.p. with FLX for 48h, after this time point, they were killed and brains processed for immunofluorescence. Synaptic signal intensity in terms of the quantification of the pre-synaptic marker was analysed. Interestingly, FLX treatment significantly reduced synaptic density in the PFC after 48 hrs of drug treatment (**figure 25**), whereas both the CA1 and CA3 regions of the hippocampus were not affected (**figure 26**). This data may suggest that the origin/location of astrocytes might be more relevant for the remodelling effect.

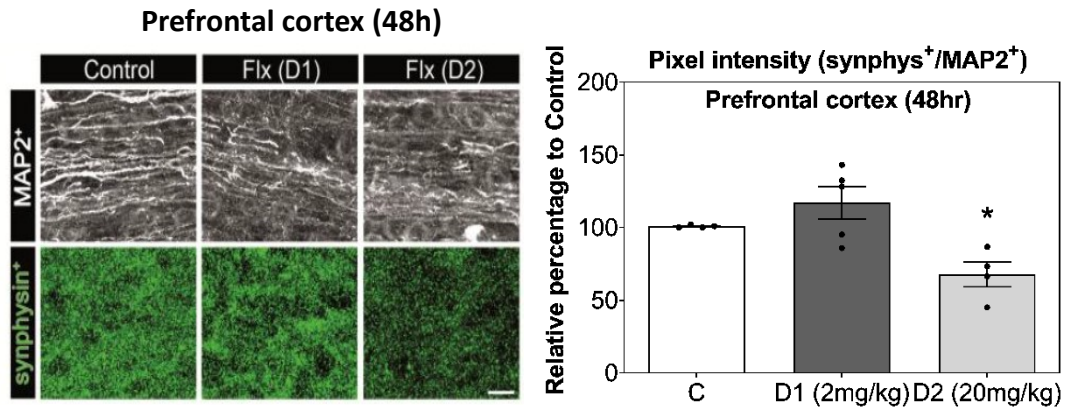


Figure 25. FLX treatment for 48h induces a synaptic remodelling *ex vivo* in the adult rat PFC with the highest dose (D2) of FLX. Pictures showing MAP2⁺ dendrites helped in the normalization of data across-sections; synphysin⁺ signal indicates pre-synaptic signal intensity. Scale bar: 10 μ m. n=4, data are expressed as mean \pm SEM. *p< 0.05. One-way ANOVA followed Dunnett’s test was used for the statistical analysis.

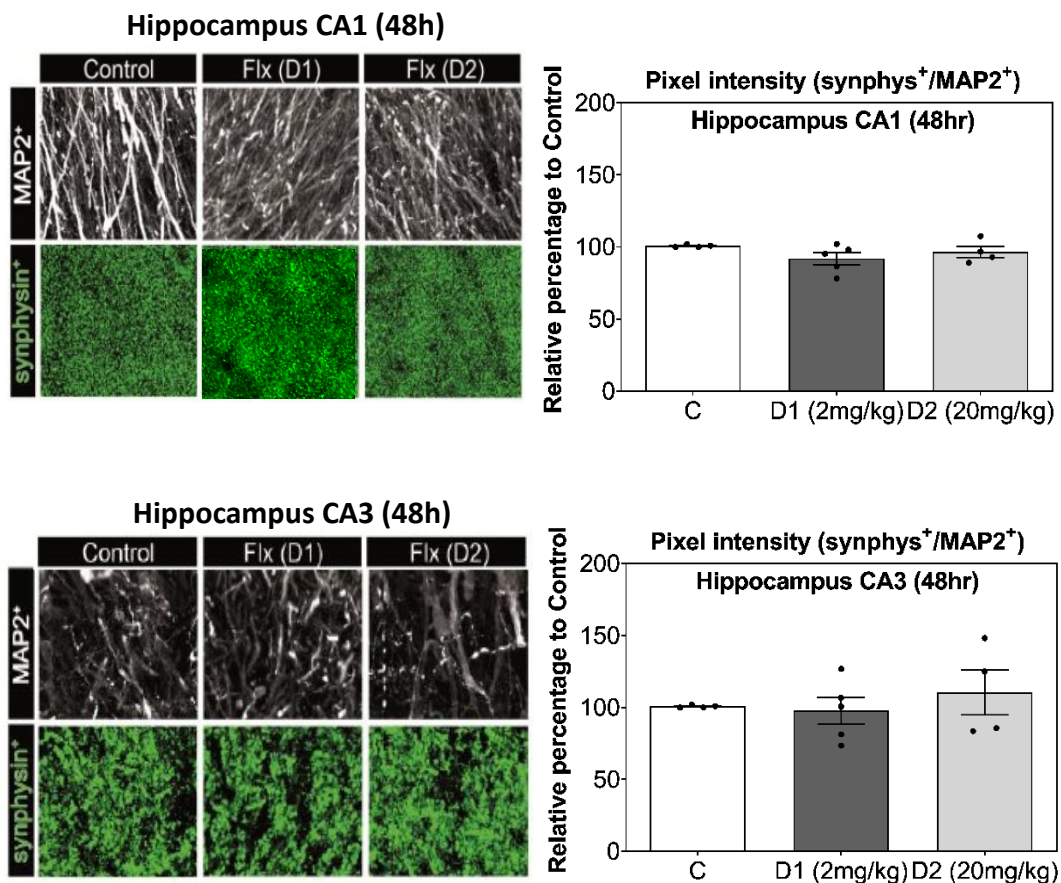


Figure 26. FLX treatment for 48h do not induce any change in synaptic signal intensity in the rat hippocampus (areas CA1 and CA3). *Ex vivo* experiments show MAP2⁺ dendrites and synphysin⁺ labelling pre-synaptic signal intensity. n=4, data are represented as mean \pm SEM. One-way ANOVA followed Dunnett’s test was used for the statistical analysis.

3.2.9 Analysis synaptic markers ex vivo in the rat PFC

A semi-quantitative analysis was also performed with the PFC samples from the rats which had saline and FLX treatment. By means of western blot I could observe a reduction in the relative amount of the presynaptic marker, synaptophysin (**figure 27 b**, control n=5, 1 ± 0.02 ; FLX n=5, 0.66 ± 0.10), and in the relative amount of the post-synaptic marker PSD95 (**figure 27 c**, control n=6, 1 ± 0.08 ; FLX n=5, 0.68 ± 0.11).

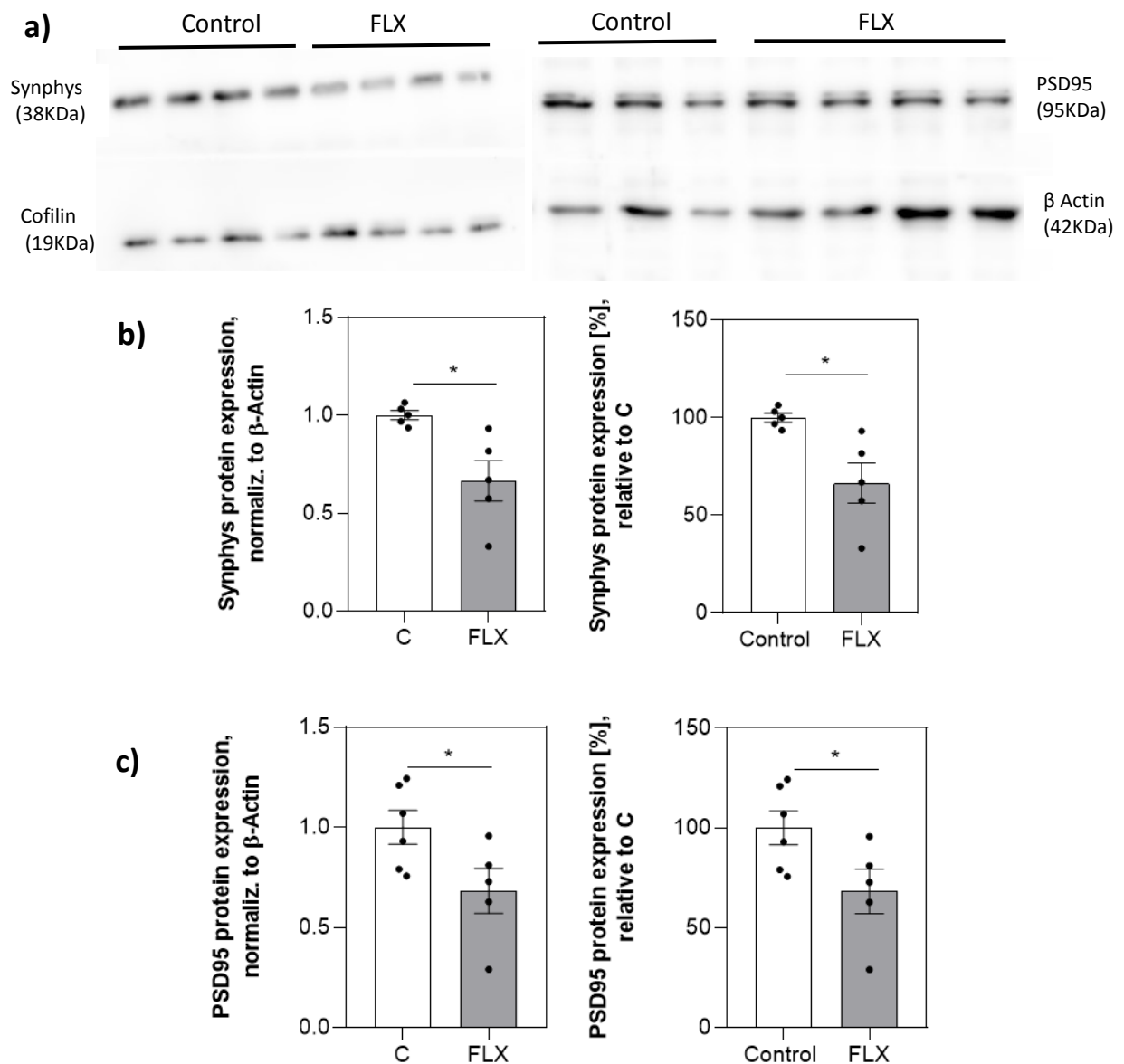


Figure 27. Western blot data from the rat PFC after saline (control) or FLX treatment. a) Representative western blot of synaptophysin (synphysis) and PSD95 with their internal controls. **b)** Relative amount of synaptophysin expression (also in %) normalized to cofilin and relative to control levels. **c)** Relative amount of PSD95 expression (also in %) normalized to β -Actin and relative to control levels. n=5-6 animals. Data are represented as mean \pm SEM. Student t-test was used for the statistical analysis.

Statistics:

Parameter	Statistic data
Synphys	$T_8 = 3.166, p=0.0133 *$
PSD95	$T_9 = 2.302; p=0.0468 *$

3.2.10 Excitatory synaptic densities in the presence of hippocampal astrocytes

I decided to check in our co-culture model *in vitro* what is the interaction between cortical or hippocampal neurons co-cultured with hippocampal astrocytes. The *in vitro* model will help to understand the role of different type of astrocytes originated in different areas. As it has been previously described both cell types grew together for two weeks and were treated with ADs for 48h. After this time point, excitatory synaptic densities were analysed in 10 μm of dendrite but no effect in the number of synaptic densities was observed in the presence of hippocampal astrocytes (for cortical neurons **figure 28 a**, **Synphys⁺**: C: n=3, 8.11 ± 0.41 ; DMI: n=3, 8.53 ± 0.71 ; MTZ: n=3, 8.61 ± 0.49 ; FLX: n=3, 8.39 ± 0.30 ; RBX: n=3, 9.35 ± 0.04 ; VLX: n=3, 8.37 ± 0.47 . **Synphys⁺/PSD95⁺**: C: n=3, 5.71 ± 0.23 ; DMI: n=3, 5.76 ± 0.48 ; MTZ: n=3, 6.11 ± 0.33 ; FLX: n=3, 5.96 ± 0.03 ; RBX: n=3, 6.24 ± 0.12 ; VLX: n=3, 5.89 ± 0.11 . **PSD95⁺**: C: n=3, 11.88 ± 0.46 ; DMI: n=3, 11.97 ± 0.26 ; MTZ: n=3, 11.02 ± 0.18 ; FLX: n=3, 11.13 ± 0.44 ; RBX: n=3, 10.93 ± 0.90 ; VLX: n=3, 11.63 ± 0.64 . For hippocampal neurons, **figure 28 b**, **Synphys⁺**: C: n=3, 9.32 ± 0.46 ; DMI: n=3, 9.38 ± 0.37 ; MTZ: n=3, 9.01 ± 0.39 ; FLX: n=3, 9.44 ± 0.45 ; RBX: n=3, 9.59 ± 0.29 ; VLX: n=3, 9.74 ± 0.32 . **Synphys⁺/PSD95⁺**: C: n=3, 6.41 ± 0.26 ; DMI: n=3, 6.30 ± 0.25 ; MTZ: n=3, 6.26 ± 0.32 ; FLX: n=3, 6.45 ± 0.12 ; RBX: n=3, 6.52 ± 0.21 ; VLX: n=3, 6.80 ± 0.21 . **PSD95⁺**: C: n=3, 11.84 ± 0.431 ; DMI: n=3, 11.93 ± 0.33 ; MTZ: n=3, 11.93 ± 0.27 ; FLX: n=3, 12.47 ± 0.26 ; RBX: n=3, 12.24 ± 0.17 ; VLX: n=3, 11.92 ± 0.77 . Ordinary one-way ANOVA followed by Dunnett's multiple comparisons test). This data goes in parallel with results *ex vivo*, indicating our *in vitro* model is a validated model useful to study the interaction between astrocytes-neurons.

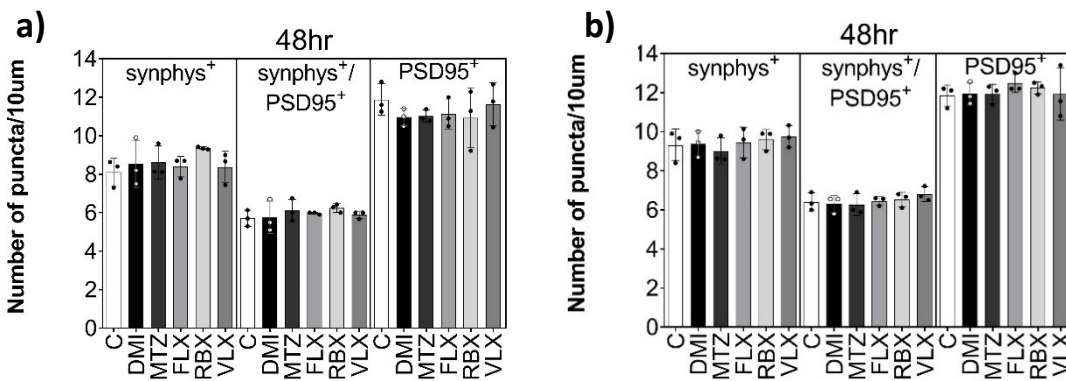
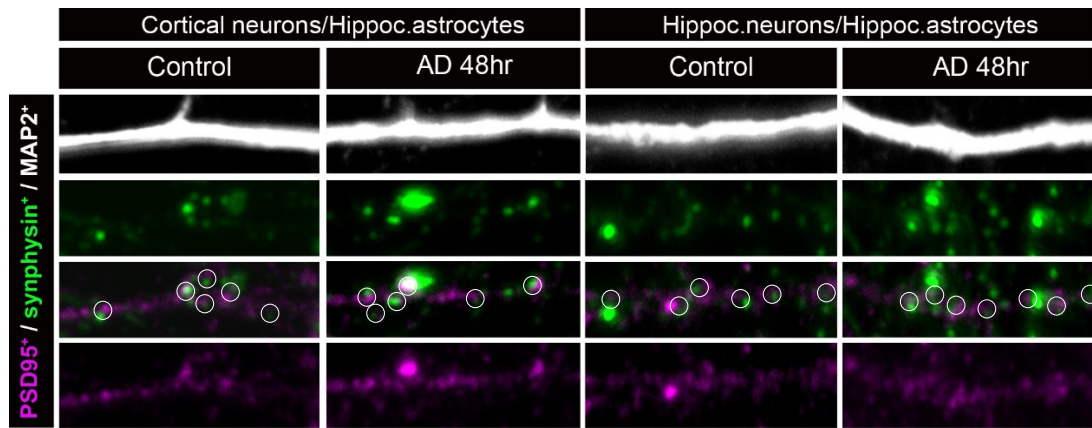


Figure 28. Synaptic densities are not affected by any AD treatment when cortical neurons a) or hippocampal neurons b) are growing with hippocampal astrocytes. Quantitative analysis of Synphys⁺ and PSD95⁺, presynaptic and postsynaptic puncta respectively and their colocalization on 10 μ m dendrites when cortical neurons (a) or hippocampal neurons (b) are growing with hippocampal astrocytes. n=3, 10-12 dendrites per treatment group. All data are represented as mean \pm SEM. Ordinary one-way ANOVA with by Dunnett's multiple comparisons *post hoc* test.

Statistics:

Parameter	ADs effects (a)	ADs effects (b)
C vs. treatment for synphys ⁺	F (5, 12) = 0.8647, p=0.5320	F (5, 12) = 0.4138, p=0.8303
C vs. treatment for synphys ⁺ /PSD95 ⁺	F (5, 12) = 0.5757, p=0.7181	F (5, 12) = 0.6603, p=0.6603
C vs. treatment for PSD95 ⁺	F (5, 12) = 0.5399, p=0.7429	F (5, 12) = 0.3670, p=0.8615

3.3 Evidences of the astrocyte-dependent remodelling of synapses

3.3.1 Analysis MEGF10 expression in the rat PFC

As we found a decrease synaptic signal intensity in the rat PFC after short AD treatment, we then looked at the effects of ADs on astrocytes. FLX also increased MEGF10 expression in astrocytes of the PFC thereby confirming the specificity of the drug effect in this cell type (**figure 29**).

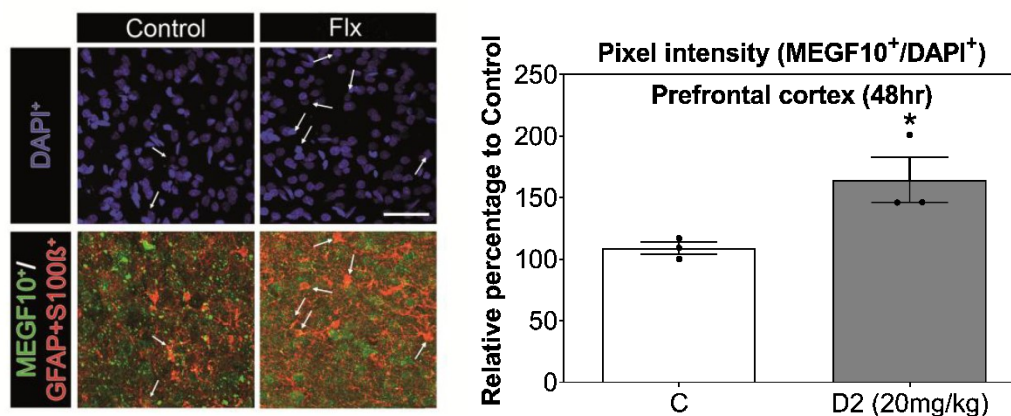


Figure 29. FLX treatment induces an increased MEGF10 expression in astrocytes. Quantitative analysis of the pixel intensity for MEGF10 (green) in the astrocytes (red) of the rat PFC after FLX injections for 48h. Increased expression of MEGF10 phagocytic protein in astrocytes is marked with arrows. Scale bar: 50 μ m. Data are represented as mean \pm SEM; n=3. Unpaired t-test *p<0.05.

3.3.2 Analysis of MEGF10 protein amount in PFC

Next, the total relative amount of MEGF10 was measured in the PFC. FLX treatment for 48h increased MEGF10 protein level (**figure 30**, control n=6, 1 ± 0.06 ; FLX n=6, 1.68 ± 0.22). As to conclude, the reduction of synaptic signal intensity observed *in vitro* and *in vivo* correlates with an increase in expression of the phagocytic receptor MEGF10 in astrocytes.

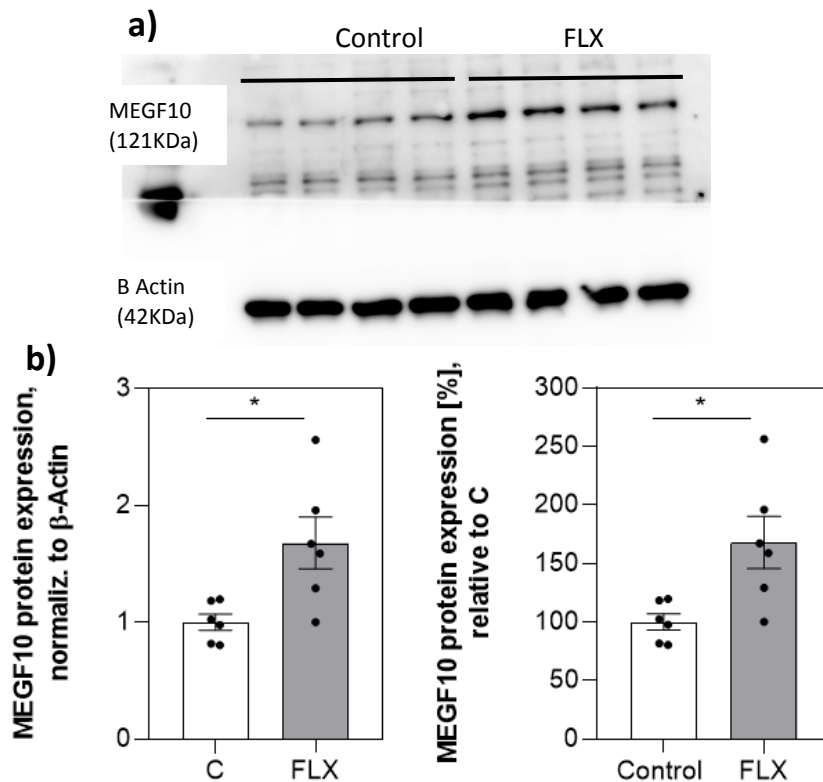


Figure 30. Western blot data from the rat PFC after saline (control) or FLX treatment. **a)** Representative western blot of MEGF10. **b)** Relative amount of MEGF10 expression (also in %) normalized to β -Actin and relative to control levels. n=6. Data are represented as mean \pm SEM. Student t-test was used for the statistical analysis.

Statistics:

Parameter	Statistic data
MEGF10	$t_{10} = 2.922, p=0.0152 *$

3.3.3 Analysis of MEGF10 in primary cortical astrocytes

Chung and colleagues found that MEGF10 is a receptor in astrocytes that work as mediator of astrocyte-dependent synaptic pruning in young and adult brains. Expression of the membrane-bound receptor MEGF10 is thought to be restricted to astrocytes in the CNS. It is particularly highly express during development in order to refine neuronal circuits but less prominent afterwards (Chung et al. 2013). Therefore, we investigated whether this protein might be a pharmacological target of ADs. Immunofluorescent-immunocytochemical staining was performed in a primary culture of cortical astrocytes. FLX treatment for 48h increased MEGF10 expression primary cortical astrocytes (**figure 31**), suggesting that a higher expression of MEGF10 could be correlated with a decrease in the number of synaptic densities.

Results

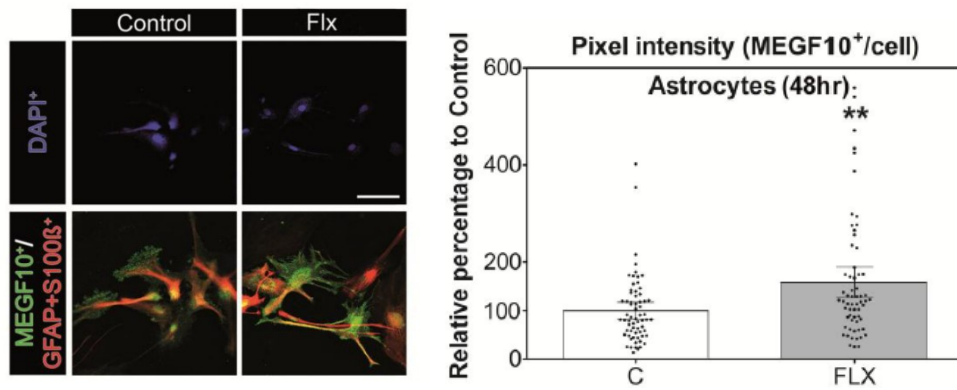


Figure 31. FLX treatment induces an increased MEGF10 expression in a primary culture of astrocytes. FLX treatment induced an increased expression of MEGF10 (green) per astrocytes in a primary culture after 48 hrs drug treatment. Scale bar: 70 μ m. Data are represented as mean \pm SEM, every symbol represents the number of astrocytes in the analysis. Unpaired t-test ** $p < 0.01$. Data provided by Di Benedetto's lab.

3.3.4 Analysis of MEGF10 protein amount in astrocytes from cortical regions

Next it was analysed whether an increase of MEGF10 was found in a primary culture of astrocytes after 10 μ M ADs treatment (**figure 32**, C: $n=13$, 100 ± 4.75 ; DMI: $n=12$, 115.9 ± 8.60 ; FLX: $n=14$, 118.6 ± 8.24 . One-way ANOVA followed by Dunnett's multiple comparisons test). This drug treatment showed variable results in the total amount of MEGF10, but neither DMI nor FLX did not change the expression of this protein significantly.

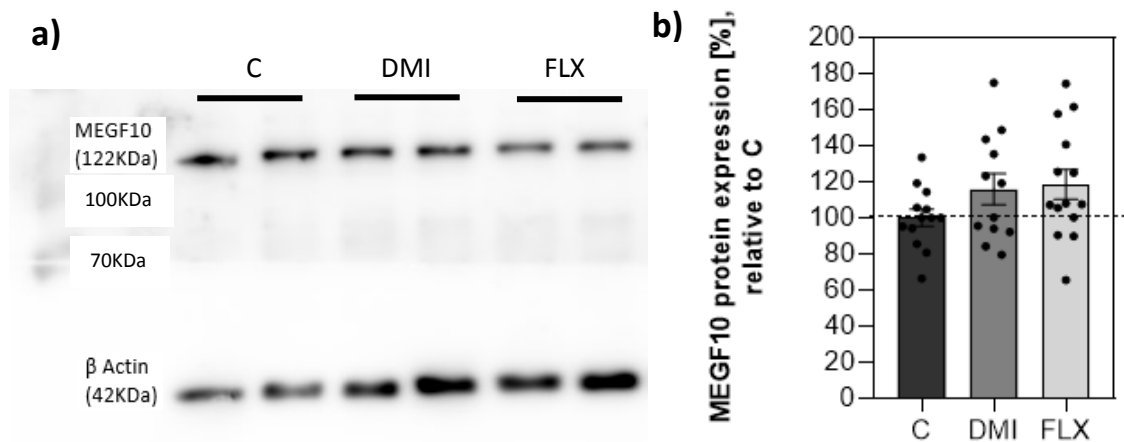


Figure 32. Western blot data from primary cortical astrocytes after 10 μ M DMI or FLX treatment. a) Representative western blot of MEGF10 on primary cortical astrocytes from NAB. **b)** Percentage of MEGF10 expression normalized to β -Actin and relative to control levels. n=13-14. Data are represented as mean \pm SEM. Ordinary one-way ANOVA followed by Dunnett's multiple comparisons test.

Statistics:

MEGF10 levels cortical astrocytes	ADs effects
C vs. DMI	F (2,36)=1.862, p= 0,2460
C vs. FLX	F (2,36)=1.862, p= 0,1402

3.3.5 Evidences MEGF10 is mediating the astrocyte-dependent remodelling of synapses

The next experiments were performed in order to see whether a blockade in the signalling pathway triggering the induction of MEGF10 or the genetic downregulation of MEGF10 could have an effect in the remodelling of synapses mediated by astrocytes and upon AD treatment. Furthermore, the MEGF10 phagocytic pathway could be implicated, therefore experiments that could reveal the participation of astrocytes in phagocytosis were performed.

3.3.6 Effects of inhibitor U0126 on the number of synapses

Given that MEGF10 is induced by ERK1/2 activation in glia cells, we next examined the significance of astrocytic ERK1/2 inhibition and therefore MEGF10 inhibition for synaptic reduction (Napoli et al. 2012). In order to see if the remodelling effect on synapses depends on AD-dependent ERK1/2 activation in astrocytes, the U0126 inhibitor was administered 30 minutes before AD treatment. This inhibitor is a synthesized organic compound that inhibit the kinase activity. As seen in **figure 20**, upon AD treatment, there is a reduction in pre- and post-synaptic markers, as well as in the number of synapses (**figure 33, coloured bars, Synphys⁺**: N=3, C: 10.13 \pm 0.33; DMI: 7.71 \pm 0.47; MTZ: 7.25 \pm 0.09; FLX: 6.69 \pm 0.69; RBX: 6.78 \pm 0.50; VLX: 7.31 \pm 0.43. **Synphys⁺/PSD95⁺**: N=3, C: 6.82 \pm 0.18; DMI: 4.72 \pm 0.66; MTZ: 4.83 \pm 0.22; FLX: 4.16 \pm 0.52; RBX: 4.16 \pm 0.22; VLX: 4.94 \pm 0.27. **PSD95⁺**: N=3, C: 10.66 \pm 0.13; DMI: 7.74 \pm 0.49; MTZ: 7.96 \pm 0.59; FLX: 8.10 \pm 0.34;

Results

RBX: 8.03 ± 0.48 ; VLX: 8.00 ± 0.61). On the other hand, it can be observed that in the presence of the inhibitor the effect of ADs are gone (**figure 35 striped bars, Synphys⁺**: N=3, C: 10.63 ± 0.33 ; DMI: 12.02 ± 0.47 ; MTZ: 9.67 ± 0.09 ; FLX: 10.72 ± 0.69 ; RBX: 9.93 ± 0.50 ; VLX: 9.66 ± 0.43 . **Synphys⁺/PSD95⁺**: N=3, C: 6.76 ± 0.158 ; DMI: 7.00 ± 0.50 ; MTZ: 5.91 ± 0.68 ; FLX 6.65 ± 0.36 ; RBX: 6.67 ± 0.89 ; VLX: 6.12 ± 0.21 . **PSD95⁺**: N=3, C: 10.63 ± 0.86 ; DMI: 9.93 ± 0.46 ; MTZ: 9.13 ± 0.51 ; FLX: 9.32 ± 0.59 ; RBX: 10.59 ± 0.54 ; VLX: 10.36 ± 0.63 . Ordinary one-way ANOVA followed by Dunnett's multiple comparisons test). There is not reduction in the number of synapses in the presence of astrocytes when they are pre-treated with U0126.

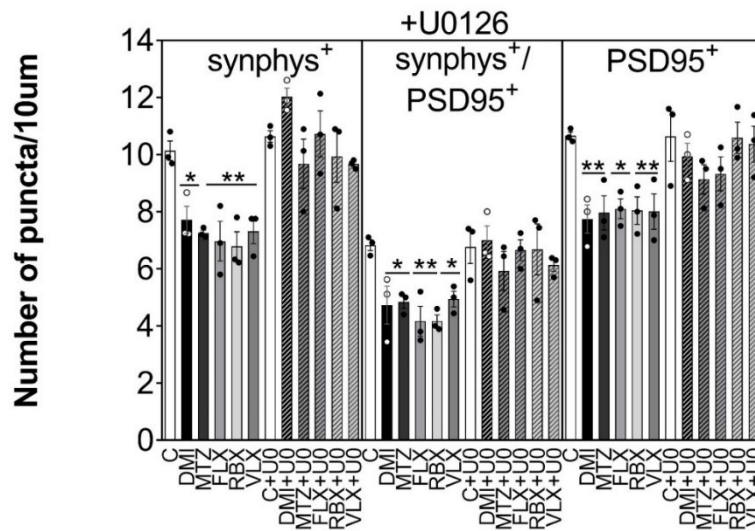


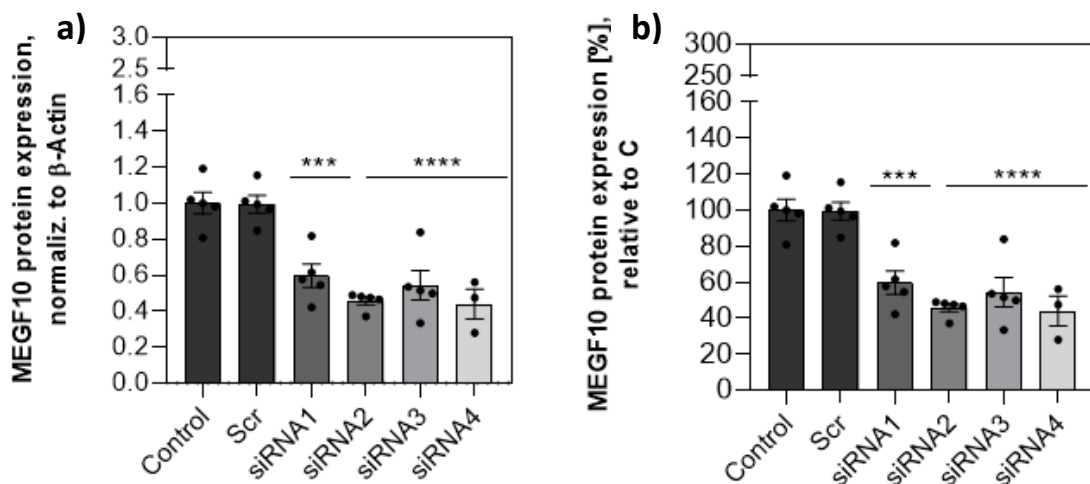
Figure 33. The pharmacological inhibition of ERK1/2 activation with U0126 prior AD treatment is sufficient to hamper drug effects on synapses in co-culture. In the left part of every graph (coloured bars) the number of synaptic densities after the effects of different ADs can be observed. ADs trigger a reduction in the number of excitatory synapses (as seen in **figure 20**). In the right part (striped bars) it can be seen the effects of U0126 on the astrocyte-mediated remodelling of synapses. All data are represented as mean \pm SEM; n=3 (10-12 dendrites per condition group). * p<0.05; ** p<0.01. Ordinary one-way ANOVA followed by Dunnett's multiple comparisons test.

Statistics:

Condition	Parameter	ADs effects
-U0126	C vs. treatment for synphys ⁺	F (5, 12) = 7.145, p=0.0026**
	C vs. treatment for synphys ⁺ /PSD95 ⁺	F (5, 12) = 6.275, p=0.0044**
	C vs. treatment for PSD95 ⁺	F (5, 12) = 5.396, p=0.0079**
+U0126	C vs. treatment for synphys ⁺	F (5, 12) = 2.042, p=0.1443
	C vs. treatment for synphys ⁺ /PSD95 ⁺	F (5, 12) = 0.5006, p=0.7704
	C vs. treatment for PSD95 ⁺	F (5, 12) = 1.099, p=0.4102

3.3.7 MEGF10 knockdown via siRNA

I designed siRNA against MEGF10 mRNA (see table 6), and transfected NAB astrocytes for 3 and 5 DIV. Two concentrations that were added to the cells, 50 nM and 100 nM, for 3 and 5 days in order to have preliminary results about the efficacy of knockdown of MEGF10. The lowest concentration showed the highest reduction in the expression of MEGF10 (122 kDa) by means of western blotting (**figure 34, relative MEGF10 protein after 50nM 3DIV**: C: n=5, 1.0 ± 0.06 ; Scr: n=5, 0.99 ± 0.04 ; si1: n=5, 0.59 ± 0.06 ; si2: n=5, 0.45 ± 0.02 ; si3: n=5, 0.54 ± 0.08 ; si4: n=3, 0.43 ± 0.08 . **Figure 35, relative MEGF10 protein expression after 50nM 5 DIV**: C: n=4, 1.0 ± 0.06 ; Scr: n=4, 0.88 ± 0.19 ; si1: n=4, 0.84 ± 0.12 ; si2: n=4, 0.58 ± 0.07 ; si3: n=4, 0.46 ± 0.10 ; si4: n=4, 0.51 ± 0.03 . One-way ANOVA with by Dunnett's multiple comparisons *post hoc test*). Taking this data into account, two of the best siRNA sequences were chosen for triggering a reduction in MEGF10 in future experiments. On the other hand, with the highest concentration (100nM) a reduction in MEGF10 was not achieved (**Figure 36, relative MEGF10 protein expression after 100nM 5 DIV**: C: n=2, 1.0 ± 0.03 ; Scr: n=3, 1.01 ± 0.04 ; si1: n=4, 0.95 ± 0.10 ; si2: n=3, 0.87 ± 0.02 ; si3: n=3, 0.96 ± 0.17 ; si4: n=4, 1.88 ± 0.49 . One-way ANOVA with by Dunnett's multiple comparisons *post hoc test*). Besides these evidences, several reports indicate that siRNA concentrations of ≤ 100 nM in mammalian cultured cells can lead to nonspecific changes in gene expression and the use of lower concentrations appears to minimize those effects (RNAi research guide, Ambion).



Results

Figure 34. Western blot data from transfection 50 nM siRNA for MEGF10 3 DIV. **a)** Relative MEGF10 protein expression normalized to β -Actin. **b)** Percentage of MEGF10 expression normalize to β -Actin and relative to control levels. Western blot analysis showed that astrocytes transfected with siRNA had a reduction around 50 to 60% total amount of MEGF10. *** $p < 0.001$; **** $p < 0.0001$. $n = 3-5$. Data are represented as mean \pm SEM. Ordinary one-way ANOVA with by Dunnett's multiple comparisons post hoc test.

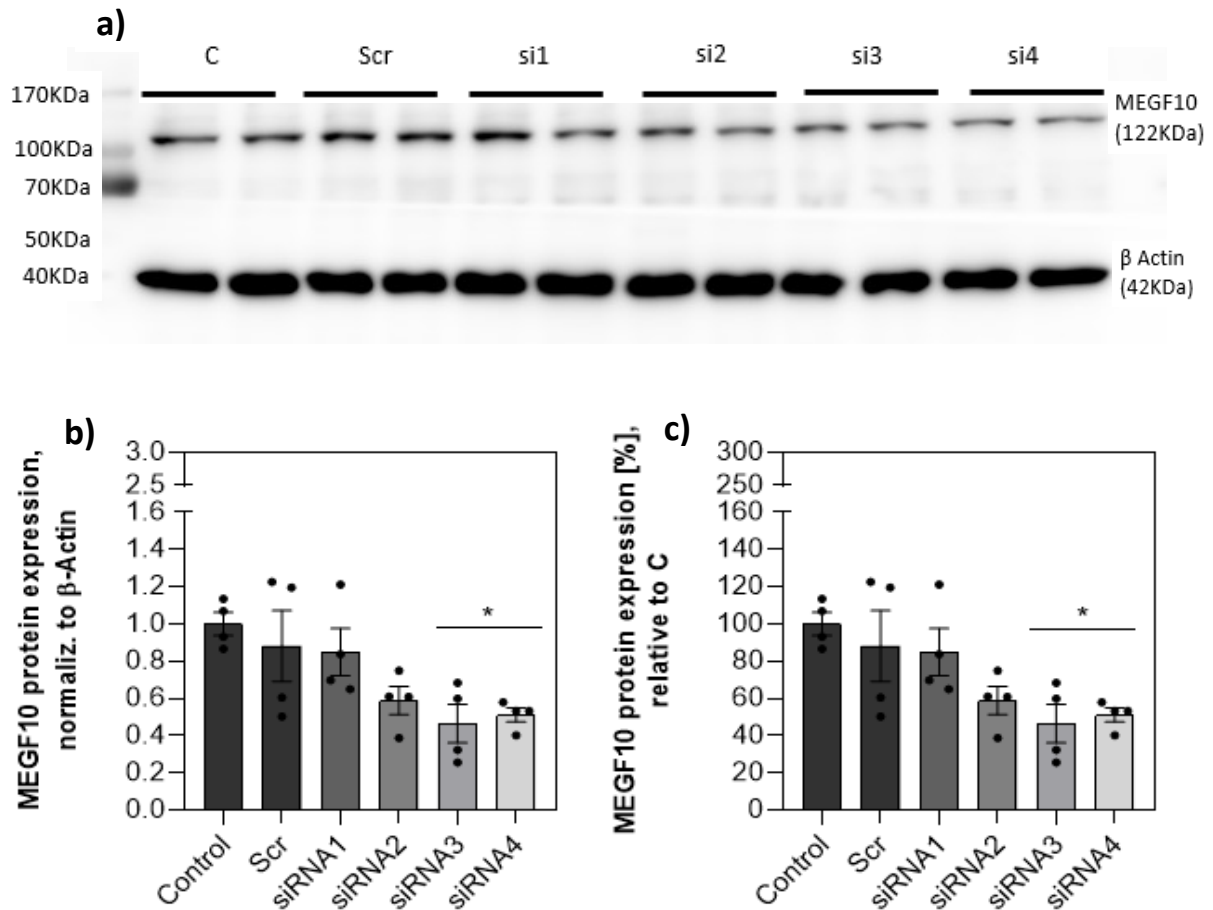


Figure 35. Western blot data from transfection 50 nM siRNA for MEGF10 5 DIV. **a)** Representative western blot of MEGF10 on primary cortical astrocytes from NAB. **b)** Relative MEGF10 protein expression normalized to β -Actin. **c)** Percentage of MEGF10 expression normalize to β -Actin and relative to control levels. Western blot analysis showed that astrocytes transfected with siRNA had a reduction around 40 to 60% total amount of MEGF10. * $p < 0.05$. $n = 4$. Data are represented as mean \pm SEM. Ordinary one-way ANOVA with by Dunnett's multiple comparisons post hoc test.

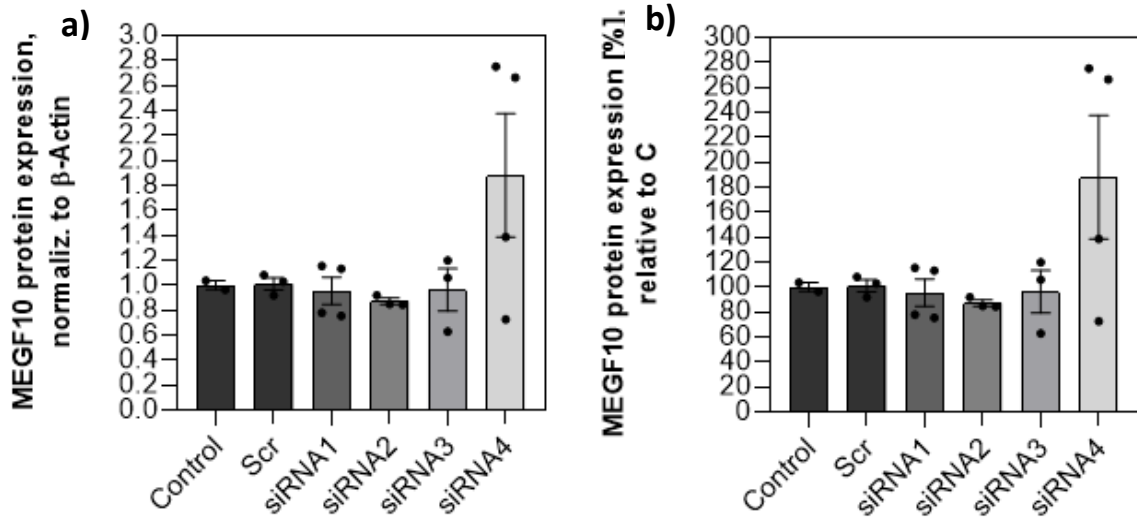


Figure 36. Western blot data from transfection 100 nM siRNA for MEGF10 5 DIV. a) Relative MEGF10 protein expression normalized to β -Actin. b) Percentage of MEGF10 expression normalize to β -Actin and relative to control levels. Astrocytes transfected with siRNA at concentration 100nM did not present any reduction in the total amount of MEGF10; n=2-4. Data are represented as mean \pm SEM. Ordinary one-way ANOVA with by Dunnett's multiple comparisons post hoc test.

As we want to study the interactions between neurons and astrocytes in a mature state, siRNA was transfected in astrocytes that were in culture with neurons for 14 DIV afterwards. After this period of time MEGF10 protein level was also seen to be reduced (**figure 37, relative MEGF10 protein expression at 14 DIV:** C: n=4, 1.0 ± 0.06 ; Scr: n=6, 0.83 ± 0.15 ; si2: n=6, 0.57 ± 0.06 ; si4: n=4, 0.46 ± 0.04 . One-way ANOVA with by Dunnett's multiple comparisons *post hoc test*) and two of the best siRNA sequences were chosen for further experiments.

Results

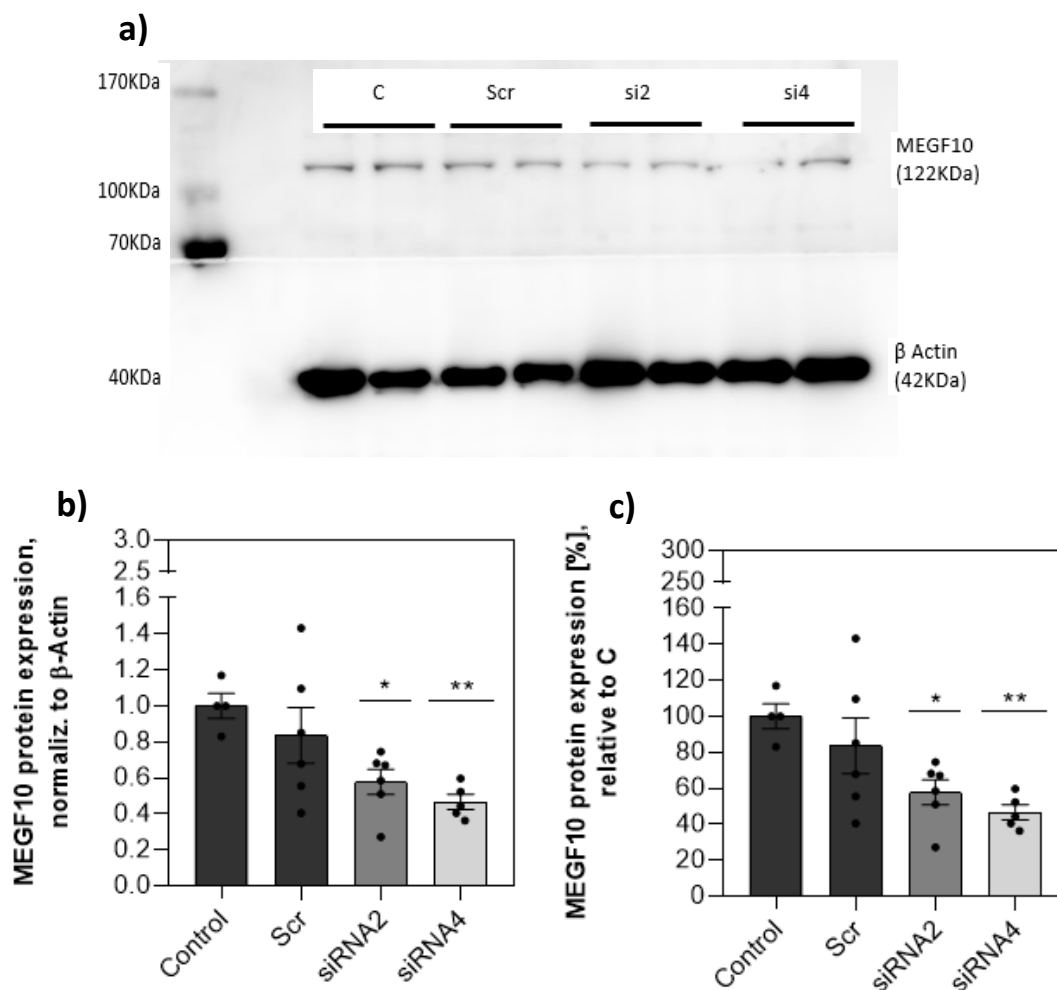


Figure 37. Western blot data from transfection 50 nM siRNA for MEGF10 for 14 DIV. a) Representative western blot of MEGF10 on primary cortical astrocytes from NAB. **b)** Relative MEGF10 protein expression normalized to β -Actin. **c)** Percentage of MEGF10 expression normalize to β -Actin and relative to control levels. Western blot analysis showed that astrocytes transfected with siRNA had a reduction around 40 to 60% total amount of MEGF10. * p<0.05; ** p<0.01. n=4-6. Data are represented as mean \pm SEM. Ordinary one-way ANOVA with by Dunnett's multiple comparisons post hoc test.

Statistics from figures 34-37.

Parameter	siRNA for MEGF10
50nm siRNA for 3 DIV	F (5, 22) = 17.59, p<0.0001****
50nm siRNA for 5 DIV	F (5, 18) = 3.991, p=0.0130*
100nm siRNA for 5 DIV	F (5, 13) = 2.166, p=0.1215
50nm siRNA for 14 DIV	F (3, 17) = 4.969, p=0.0118*

3.3.8 Analysis of excitatory synaptic densities in the presence of knockdown MEGF10 astrocytes

The siRNA sequences which triggered the higher reduction in MEGF10 protein expression were used for further analysis. Neurons growing in co-culture and treated with FLX for 48h displayed a reduction in the number of excitatory synapses (see white bars **figure 38 c**, C+FLX and Scr+FLX) while neurons growing with MEGF10 knockout astrocytes did not show any change in the number of synaptic densities (see grey bars **figure 38 c**, si2 and si4. **Figure 38, Synphys⁺**: N=3, C: 12.29 ± 0.26 ; Scr: 10.82 ± 0.63 ; C+FLX: 8.90 ± 0.35 ; Scr+FLX: 8.49 ± 0.50 ; si2: 12.80 ± 0.58 ; si2+FLX: 14.18 ± 0.91 ; si4: 14.11 ± 1.13 ; si4+FLX: 13.79 ± 1.28 . **Synphys⁺/PSD95⁺**: N=3, C: 8.22 ± 0.18 ; Scr: 7.77 ± 0.29 ; C+FLX: 5.76 ± 0.20 ; Scr+FLX: 5.72 ± 0.31 ; si2: 8.54 ± 0.18 ; si2+FLX: 9.04 ± 0.49 ; si4: 9.20 ± 0.92 ; si4+FLX: 8.81 ± 0.63 . **PSD95⁺**: N=3, C: 13.53 ± 0.53 ; Scr: 12.22 ± 0.58 ; C+FLX: 10.91 ± 0.31 ; Scr+FLX: 10.96 ± 0.09 ; si2: 13.26 ± 0.47 ; si2+FLX: 13.82 ± 0.46 ; si4: 13.59 ± 1.04 ; si4+FLX: 13.58 ± 0.83 . Ordinary one-way ANOVA followed by Dunnett's multiple comparisons test). Furthermore, neurons together with knockdown MEGF10 astrocytes and treated with FLX did not show any reduction in synphys⁺/PSD95⁺ colocalization (see grey bars with stripes **figure 38 c**, si2+Flx/si4+flx). This data indicates FLX cannot target MEGF10 and mediate synaptic remodelling when it is reduced, as compared to what it happens with control astrocytes after treatment with FLX for 48h. For this experiment, normal astrocytes (control) and astrocytes transfected with non-targeting sequence (Scr) were used as controls. Even if there is a small reduction in synphys⁺ or PSD95⁺ puncta with the Scr sequence, this is not reflecting any significant difference with the principal control.

Results

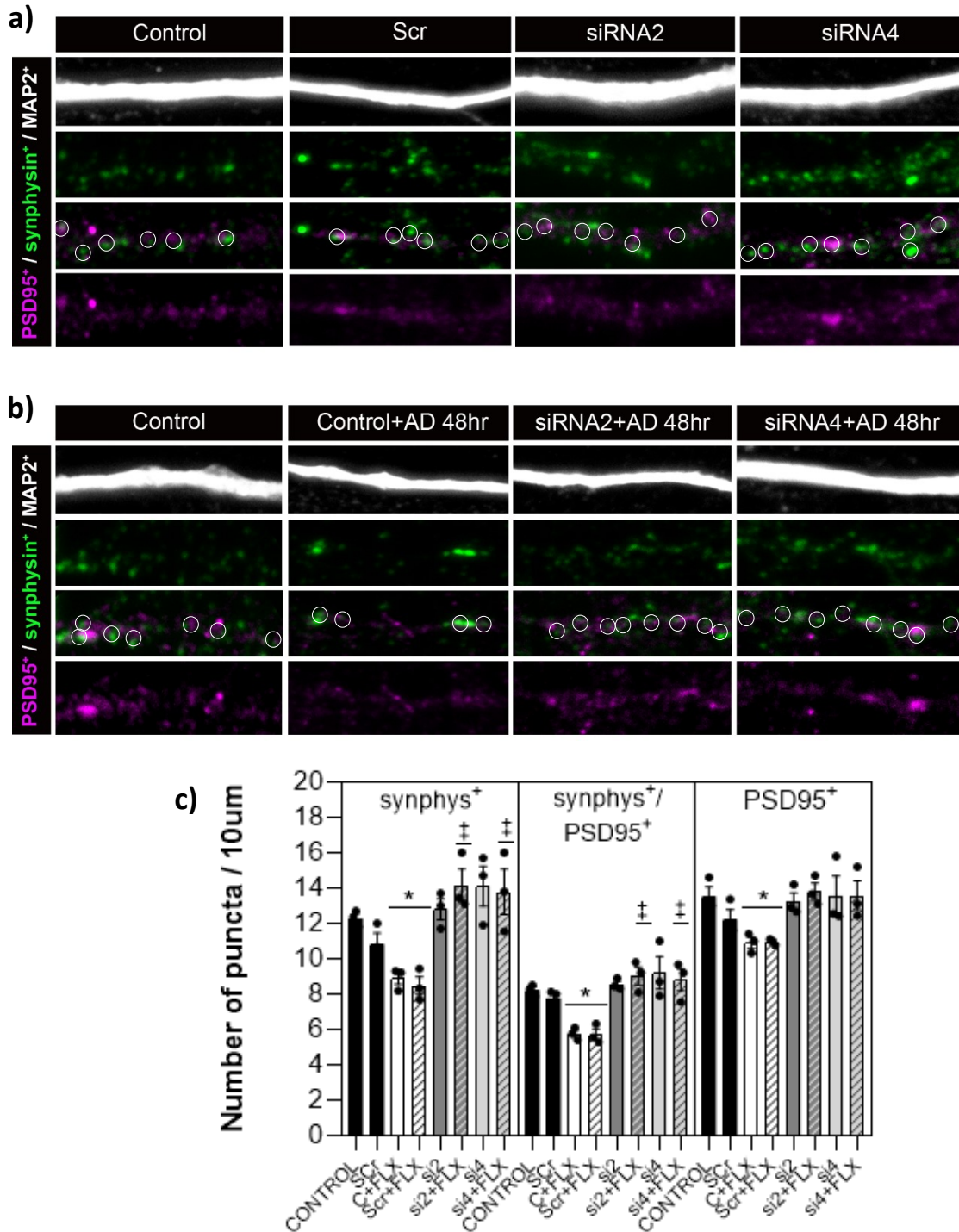


Figure 38. Excitatory synaptic densities in neurons are not affected after knocking down MEGF10 in astrocytes and following 48h FLX treatment. **a)** Representative images with the quantification of synapses in control conditions and in the presence of siRNA2 and siRNA4 transfected astrocytes. **b)** Representative images with the quantification of synapses when the AD FLX was added for 48h and in the presence of siRNA2 and siRNA4 transfected astrocytes. **c)** Quantification of excitatory synapses in 10µm of dendrite. Both control and control cells transfected with Scr show a reduction in synaptic densities. Those results are rescued by knocking down MEGF10 with siRNA2 and siRNA4. The AD treatment of cells transfected with siRNA does not show any reduction in the number of synapses. All data are represented as mean ± SEM; n=3

(10-12 dendrites per condition). * $p < 0.05$ (compared to control); ++ $p < 0.01$ (compared to C+FLX). Ordinary one-way ANOVA followed by Tukey's multiple comparisons test.

Statistics:

	Parameter	siRNA/ADs effects
All conditions	C vs. siRNA/ADs effects for synphys ⁺	F (7, 16) = 8,347 p=0.0002 ***
	C vs. siRNA/ADs effects for synphys ⁺ /PSD95 ⁺	F (7, 16) = 8,664 p=0.0002 ***
	C vs. siRNA/ADs effects for PSD95 ⁺	F (7, 16) = 3,811 p=0.0127 *

3.3.9 Phagocytic properties of astrocytes *in vitro*

LAMP1, lysosomal marker, was quantified in astrocytes with and without FLX treatment. LAMP1 was quantified in the juxtannuclear area of the astrocytes (**figure 39 a**). Analysis revealed higher amount of LAMP vesicles after FLX treatment in primary astrocytes (**figure 39 b**, C: n=3, 1.43 ± 0.23 ; FLX: n=3, 2.25 ± 0.27 ; unpaired t-test, $p=0.0359$). Second analysis was the colocalization of synphys⁺/LAMP1⁺, their colocalization might indicate synaptophysin was engulfed by the astrocytes and got inside the vesicles before being digested (**figure 39 c**, C: n=3, 38.44 ± 1.83 ; FLX: n=3, 48.75 ± 2.76 ; unpaired t-test, $p=0.0864$). After FLX treatment an increase in the amount of synphys⁺ was found to be colocalizing with LAMP1⁺ vesicles, indicating an increase in internalized synphys⁺ although those results did not show any statistical significance.

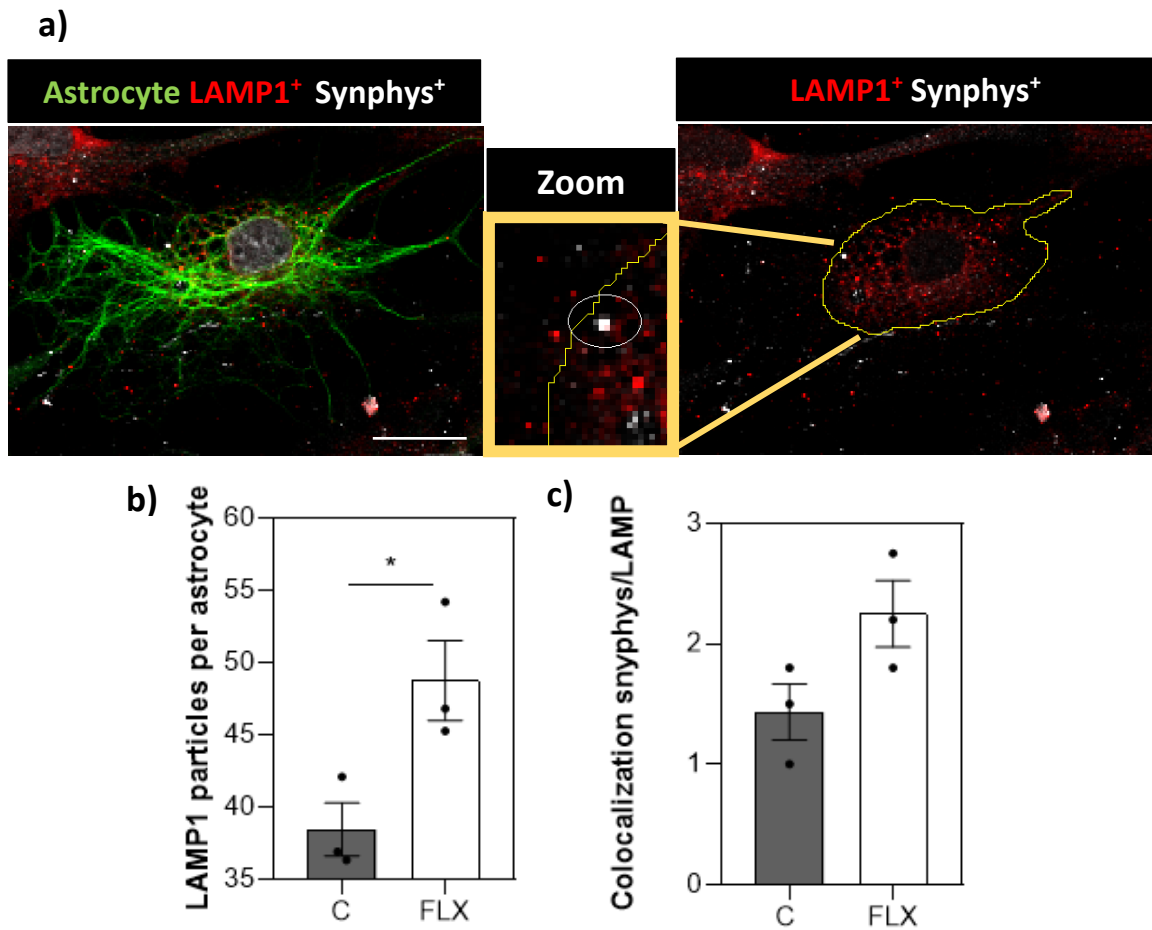


Figure 39. Higher number of lysosomes in astrocytes after FLX treatment and their co-localization with synphys⁺ particles. a) Representative microphotographs (Z-stack series of 40 μm) from control astrocytes and the co-localization of LAMP1⁺/synphys⁺ in the yuxtannuclear area, scale bar 20 μm . **b)** Analysis LAMP1 particles per astrocyte. **c)** Analysis of the co-localization of LAMP1⁺/synphys⁺. n=3 (10 astrocytes per treatment group), data are represented as mean \pm SEM. * p<0.05. Unpaired t-test.

Statistics:

Parameter	siRNA for MEGF10
Number LAMP particles	t=3,108, df=4, p=0.0359 *
LAMP ⁺ /synphys ⁺	t=2,263, df=4, p=0.0864

3.4 Studying astrocytes and their interaction with neurons in animal models for depression

The aim of the next experiments was to validate WKY rats as an additional animal model to study depressive phenotype. Furthermore, I wanted to uncover whether the number of synapses and complexity of neurons are modified in depressive-like behaviours.

3.4.1 Characteristics of the depressive-like phenotype in Wistar Kyoto rats on a cellular basis

The aim of these experiments was to validate WKY rats as an additional animal model to HAB for our experiments to more realistically demonstrate the heterogeneity found in depression throughout further experiments. Therefore, it is important to determine whether WKY rats, although having a distinct molecular background to HAB, could have similar alteration in astrocyte number and H3K4me3 abundance (characterized epigenetic mark known to be highly enriched at transcriptional start sites and then associated with active transcription). In order to analyse these aspects in adult NAB and WKY rats, IF-IHC on PFC brain slices was performed. A significant decrease in GFAP/S100 β positive astrocyte cell number was seen in the PFC of WKY rats compared to NAB (**figure 40 b**. NAB: n=6, $100 \pm 3.15\%$; WKY: n=6, $80.68 \pm 4.53\%$. Student's t test). Further, to investigate if there is an astrocyte-specific enrichment of H3K4me3, a colocalisation analysis was performed. For this, co-localization of H3K4me3 with astrocytic nuclei was analysed. A significant increase of this activating methylation marker was found in WKY PFC adult brain slices (**figure 40 c**. NAB: n = 6, 100 ± 13.10 ; WKY: n = 6, 135 ± 8.91 . Student's t test).

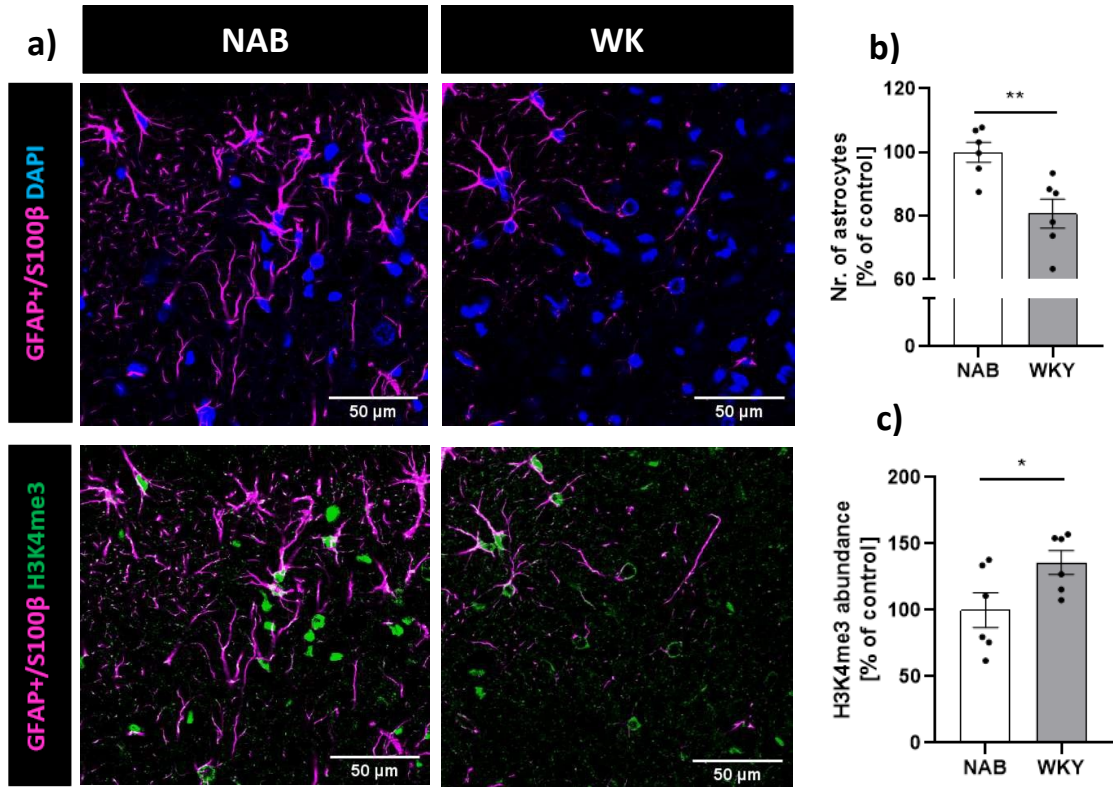


Figure 40. Severe alterations in astrocyte density and H3K4-trimethylation marker abundance in PFC of adult WKY rats in comparison to NAB rats. a) Representative image of adult rat PFC with astrocytes labelled for GFAP and S100β (magenta), and DAPI-stained DNA (blue). Scale bar: 50 μm. **b)** Quantification of astrocyte density in PFC of NAB. **c)** Quantification of H3K4me3 abundance in NAB vs. WKY astrocytic nuclei. n=6. Data is depicted as mean ± SEM. Unpaired, two-tailed Student’s t-test. * p<0.05; ** p<0.01.

Statistics:

Parameter	Statistic data
Number of astrocytes	t10 = 3.496, p=0.006**
H3K4me3 abundance	t10 = 2.262; p=0.0472*

3.4.2 Sholl analysis: Alteration of morphological properties and complexity of NAB neurons co-cultured with HAB or WKY astrocytes

To determine how the morphology of neurons isolated from NAB rats is influenced by growing on astrocytes isolated from different animal models for depressive-like behaviour, HAB or WKY, Sholl analysis was performed. As indicated in the representative pictures (**figure 41**), growth of wildtype neurons on depression model astrocytes, strongly affects branching complexity. Total Sholl analysis shows a significant decrease in neuronal branches at 70 – 100 μm , 120 μm and 140 – 170 μm from soma, when grown on HAB astrocytes and at 70 - 120 μm and 160 μm from soma when grown on WKY astrocytes (**figure 41 b**; NAB: n=4; HAB: n=3; WKY: n=3; Two-way ANOVA: Distance from soma (in μm) x genetic background). The mean path length of neuronal dendrites, showed only insignificant changes, under the three different co-culture conditions (**figure 41 c**, NAB: n=4, 85.46 ± 8.84 ; HAB: n=3, 86.22 ± 4.40 ; WKY: n=3, 85.70 ± 13.15 ; Ordinary one-way ANOVA, NAB vs. HAB $p=0.96$; NAB vs. WKY $p=0.99$). The number of the main primary processes is decrease in neurons growing on WK astrocytes, although this parameter does not reach statistically significance (**figure 41 d**, NAB: n = 4, 6.10 ± 0.50 ; HAB: n = 3, 5.86 ± 0.40 ; WKY: n = 3, 5.00 ± 0.41 ; Ordinary one-way ANOVA followed by Dunnett's multiple comparisons test, NAB vs. HAB $p=0.91$; NAB vs. WKY $p=0.23$).

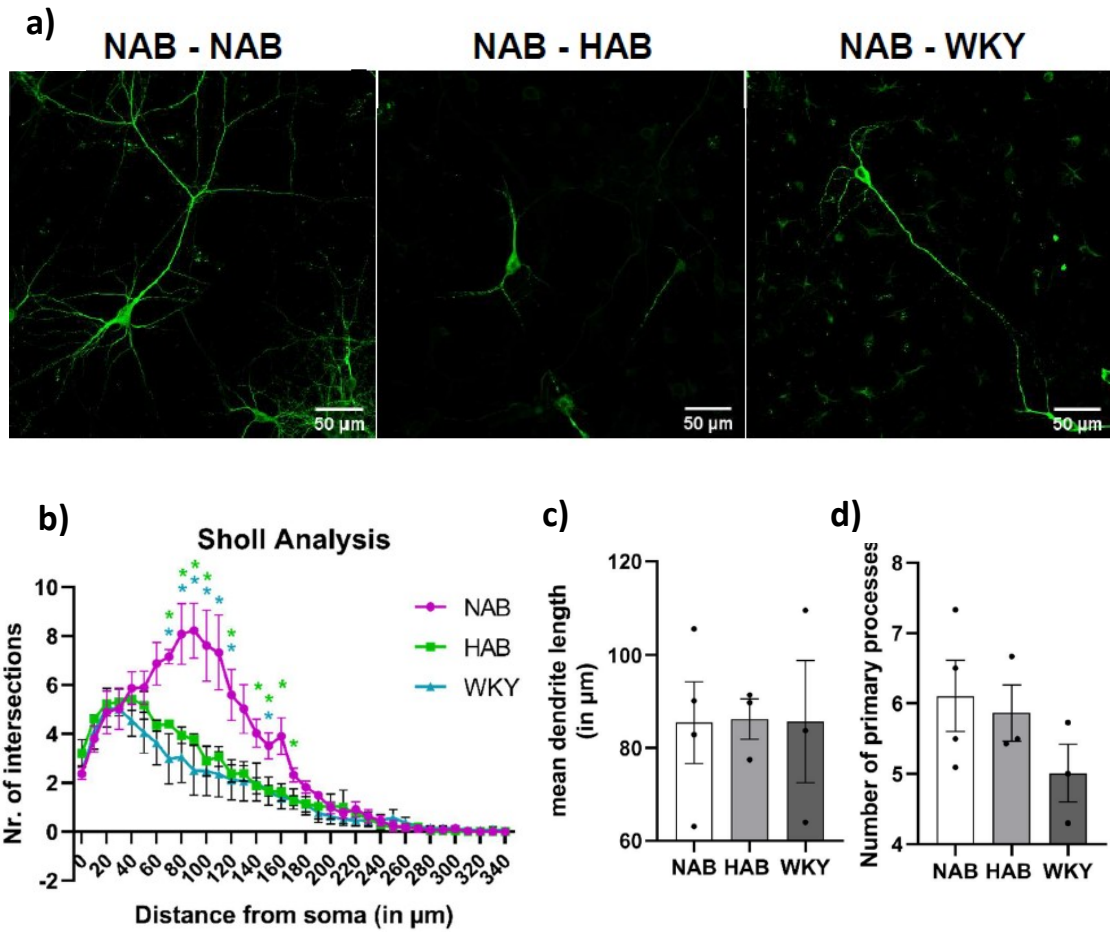


Figure 41. Neuronal morphology from neurons growing in the presence of NAB, HAB or WKY astrocytes. **a)** Representative images of MAP2-stained (green) cortical neurons co-cultured for 14 DIV with astrocytes from either NAB, HAB or WKY rats. Scalebar: 50 μm . **b)** Sholl quantification of MAP2-stained neuron complexity, under conditions from a) * $p \leq 0.05$, significant differences calculated by two-way ANOVA followed by Fisher’s lowest significant difference (LSD). **c)** Mean dendrite length under conditions from a). Ordinary one-way ANOVA followed by Dunnett’s multiple comparisons test. **d)** Number of primary processes on neurons under conditions from a). Data are represented as mean \pm SEM. NAB: $n=4$, HAB $n=3$, WKY $n=3$ (from 2 to 14 neurons per condition and treatment).

Statistics:

Analysis	Parameter	Statistic data
Sholl analysis		$F(68,238)=3.692; p<0,001$
Mean dendrite length	NAB vs. HAB	$F(2,7)=0.00165, p>0.99$
	NAB vs. WKY	$p=0.997$
N° primary processes	NAB vs. HAB	$F(2,7) = 1.508, p=0.29$
	NAB vs. WKY	$p=0.91$
		$p=0.23$

3.4.3 Sholl analysis after AD treatment

Next, it was important to determine the effect of acute AD treatment on neurons growing with HAB and WKY astrocytes. Sholl analysis was performed on neurons from co-cultures treated with ADs. AD treatment affected neuronal arborisation complexity by partially rescuing the morphology of the diseased phenotype (**figure 42**; NAB: n=3; NAB+FLX: n=3; HAB: n=4; HAB+FLX: n=4; WKY: n=3; WKY+FLX: n=3. Two-way ANOVA: Distance from soma (in μm) x genetic background).

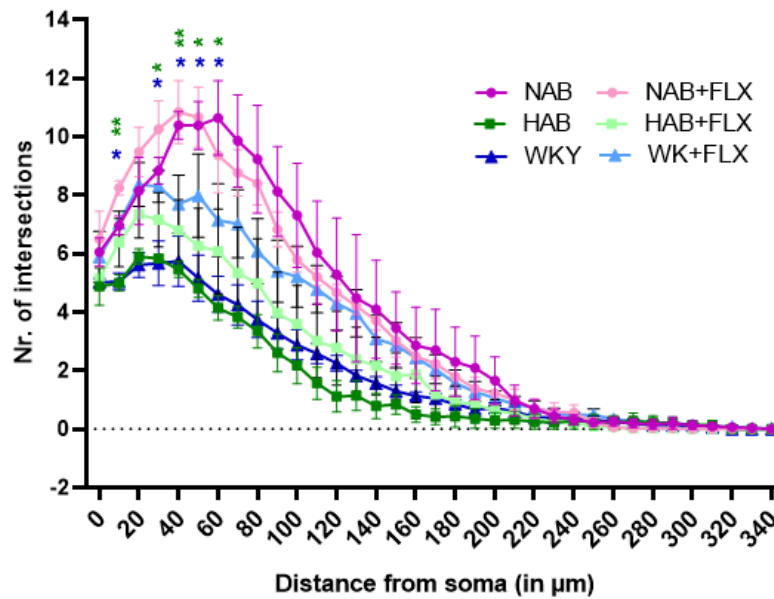


Figure 42. Neuronal morphology from neurons growing in the presence of NAB, HAB or WKY astrocytes treated with ADs for 48h. Sholl quantification revealed a higher arborisation complexity in neurons growing with HAB or WKY astrocytes treated with FLX (see HAB+FLX and WKY+FLX). All comparisons were made relative to control NAB. Neurons treated with FLX do not present significant difference, except for HAB+FLX at 40 and 50 μm from the soma $*p \leq 0.05$ (stars not shown), when compared to NAB. n= 3-4 (10-12 neurons per condition). Significant differences were calculated by two-way ANOVA followed by Fisher's lowest significant difference (LSD) $*p \leq 0.05$, $**p \leq 0.01$.

Statistics:

Analysis	Statistic data
Sholl analysis	F (170, 510) = 2,972 p<0,0001

3.4.4 Synaptic density in NAB Neurons co-cultured with HAB or WKY Astrocytes

Functional and structural alterations in synapse density have been linked to MDD (Duman et al., 2016; Holmes et al., 2019). I examined whether the growth of NAB cortical neurons

Results

on astrocytes derived from the cortex of HAB or WKY rats show differences in synapse number per 10 μm dendrite. No significant differences in these three aspects were found between NAB neurons grown on NAB or HAB astrocytes. However, a significant decrease in synapse numbers, as well as pre- and postsynaptic puncta was discovered in NAB neurons grown on WKY astrocytes when compared to NAB neurons grown on NAB astrocytes (**figure 43, synphys⁺**, n=3, NAB 10.82 ± 0.91 ; HAB 9.06 ± 0.54 ; WKY 7.03 ± 0.95 ; **synphys⁺/PSD95⁺**, n=3, NAB 6.12 ± 0.28 ; HAB 5.87 ± 0.19 ; WKY 3.81 ± 0.26 ; **PSD95⁺**, n=3, NAB 9.97 ± 0.51 ; HAB 10.26 ± 0.29 ; WKY 8.03 ± 0.57).

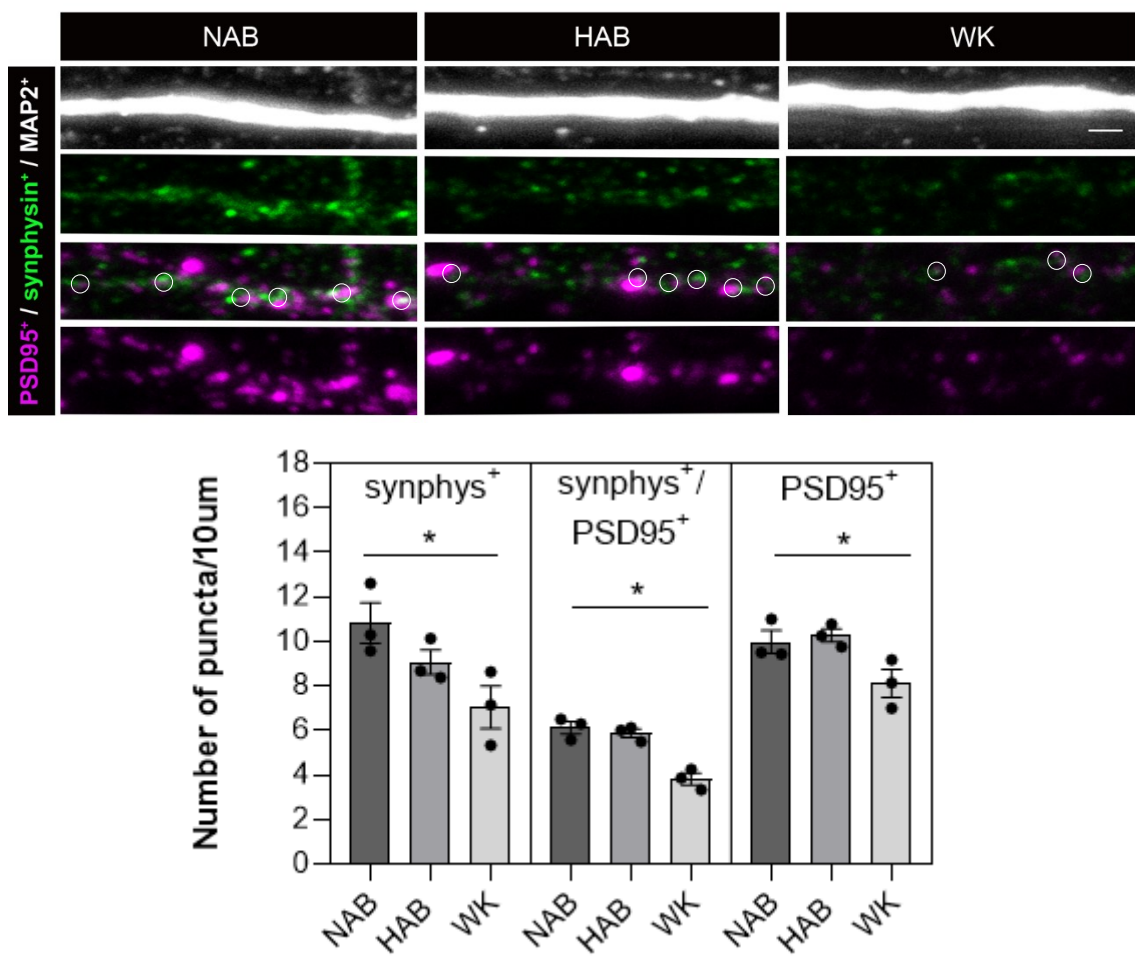


Figure 43. Excitatory synaptic densities in neurons growing with NAB, HAB or WK astrocytes. a) Representative image of 10 μm dendrite from NAB neurons growing with NAB, HAB or WK astrocytes. **b)** Quantitative analysis of presynaptic puncta synphys⁺, postsynaptic puncta PSD95⁺ and their co-localization synphys⁺/PSD95⁺, representing true excitatory synapses (white dots). n=3, 10 dendrites per treatment group. All data are represented as mean \pm SEM. * p<0.05 between NAB and WKY. Ordinary one-way ANOVA with by Dunnett's multiple comparisons post hoc test.

Statistics:

Parameter	Statistic data
Synphys ⁺	F (2, 6) = 5,283 NAB vs. HAB p=0.29; NAB vs. WK p=0.03 *
Synphys ⁺ /PSD95 ⁺	F (2, 6) = 25,73 NAB vs. HAB p=0.72; NAB vs. WK p=0,0011 **
PSD95 ⁺	F (2, 6) = 6,433 NAB vs. HAB p=0.88; NAB vs. WK p=0,0049 *

3.4.5 MEGF10 levels in primary astrocytes derived from animal models of depression

Proteins isolated from primary cortical astrocytes derived from NAB, HAB and WKY rats were analysed for the MEGF10 protein amount using WB method. No significant changes of MEGF10 level could be detected (**figure 44**; NAB: n=8, 1 ± 0.19; HAB: n=8, 1.06 ± 0.19; WKY: n=8, 1.32 ± 0.24; Ordinary one-way ANOVA).

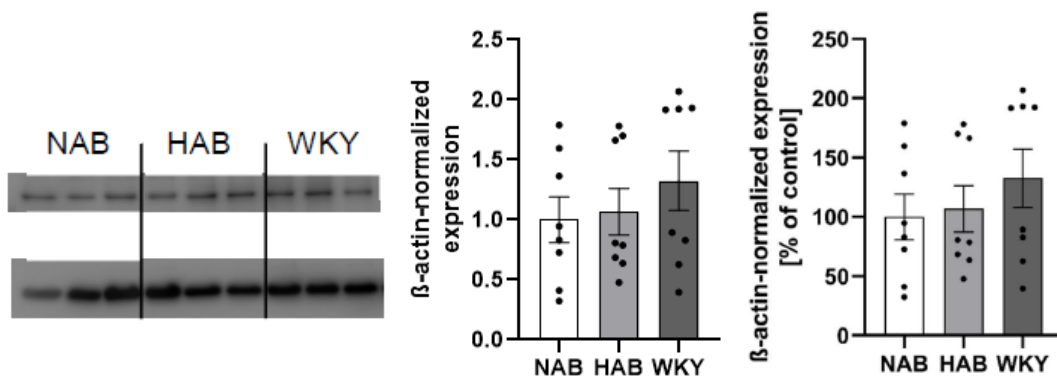


Figure 44. Western blot data from primary astrocytes NAB and from the animal models HAB and WK. **a)** Representative western blot of MEGF10 isolated from primary NAB, HAB or WKY cortical astrocytes. **b)** Relative MEGF10 protein expression normalized to β -Actin. **c)** Percentage of MEGF10 expression normalize to β -Actin and relative to NAB levels. n=8, data represented as mean \pm SEM. Ordinary one-way ANOVA.

Statistics:

Parameter	MEGF10 expression
NAB vs. HAB	F(2,21) = 0.6526; p=0.962
NAB vs. WK	F(2,21) = 0.6526; p=0.461

4 Discussion

Depression is a leading cause of disability worldwide and a major contributor to the overall global burden of disease (WHO). The exact underlying mechanism of MDD and the action of ADs are not fully understood. There are evidences showing that not only neurons, but also glial cells present aberrancies in MDD. It is still unknown whether those changes may be the underlying causes or consequences of a depressive phenotype. Treatment of depression depends on our understanding of the pathophysiology of the disease and of the mechanisms by which drugs relieve symptoms of depression. Therefore, some of the scientific efforts aim to find novel, faster-acting compounds and biomarkers that might predict the outcome of pharmacological treatments.

Communication between glia cells and neurons has been studied in the context of physiology and pathology. In the present thesis, I was able to advance the understanding of the interactions between astrocytes and neurons, more specifically with the synapses. ADs have been used in this study in order to elucidate new targets that might help to improve current treatment strategies. First, I described the effects of ADs on the different types of synapses. Furthermore, how astrocytes could mediate this effect in normal physiological conditions after the treatment with ADs. In particular a receptor found in astrocytes, MEGF10 was studied in this project, as this molecule could mediate the effects on ADs with an increase in its phagocytic properties. The results presented in this thesis point out the role of astrocytes in the maintenance of synaptic connections, and highlight these cells as potential targets to get a remodelling effect in brains of people suffering from mood disorders. Finally, animal models of depression have been studied to gain a deeper understanding of the underlying pathophysiological changes found in the disease and how a pharmacological treatment may help to re-establish some of those changes. Below, I will discuss the individual major findings revealed in this project.

4.1 Synaptic remodelling and the implication of astrocytes

For the previous experiments, cells from normal naïve animals have been used as preclinical tests are performed on normal animals. The reason is to understand how the drugs target certain molecules or cells, not interfering with other physiological changes produced with the disease itself (Trullas, 1997). I focused on the analysis of cortical and hippocampal areas, as those areas are implicated in mood disorders. The frontal cortex is responsible for higher executive functions such as cognition, working memory and the integration of sensory information (Duman, 2016), while the hippocampus plays a critical role in learning and memory (Sapolsky, 2001). Both regions control emotion, mood and cognition in response to physical or psychological stress (Harmer, Duman and Cowen, 2017). Reduction in the size, atrophy or loss of neurons and glial cells have been found in the PFC and hippocampus in MDD (Radley et al., 2005; Liu & Aghajanian, 2008; Duman & Li, 2012). Therefore, it is important to know how astrocytes and neurons interact in those areas and what are their responses upon AD treatment. *In vitro* experiments as mono-cultures or co-cultures were broadly used in this project. They are highly relevant for drug research because they provide a more representative human *in vivo*-like tissue model than animal models and allow for high-throughput testing and in-depth monitoring of drug effects on cell–cell interactions (Goers, Freemont and Polizzi, 2014).

The onset of beneficial drug effects in depression is delayed for two or three weeks. In other cases, patients with MDD do not achieve remission when trials with antidepressant medication are given (Duman et al. 2016). The delay response of some patients to ADs suggest that their secondary actions might involve changes in gene expression and/or synaptic plasticity contributing to their therapeutic mechanisms (Price and Drevets 2010). The search for alternative targets of ADs in order to increase their efficacy, might help to improve current treatment strategies (Bessa et al. 2009; Duric et al. 2010) or develop new drugs with AD properties. Here, I investigated the role of astrocytes in mediating a remodelling effect of ADs by targeting adult neuronal synaptic connections. Five different types of ADs corresponding to different classes have been used in this study: Desipramine (tricyclic AD), Mirtazapine (tetracyclic AD), Fluoxetine (SSRI), Reboxetine (NRI) and Venlafaxine (SNRI). The objective of these tests was to identify potential drugs with a

common mechanism of action, in particular to detect whether they all targeted the same molecules or pathways. Thus, the discovery of other pharmacological effects could be used to improve ADs efficacy in MDD and therefore be part of the development of new drugs.

It has been described how ADs target glial cells. In the case of astrocytes, ADs affect intracellular pathways and gene expression, expression of receptors and release of trophic factors (for review see Czéh & Di Benedetto, 2013). Several groups have confirmed that the ERK/MAPK pathway is a common target in glial cells after acute or chronic AD treatment (Hisaoaka et al. 2007; Li et al. 2009). For this study we have also studied the ERK/MAPK pathway in astrocytes, as this pathway plays a role in a broad spectrum of biological responses, even in the context of mood disorders. For instance, acute blockade of ERK/MAPK signalling in mice with pharmacological inhibition of ERK activity produced a depressive-like phenotype and blocked behavioral actions of antidepressants (Duman et al., 2007). A decreased activity of ERK1 and ERK2, modulators of this pathway, have been found in *post-mortem* brains of depressive patients (Dwivedi et al., 2001). The modulation of the ERK signalling pathway might have consequences on remodelling processes, for example in dendritic morphology in neurons (Kumar et al., 2005). That is the reason why ERK/MAPK pathway has been studied in astrocytes and C6 cells. Previous work from my laboratory was focused on the study of these cells, as they belong to a cell line which shares similar ERK activation patterns with astrocytes in response to ADs and might therefore be used as an astrocytic model to analyse an AD-dependent modulation of ERK activation (Di Benedetto et al. 2012). The five different ADs have been seen to activate pERK1/2 in C6 cells and astrocytes. Interestingly, the specificity of simultaneous ERK1/2 activation is a common and exclusive downstream target of several classes of ADs in astrocytes, but not of other drugs such as psychotropic drugs. Previous work revealed no effect in the amount of ERK1/2 molecules when benzodiazepines or antipsychotics were used (Di Benedetto et al. 2012), thus indicating that this effect is due to a common and selective action of antidepressants. This drug specificity is important because the knowledge about the specific molecular targets – which trigger therapeutic efficacy– and the general nonspecific pharmacological targets

–which might be responsible for unwanted side effects– is crucial for the generation of new ADs.

ERK1/2 regulates astrocyte features as morphology, growth, maturation or cell proliferation (Rossi et al. 2011; Fields et al. 2013). On the other hand, ERK signalling and function have been linked with synaptic plasticity and survival of neurons (Duric et al. 2010). Glial cells are very close to synapses and dynamically interact with them, this engages a bidirectional communication that is critical for the processing of synaptic information (Rial et al. 2016). It is proposed that changes in their interaction could further affect the number and density of synapses. I focused on the study of excitatory synapses as the majority of studies on astrocyte modulation of synapse formation were tested on this type of synapses (Farhy-Tselnicker and Allen, 2018). Firstly, I worked with *in vitro* experimental models validated in other studies, which allowed me to analyse both the properties of neurons and astrocytes separately and their interactions, and thus to get robust and reproducible data. I started analysing the number of excitatory synaptic densities after acute treatment of ADs. I aimed to know pharmacological effects of ADs in an early time point, in order to figure out whether acute treatment give rise to molecular changes in the brains, which could then trigger a remodelling in the adult neuronal networks and thus improve some of the symptoms of MDD. Most of the current knowledge of the mechanisms of ADs has come from animal studies examining neurobiological changes following chronic antidepressant administration. In the same way as in humans, long term treatments alleviate some of the depressive symptoms, but the mechanism responsible for such changes might originate in the first days of the treatment.

Increasing evidence demonstrates that neuroplasticity, a fundamental mechanism of neuronal adaptation, is disrupted in mood disorders and in animal models of stress. On the other hand, AD treatment produces opposing effects and can enhance neuroplasticity. Neuroplasticity can be studied in terms of structural (changes in spine and dendrite morphology) or functional (changes in communication and the molecular and cellular mechanisms accompanying such changes) synaptic plasticity (Pittenger and Duman, 2008). Coming from this knowledge, primary cortical neurons in a monoculture

model were used to assess whether the drugs could have any direct effect in the number of synapses. Although the presence of single neurons do not model the characteristics of a real brain, it may be helpful to see direct changes in this cell type. Single functional synapses were detected as whitish puncta, representing colocalization or closeness of immunoreactivity to the pre- and postsynaptic markers synaptophysin and PSD95, respectively (Ullian et al., 2001). These pre- and postsynaptic markers were used due to their presence in mature neuronal networks (El-Husseini et al., 2000; Glantz et al., 2007). No changes in the number of excitatory synapses were found after acute 48h treatment with ADs. On the other hand, inhibitory synaptic densities were quantified, but ADs seemed not to have an effect on them neither. In my experiments, lower number of inhibitory synapses were found in baseline conditions corresponding approximately to 20% of the inhibitory synapses found in the mammalian cortex, versus 80% of the excitatory synapses that can be found in cortical regions (King, Zylberberg and Dewese, 2013).

Secondly, primary cortical neurons and astrocytes were studied in a co-culture model. Co-culture systems have long been used to study the interactions between cell populations and are fundamental to acknowledge the cell–cell interaction, in this case similar to a neural network. The cells were treated with ADs for 48h and excitatory synaptic densities were quantified in the dendrites of neurons. Interestingly, a reduced amount of pre- and postsynaptic markers and therefore in synaptic densities were found in an early-time treatment. Similar results were found for the five ADs, but this reduction was not seen after 120h continuous AD treatment. This may be explained as a remodelling effect produced in the neuronal network which would be part of a neural circuit refinement and important to the further information processing. An interaction between astrocytes and neurons seem to be crucial to interpret these results. On the other hand, I could exclude that our *in vitro* model had a relevant amount of other cell types (for instance microglial cells) which could interfere with the aforementioned results. Next step was important to figure out whether a contact-mediated action by astrocytes or changes triggered by the release of soluble substances were responsible for the reduction in synaptic densities found after 48h treatment. An assay with ACM has been used in other studies to control if astrocyte-secreted proteins like Hevin and SPARC

or Glypicans have synaptogenic function (Kucukdereli et al. 2011; Allen et al. 2012). In my experiments, it is important to figure out whether the combination of ANCM + ADs played a role in terms of the density of synapses. For this reason, this combination was added to primary cortical neurons. ANCM + 48h ADs did not produce any reduction in the number of excitatory synaptic densities. I also analysed if any delayed effect could be present after 120h AD treatment, but similar numbers were found after this time period. This data provided me with the information that a membrane bound protein found in astrocytes may underlie the synaptic reduction to favour a subsequent early remodelling effect, rather than the release of soluble factors in the medium.

Next, it was evaluated whether ADs induced synaptic remodelling in adult rat brains, as in the co-culture experiments. By studying the effects of ADs in the brain, we can get an idea of the effects in a more complex network. Male rats were injected with the AD FLX for 48h (20mg/kg). Previous work from my laboratory revealed the lowest dosis of FLX (2mg/kg) was not sufficient to induce any change in the rat PFC. Rats treated with 20mg/kg presented a reduction of pre-synaptic signal intensity (synaptophysin⁺ pixel intensity) in the PFC, but not in hippocampal areas. The relative protein amount of the presynaptic (synaptophysin) and post-synaptic marker (PSD95) was also analysed in the PFC. A reduced amount of synaptic markers (protein level) was observed in the PFC of FLX treated rats compared to saline treated rats. Nevertheless, there still remain large gaps in the understanding of the neuroanatomical sites of action of current antidepressant agents. Are the effects of antidepressants confined to particular brain areas or do they occur more ubiquitously throughout the brain? For this reason –and to interpret the data of the *ex vivo* experiments– I performed *in vitro* experiments, studying the interaction between hippocampal astrocytes and cortical or hippocampal neurons. For all the *in vitro* studies, the combinations –cortical astrocytes with cortical or hippocampal neurons; hippocampal astrocytes with hippocampal or cortical neurons– allowed me to better understand whether changes in synapses were region-specific and cell-specific and even whether astrocytes from different areas may have different functions. Interestingly, I could observe that when hippocampal astrocytes were present in the co-culture, the ADs could not induce the astrocyte-dependent remodelling of synapses, in a similar way as it was seen in the hippocampus *ex vivo*. Since Cahoy and

colleagues performed a genome-wide analysis of the mRNA from acutely isolated, highly purified astrocytes, we had a higher acknowledgement about the transcription factors, signalling transmembrane receptors and secreted proteins that are specifically and highly expressed by astrocytes (Cahoy et al. 2008). The astrocyte transcriptome also pointed to many hypotheses about astrocyte function. Many recent papers have revealed transcriptional and functional differences between astrocytes from different areas, or even between rodent and human astrocytes. From all the discoveries, it should be noted that different populations of astrocytes have differences in their expression of ion channels and coupling molecules (Regan et al., 2007; Chaboub, 2012). Astrocytes from different regions also demonstrate heterogeneity for the gene expression profile in some of their synaptogenic factors. For instance Glypicans, Hevin and SPARC have different expression in cortical or hippocampal areas (Buosi et al. 2017; Singh et al., 2016). In the human and mouse transcriptome, it has been found that some of the human astrocyte-enriched genes were not similarly enriched in mouse astrocytes (Zhang et al. 2016). All of these results show the molecular and functional heterogeneity of astrocytes in the nervous system. Furthermore, this data is demonstrating that astrocytes are able to exert particular synaptogenic effects in specific synapses and different brain areas. In parallel with our data, we could see that astrocytes in PFC are able to remodel excitatory synaptic densities after 48h ADs treatment but hippocampal astrocytes are not able to undergo any change at this time point. There are still open questions that need to be answered, about whether ADs target cells in the hippocampus after longer treatments or whether astrocytes from hippocampal areas may trigger the same effects or functions as cortical astrocytes.

Chronic stress –one of the risk factors to develop depression- and long-term glucocorticoid treatment leads to the loss of dendritic spines and synaptic contacts in the hippocampus and the PFC (Radley et al. 2005; Hajszan et al. 2010). Chronic mild stress also increases the number of immature spines compared to mushroom-like mature spines in the apical dendrites of pyramidal neurons in the hippocampus and PFC, and these changes are largely reversible by AD drug treatment that increases spine number back to the baseline level (Bessa et al. 2009; Castrén and Hen, 2013). However, it is important to notice that those effects of ADs in animal models of stress are only seen

after long-term treatments. On the contrary, the reduction in the number of synapses I observed in early-term treatments may be interpreted as a remodelling effect, so that unwanted synapses are eliminated triggering neuronal circuit refinement. In other words, the elimination of weakly synapses may be critical for optimizing the signal-to-noise ratio in neuronal networks. As other groups have pointed out, the re-establishment of neuronal plasticity (dendritic and synaptic contacts remodelling) in the hippocampus and PFC may be the basis for the restoration of behavioral homeostasis by ADs (Bessa et al. 2009). We observed ADs target astrocytes and enhance synaptic remodelling. The modulation of signalling pathways that involve the presence of 'eat me signals' in certain spines may be a putative mechanism underlying the remodelling effect. Some of the 'eat me signals' which can participate in this process, such as phosphatidylserine, are externalized and they may be recognized by the astrocytes (Chung et al. 2013). This suggests that contact-mediated mechanisms might underlie the synaptic pruning to favour a subsequent remodelling. An important question is whether the weak synapses that need to be eliminated present 'eat me signals' locally and if so, what their identities are.

Another of my goals was also to understand whether ADs target a particular type of synapses. Our data indicated that inhibitory synaptic densities are not affected after acute ADs treatments. It is important to notice that an imbalance between excitation/inhibition (E/I) has been described in the context of psychiatric disorders (Rubenstein and Merzenich, 2003). Excitatory and inhibitory activity can be affected by glia-mediated synapse engulfment. The proximity of astrocytes to the synapse renders them ideal candidates for controlling and eventually restoring E/I balance in the brain. Altered excitatory and inhibitory activity occurring already since development may lead to subsequent synaptic dysfunction in specific networks. This in turn could affect signal processing, which could be the cause for phenotypic changes observed in various psychiatric disorders. Therefore, the understanding of which synapses are target of certain drugs in healthy conditions may help to understand how they are working under disease conditions and if they can be a possible target for the improvement of symptoms.

4.2 MEGF10 and its role in the remodelling of synapses

Among the candidate molecules in astrocytes, I investigated which receptor or membrane bound protein could be able to mediate such remodelling effect in synapses. The candidate that was studied was MEGF10. Cahoy and colleagues published a transcriptome database for astrocytes in 2008. In this study, a complete astrocytic molecular pathway for engulfment and phagocytosis was discovered in those cells. Interestingly, this pathway and functions are highly conserved between species. MEGF10 was seen to participate in this phagocytic pathway and was enriched in astrocytes (Cahoy et al. 2008). Some years later, Chung and colleagues reported a new role for astrocytes in actively engulfing central nervous system synapses in the mammalian brain. This process helped to mediate synapse elimination and required the MEGF10 phagocytic pathway. Together with MERTK phagocytic pathway, MEGF10 participated in synapse remodelling underlying neural circuit refinement (Chung et al. 2013). On the other hand, MEGF10 mRNA has been seen to be upregulated after the ERK-signalling pathway was activated triggering cell plasticity (Napoli et al. 2012). Our data showed a simultaneous ERK1/2 activation, with increased in pERK1/2 molecules after astrocytes were treated with ADs. MEGF10 is induced by ERK1/2 activation in glia cells and inhibition of ERK1/2 activation hinders ADs efficacy (Duman et al. 2007; Napoli et al. 2012). By studying MEGF10 in this context, I could provide a higher knowledge about its possible implication in the remodelling of synapses and its role as a pharmacological target of ADs.

As a decrease synaptic protein expression was found in the rat PFC after short AD treatment, we looked at the effects of ADs on astrocytes. FLX also increased MEGF10 expression in astrocytes of the PFC, thereby confirming the specificity of the drug effect in this cell type. Further studies confirmed that the relative amount of MEGF10 protein was increased in the PFC after AD treatment. Immunocytochemical staining also revealed increased MEGF10 expression a primary culture of cortical astrocytes after FLX treatment was given for 48h. This data may suggest that a higher expression of MEGF10 could be correlated with the decrease number of synaptic densities found *in vitro* and the decrease synaptic protein expression found *ex vivo*. Moreover, it was analysed whether an increase of MEGF10 was found in a primary culture of astrocytes after 10 μ M ADs treatment. In

this study, I got variable results with regard to the relative MEGF10 expression. The ADs DMI and FLX were used in the study; some treatments triggered an increased in the total amount of MEGF10 after 48h but others maintained the relative amount of protein at the same level as controls; none of the treatments changed the expression of this protein significantly. This may be explained due to technical reasons, as some of the astrocytes growing in culture may have an increase in the amount of MEGF10 but not others, and the confluency of the astrocytes may play an important role for this experiment. Another reason could be the lack of cell-region specificity as the primary astrocytes come from a pool of cells from the entire cortex, showing once more the presence of heterogeneous astrocytes. These results may be also explained by a more complex mechanism, ADs may target MEGF10 and this molecule can be more available and present in the fine processes of the astrocytes ready to participate in the pruning activity as the processes of astrocytes are closer and highly interacting with synapses. To study this approach, a more complex technique is required rather than the use of normal immunohistochemistry or immunocytochemistry. On the other hand, the low availability of astrocytic markers that stain the whole cell body plus the fine processes is a limitation for this technique. Future approach is the study of the specimen and the distribution of MEGF10, following the principle of expansion microscopy in transgenic mice.

Thereafter, I was able to ascertain the pharmacological and genetic manipulation of the MEGF10 pathway. Given that MEGF10 is induced by ERK1/2 activation in glia cells, I first examined the significance of astrocytic ERK1/2 inhibition and therefore MEGF10 inhibition for synaptic reduction (Napoli et al., 2012). In order to see if the remodelling effect on synapses depends on AD-dependent ERK1/2 activation in astrocytes, the U0126 inhibitor was administered. This particular inhibitor is a synthesized organic compound that inhibit the kinase activity of MAPKK or MEK. It was observed that the effects of ADs are gone in the presence of the inhibitor. This means there is not reduction in the number of synapses in the presence of astrocytes and the blockade of ERK1/2 activation was sufficient to inhibit the remodelling effect. Secondly, the genetic manipulation of MEGF10 allowed to obtain a reduction in the protein expression by 40 to 60%. This was sufficient to see that, by knocking-down MEGF10 in astrocytes, no reduction in synphys⁺/PSD95⁺ colocalization after 48h FLX treatment was seen. Contrarily to the effects I observed in

control astrocytes treated with FLX, the reduction in MEGF10 protein in the knockdown astrocytes was sufficient to eliminate the pharmacological effect of FLX.

Finally, the phagocytic properties of astrocytes were analysed *in vitro*. LAMP1, lysosomal marker, was quantified in the juxtannuclear area of astrocytes. I observed a higher amount of LAMP vesicles in the astrocytes treated with FLX for 48h, indicating that a higher digestion may be occurring; although the amount of synphys⁺ to be colocalizing with LAMP1⁺ vesicles, indicating a possible internalization did not reach significant differences. In parallel with those results, a recent publication has shown that FLX increased phagosome formation and enhanced the fusion of phagosomes with lysosomes in a chronic mild stress mouse model of depression (Shu et al. 2019). Further studies on this point need to probe the putative phagocytic activity mediated by MEGF10 in the astrocytes when FLX treatment is given. A good approach will be to perform a phagocytic assay in MEGF10^{-/-} mice treated with FLX. This experiment will be done in collaboration with Chung's research group.

Concerning synapse elimination by astrocytes in adult brains, similar results have been obtained by Chung and colleagues. They observed synapse elimination in adult brains mediated by MEGF10. Interestingly, they found that more excitatory synapses were engulfed by 1-month-old than 4-month-old cortical astrocytes, probably due to a higher synapse pruning during development. In contrast, engulfed inhibitory synapses showed the same density within 1- and 4-month-old cortical astrocytes (Chung et al. 2013).

4.3 Animal models of depression and targeting astrocytes as therapeutic value

The decreased ERK1/2 activity found in depressed patients (Dwivedi et al. 2001) might indeed negatively affect MEGF10 and reduce its potential to refine neuronal circuits during development, leading to the formation of unwired adult neuronal networks and predisposing to the onset of neuropsychiatric disorders.

MEGF10 receptor plays a role in an evolutionarily conserved phagocytic pathway. From *Drosophila* to worms, receptors help to mediate axon pruning by glia cells and phagocytosis of apoptotic cells (Zhou et al. 2001; MacDonald et al. 2006; Ziegenfuss et al.

2008). The importance of this pathway in maintaining homeostasis and remodelling the synaptic architecture seems crucial. For this reason, it is important to see how this pathway works in the context of disease. Dysregulation of MEGF10 is suggested as a possible cause for depressive-like phenotypes and could represent a suitable target for novel ADs. To lay the foundation for testing this hypothesis in the context of the heterogeneity of depression, WKY rat as additional animal model to HAB rat was validated. A crucial method to gain a deeper understanding of the neurobiological background of brain pathologies is the use of animal models that reproduce main features of the respective diseases in human. Both animal models are well validated models for depressive behaviour with regards to responses in behavioural tests, neuroendocrine system, gene expression and cellular level (Neumann et al., 2011; Nam et al., 2014). In previous experiments, our group found a significant decrease in astrocyte density of HAB rats in comparison to normal anxiety-related behaviour (NAB) rats. In the case of WKY astrocytes, deficits in GFAP expression have been found in cortico-limbic areas (Gosselin et al., 2009). Moreover, we have found reductions in astrocyte density in WKY rat consistent with the observed reduction of glia cells, especially astrocytes, in *post-mortem* fronto-limbic brain regions of MDD patients (Rajkowska et al., 1999; Rajkowska and Miguel-Hidalgo, 2007). We also found changes in the abundance of trimethylation on 4th lysine residue of histone H3 protein (H3K4me3). H3K4me3 is necessary for packaging DNA in eukaryotic cells by increasing the accessibility of DNA. Thus, changes in abundance of these methylation markers strongly affect the accessibility of genomic regions for the initiation of transcription (Santos-Rosa et al. 2002). A similar alteration of H3K4me3, as the one seen in HAB and WKY rat, has been described in depressive patients (Cruceanu et al., 2013; Bagot et al., 2014).

Next, it was determined whether diseased astrocytes could influence neuronal properties as their morphology. Sholl analysis revealed a decreased in neuronal branches at a certain distance from the soma when normal neurons were growing with HAB or WKY astrocytes. These altered morphological properties related to the neuronal arborisation may have an influence in neuron to neuron connectivity and may affect the electrophysiological properties on the neurons. Astrocytes are known to influence synaptogenesis, for instance synapse number and maturation (Ullian et al. 2001). Hence, I was interested in

the effects of astrocytes exhibiting a depressive-like phenotype on synapse homeostasis. Therefore, synapse density was quantified in neurons growing with diseased astrocytes. Reduced number of excitatory synaptic densities was found on neuron growing with WKY astrocytes, while no differences were found when HAB astrocytes were interacting. These alterations in synaptic structures may be the consequences of improper neuronal refinement and could be consistent with the observed reduction of astrocytes in WKY rats. The differences between animal models may be sustained by heterogeneity found in depression, including all the identified subtypes of affective disorders and their symptoms. Next approach was focused on the understanding of whether ADs could rescue these structural changes. Sholl analysis revealed a partial rescued in the arborisation of neurons when the cells were treated with ADs. This data suggest an improvement in neuronal morphology which may be also relevant for the circuit connectivity.

Prior to this thesis, our group performed native chromatin-Immunoprecipitation (ChIP) on astrocytes derived from HAB and NAB rat under baseline conditions to analyse H3K4me3 histone modification on a genome-wide scale. The results showed a global increase of H3K4me3 in astrocytes from in HAB rats, when compared to NAB rats. However, individual genomic loci displayed a significant decrease in H3K4me3, for example the *megf10* gene. This data led us to the hypothesis that dysregulation of MEGF10 could be one of the causes of a default neuronal communication and the underlying mechanism of depressive-like phenotypes. To broaden our understanding, we aimed to describe changes of MEGF10 on a translational and transcriptional level. No differences could be detected when analysing MEGF10 protein levels in primary cortical astrocytes from the different animal models. Although preliminary data suggested a decrease in MEGF10 mRNA levels in HAB astrocytes (**supplementary figure 1**) which may go in parallel with the previous data. A possible explanation for the decrease in mRNA transcripts in HAB astrocytes could be dysregulation of posttranscriptional processes, for example, mRNA could be more preferentially translated under certain conditions (Pereira et al., 2005). Additionally, MEGF10 could be enriched in HAB astrocytes due to a higher protein's half live and an extreme low protein turnover *in vivo*. Furthermore, multiple

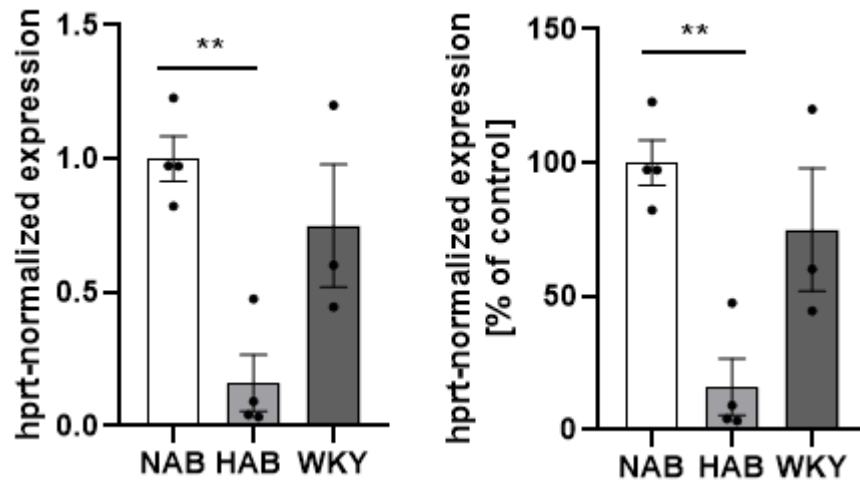
post-transcriptional processes, e.g. splicing or addition of a poly-A-tail, could be altered in disease (Greenbaum et al., 2003).

In order to see alterations in MEGF10 abundance during development I will perform experiments analysing the relative amount of MEGF10 during the critical period when most of the plastic changes and remodelling of neuronal circuits take place. Our preliminary data from the two first postnatal weeks revealed no differences between the MEGF10 relative protein expression in the brains of the animal models versus control **(supplementary figure 2)**. A drawback of this method is the protein isolation step, since not only astrocytes but all cells present in the PFC were lysed. Even though mainly astrocytes express MEGF10 in the CNS, the possibility of other cells expressing it cannot be excluded.

On the other hand, the distribution and availability of MEGF10 need to be studied. Those results could also indicate that MEGF10 maybe not in a fully functional state. There is a dependence of MEGF10 on ATP-binding cassette transporter ABCA1 (and PTB domain-containing engulfment adapter protein 1 (GULP1)) for their transport to the membrane into the phagocytic cup in HeLa cell line (Hamon et al. 2006). On this basis, it is plausible to consider alteration of interactions between ABCA1 and MEGF10 as a further cause of pathological dysfunction of the MEGF10 pathway.

Given the lack of success and delayed onset of action of current antidepressants, research turned towards other systems as potential treatment. The present thesis revealed a new target and potential candidate of AD drugs which revealed structural synaptic changes in an early time point. Future studies to unravel the mechanisms by which MEGF10 may be affected in disease will give some indication about potential mechanisms underlying the behavioural and physiological phenotype as well as the treatment response.

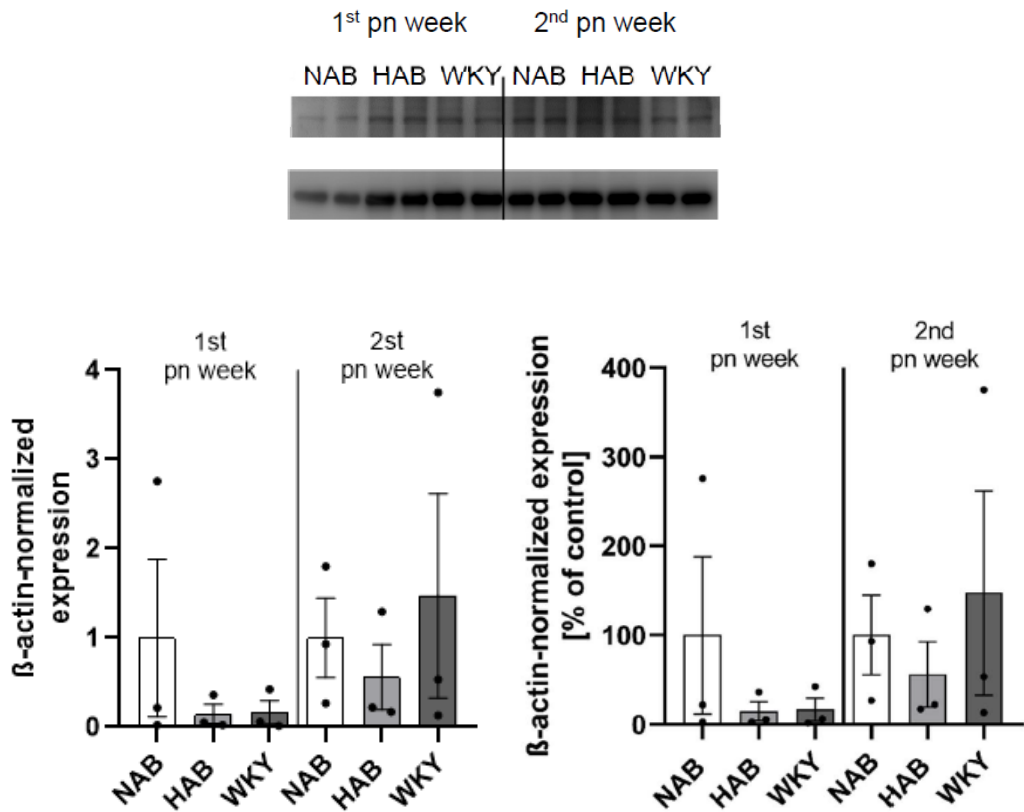
Supplementary



Supplementary figure 1. Analysis of MEGF10 of transcriptional level. a) qPCR analysis of mRNA levels of megf10 isolated from cortical NAB, HAB and WKY astrocytes. Hprt-normalized expression is illustrated as fold change compared to control. All data is depicted as mean (% of control) \pm SEM, ** $p \leq 0.01$ significant differences marked with asterisk were calculated by ordinary one-way ANOVA followed by Dunnett's multiple comparisons test. NAB: $n = 4$, 1 ± 0.083 ; HAB: $n = 4$, 0.161 ± 0.105 ; WKY: $n = 3$, 0.749 ± 0.230 . Ordinary one-way ANOVA. **b)** Graph indicating the percentage relative to control NAB.

Statistics:

Parameter	MEGF10 expression (mRNA level)
C vs HAB	F (2, 8) = 10,98 P=0,005
C vs WKY	NAB vs. HAB: $p = 0,003^{**}$ NAB vs. WKY: $p = 0,39$ n.s.



Supplementary figure 2. Expression MEGF10 in the cortex during the critical period. a) Western blot image of proteins extracted from PFA fixed PFC tissue isolated from NAB, HAB and WKY rat brains from first and second postnatal (pn) week. 2 replicates per condition. b) Relative data normalization to β -Actin; 1st week: NAB: n=3, 1 ± 0.88 ; HAB: n = 3, 0.148 ± 0.107 ; WKY: n = 3, 0.168 ± 0.129 ; 2st week: NAB: n = 3, 1 ± 0.443 ; HAB: n = 3, 0.56 ± 0.366 ; WKY: n = 3, 0.147 ± 0.145 ; Ordinary one-way ANOVA. c) Percentage relative to control NAB.

Statistics:

Parameter	MEGF10 expression (protein level)
1 st week	F (2, 6) = 0,8817 P=0,4616 NAB vs. HAB: p = 0.448, n.s; NAB vs. WKY: p = 0.463, n.s
2 nd week	F (2, 6) = 0,3787 P=0,7000 NAB vs. HAB: p = 0.883, n.s; NAB vs. WKY: p = 0.865, n.s

List of abbreviations

ACM	Astrocyte Condition Media
ACTH	Adrenocorticotropin hormone
ADs	Antidepressants
ALDH1L1	Aldehyde dehydrogenase 1 family member L1
AMPA	α -amino-3-hydroxy-5-methyl-4-isoxazolepropionic acid
AMY	Amygdala
ANCM	Astrocyte Neuron Condition Media
AQP4	Aquaporin 4
ATP	Adenosine triphosphate
AVP	Arginine vasopressin
BDNF	Brain-derived neurotrophic factor
BGs	Bergmann glial
C1q	Complement component 1
C3	Complement component 3
cDNA	Complementary DNA
CHR	Corticotropin-releasing hormone
CNS	Central nervous system
Ct	Cycle threshold
CUS	Chronic unpredictable stress
Cx	Connexins
DA	Dopamine
DMI	Desipramine
DIV	Days in vitro
E	Embryonic day
ECT	Electroconvulsive therapy
Erk	Extracellular signal-regulated-protein kinase
FACS	Fluorescence-activated cell sorting
FLX	Fluoxetine
FST	Forced swimming test

GABA	γ -aminobutyric acid
GluA1	Glutamate receptor 1
GFAP	Glial fibrillary acidic protein
GLT	Glutamate transporter
GS	Glutamine synthetase
Gpc4 - Gpc6	Glypicans 4 and 6
h or hr	Hours
HAB	High Anxiety-like Behaviour
HPA	Hypothalamic-pituitary-adrenal
H3K4me3	Tri-methylation at the 4th lysine residue of the histone H3
5-HT	5-hydroxytryptamine, serotonin
Iba-1	Ionized calcium-binding adapter molecule 1
IF-IHC	Immunofluorescence-immunohistochemistry
IF-ICC	Immunofluorescence-immunocytochemistry
i.p.	Intraperitoneally
IP3R	1,4,5-trisphosphate receptor
MAP	Mitogen-associated protein
MAP2	Microtubule-associated protein 2
MDD	Major depressive disorder
MEGF10	Multiple EGF-like-domains 10
MERTK	Proto-oncogene tyrosine-protein kinase MER
mGluRs	Metabotropic glutamate receptors
min	Minutes
mPFC	Medial prefrontal cortex
mRNA	Messenger RNA
MTZ	Mirtazapine
NAB	Rats non-selected for anxiety-like behaviour
NE	Norepinephrine
NGS	Normal goat serum
NMDA	N-methyl-D-aspartate
O/N	Overnight

List of abbreviations

P	Postnatal day
PBS	Phosphate buffered saline
PFA	Paraformaldehyde
p.n.	postnatal week
PSD95	Postsynaptic density protein 95
PVN	Paraventricular nuclei
RBX	Reboxetine
RG	Radial glia cells
RGCs	Retinal ganglion cells
RT	Room temperature
S100 β	S100 calcium-binding protein β
Scr	Scramble
SCAP	SREBP cleavage-activating protein
Sec	Seconds
SEM	Standard error of the mean
Shh	Sonic hedgehog signal
siRNAs	Short interfering RNAs
SNRIs	Serotonin (5-HT) and norepinephrine dual-reuptake inhibitors
SSRIs	Selective serotonin (5-HT) reuptake inhibitors
SPARC	Secreted protein acidic and rich in cysteine
SREBPs	Sterol regulatory element binding proteins
Synphys/ synphysin	Synaptophysin
TCAs	Tricyclic ADs
TGF- β	Transforming growth factor β
TNF- α	Tumor necrosis factor α
TSP	Thrombospondins
VA	Vellate astrocytes
VGAT	Vesicular GABAergic transporter
VLX	Venlafaxine
vs.	versus
WKY	Wistar–Kyoto

References

- Abbott, C. C., Jones, T., Lemke, N. T., Gallegos, P., McClintock, S. M., Mayer, A. R., Bustillo J., Calhoun, V. D. (2014). Hippocampal structural and functional changes associated with electroconvulsive therapy response. *Translational Psychiatry*, 4(11), e483-7.
- Allen, N. J., Bennett, M. L., Foo, L. C., Wang, G. X., Chakraborty, C., Smith, S. J., & Barres, B. A. (2012). Astrocyte glypicans 4 and 6 promote formation of excitatory synapses via GluA1 AMPA receptors. *Nature*, 486(7403), 410–414.
- Araque, A., Parpura, V., Sanzgiri, R. P., & Haydon, P. G. (1999). Tripartite synapses: Glia, the unacknowledged partner. *Trends in Neurosciences*, 22(5), 208–215.
- Bagot, R. C., Labonté, B., Peña, C. J., & Nestler, E. J. (2014). Epigenetic signaling in psychiatric disorders: Stress and depression. *Dialogues in Clinical Neuroscience*, 16(3), 281–295.
- Banasr, M., & Duman, R. S. (2008). Glial Loss in the Prefrontal Cortex Is Sufficient to Induce Depressive-like Behaviors. *Biol Psychiatry*. 10-863–870.
- Bayraktar, O. A., Fuentealba, L. C., Alvarez-buylla, A., & Rowitch, D. H. (2019). Astrocyte Development and Heterogeneity. *Cold Spring Harb Perspect Biol.*, 7(1)a020362
- Beattie, E. C., Stellwagen, D., Morishita, W., Bresnahan, J. C., Ha, B. K., Zastrow, M. Von, ... Malenka, Robert C. (2002). Control of Synaptic Strength by Glial TNF. *Science*. 295(5563):2282-5.
- Belzung, C., & Lemoine, M. (2011). Criteria of validity for animal models of psychiatric disorders: focus on anxiety disorders and depression. *Biol Mood Anxiety Disord.*, 1(1):9.
- Bernard, R., Kerman, I. A., Thompson, R. C., Jones, E. G., Bunney, W. E., Barchas, J. D., Schatzberg AF, Myers RM, Akil H & Watson, S. J. (2011). Altered expression of glutamate signaling, growth factor, and glia genes in the locus coeruleus of patients with major depression. *Molecular Psychiatry*, 16(6), 634–646.
- Bessa, J. M., Ferreira, D., Melo, I., Marques, F., Cerqueira, J. J., Palha, J. A., ... Sousa, N. (2009). The mood-improving actions of antidepressants do not depend on neurogenesis but are associated with neuronal remodeling. *Molecular Psychiatry*, 14(8), 764–773.
- Bosworth, A. P., & Allen, N. J. (2017). The diverse actions of astrocytes during synaptic development. *Current Opinion in Neurobiology*, 47, 38–43.
- Buosi, A. S., Matias, I., Araujo, A. P. B., Batista, C., & Gomes, F. C. A. (2017). Heterogeneity in Synaptogenic Profile of Astrocytes from Different Brain Regions. *Molecular Neurobiology*. 55(1):751-762
- Bushong, E. A., Martone, M. E., Jones, Y. Z., & Ellisman, M. H. (2002). Protoplasmic Astrocytes in CA1 Stratum Radiatum Occupy Separate Anatomical Domains. *The Journal of Neuroscience*, 22(1), 183–192.

References

- Cabras, S., Saba, F., Reali, C., Scorciapino, M. L., Sirigu, A., Talani, G., Biggio G. & Sogos, V. (2010). Antidepressant imipramine induces human astrocytes to differentiate into cells with neuronal phenotype. *International Journal of Neuropsychopharmacology*, 13(5), 603–615.
- Cahoy, J. D., Emery, B., Kaushal, A., Foo, L. C., Zamanian, J. L., Christopherson, K. S., Yi Xing, & Barres, B. A. (2008). A transcriptome database for astrocytes, neurons, and oligodendrocytes: a new resource for understanding brain development and function. *The Journal of Neuroscience*. 28(1), 264–278.
- Cao, X., Li, L. P., Wang, Q., Wu, Q., Hu, H. H., Zhang, M., Fang YY. & Gao, T. M. (2013). Astrocyte-derived ATP modulates depressive-like behaviors. *Nature Medicine*, 19(6), 773–777.
- Castrén, E., & Rantamäki, T. (2009). The role of BDNF and its receptors in depression and antidepressant drug action: Reactivation of developmental plasticity. *Developmental Neurobiology*, 70(5), 289–297.
- Castrén E. and Hen R. (2013). Neuronal plasticity and antidepressant actions. *Trends Neurosci*. 36(5): 259–267.
- Chaboub, L. S. (2012). Developmental Origins of Astrocyte Heterogeneity: The Final Frontier of CNS. *Dev Neurosci*. 34(5):379-88
- Chen, X., Sun, C., Chen, Q., O'Neill, F. A., Walsh, D., Fanous, A. H., ... Kendler, K. S. (2009). Apoptotic engulfment pathway and schizophrenia. *PLoS ONE*, 4(9).
- Christian, K. M., Miracle, A. D., Wellman, C. L., & Nakazawa, K. (2011). Chronic stress-induced hippocampal dendritic retraction requires CA3 NMDA receptors. *Neuroscience*, 174, 26–36.
- Christopherson, K. S., Ullian, E. M., Stokes, C. C. A., Mallowney, C. E., Hell, J. W., Agah, A., ... Barres, B. A. (2005). Thrombospondins are astrocyte-secreted proteins that promote CNS synaptogenesis. *Cell*, 120(3), 421–433.
- Chung, W., Clarke, L. E., Wang, G. X., Stafford, B. K., Sher, A., Chakraborty, C., ... Barres, B. A. (2013). Astrocytes mediate synapse elimination through MEGF10 and MERTK pathways. *Nature*. 504, 394–400
- Cruceanu, C., Alda, M., Nagy, C., Freemantle, E., Rouleau, G. A., & Turecki, G. (2013). H3K4 tri-methylation in synapsin genes leads to different expression patterns in bipolar disorder and major depression. *International Journal of Neuropsychopharmacology*, 16(2), 289–299. 363
- Czéh, B., & Di Benedetto, B. (2013). Antidepressants act directly on astrocytes: Evidences and functional consequences. *European Neuropsychopharmacology*, 23(3), 171–185.
- Czeh, B., Michaelis, T., Watanabe, T., Frahm, J., de Biurrun, G., van Kampen, M., ... Fuchs, E. (2001). Stress-induced changes in cerebral metabolites, hippocampal volume, and cell

proliferation are prevented by antidepressant treatment with tianeptine. *Proceedings of the National Academy of Sciences*, 98(22), 12796–12801.

Czéh, B., Müller-Keuker, J. I. H., Rygula, R., Abumaria, N., Hiemke, C., Domenici, E., & Fuchs, E. (2007). Chronic social stress inhibits cell proliferation in the adult medial prefrontal cortex: Hemispheric asymmetry and reversal by fluoxetine treatment. *Neuropsychopharmacology*, 32(7), 1490–1503.

Czéh, B., Simon, M., Schmelting, B., Hiemke, C., & Fuchs, E. (2006). Astroglial plasticity in the hippocampus is affected by chronic psychosocial stress and concomitant fluoxetine treatment. *Neuropsychopharmacology*, 31(8), 1616–1626.

Dave, V., & Kimelberg, K. (1994). Na⁺-Dependent, Fluoxetine-Sensitive Serotonin Uptake by Astrocytes Tissue-printed from Rat Cerebral Cortex. *The Journal of Neuroscience*, 14(8): 4972-4986

Di Benedetto, B., Radecke, J., Schmidt, M. V., & Rupprecht, R. (2013). Acute antidepressant treatment differently modulates ERK/MAPK activation in neurons and astrocytes of the adult mouse prefrontal cortex. *Neuroscience*, 232, 161–168.

Di Benedetto, B., Kühn, R., Nothdurfter, C., Rein, T., Wurst, W., & Rupprecht, R. (2012). N-desalkylquetiapine activates ERK1/2 to induce GDNF release in C6 glioma cells: A putative cellular mechanism for quetiapine as antidepressant. *Neuropharmacology*, 62(1), 209–216.

Di Benedetto, B., Malik, V. A., Begum, S., Jablonowski, L., Gómez-González, G. B., Neumann, I. D., & Rupprecht, R. (2016). Fluoxetine requires the endfeet protein aquaporin-4 to enhance plasticity of astrocyte processes. *Frontiers in Cellular Neuroscience*, 2;(10):8.

Diniz, L. P., Almeida, J. C., Tortelli, V., Lopes, C. V., Setti-Perdigão, P., Stipursky, J., ... Gomes, F. C. A. (2012). Astrocyte-induced synaptogenesis is mediated by transforming growth factor β signaling through modulation of d-serine levels in cerebral cortex neurons. *Journal of Biological Chemistry*, 287(49), 41432–41445.

Dossi, E., Vasile, F., & Rouach, N. (2018). Human astrocytes in the diseased brain. *Brain Research Bulletin*, 136, 139–156.

Dowlati, Y., Herrmann, N., Swardfager, W., Liu, H., Sham, L., Reim, E. K., & Lanctôt, K. L. (2010). A Meta-Analysis of Cytokines in Major Depression. *Biological Psychiatry*, 67(5), 446–457.

Duman, C. H., Schlesinger, L., Kodama, M., Russell, D. S., & Duman, R. S. (2007). A Role for MAP Kinase Signaling in Behavioral Models of Depression and Antidepressant Treatment. *Biological Psychiatry*, 61(5), 661–670.

Duman, R. S., Aghajanian, G. K., Sanacora, G., & Krystal, J. H. (2016). Synaptic plasticity and depression: New insights from stress and rapid-acting antidepressants. *Nature Medicine*, 22(3), 238–249. 0

References

- Duman, R. S., & Li, N. (2012). A neurotrophic hypothesis of depression: Role of synaptogenesis in the actions of NMDA receptor antagonists. *Philosophical Transactions of the Royal Society B: Biological Sciences*, 367(1601), 2475–2484.
- Duric, V., Banasr, M., Licznarski, P., Schmidt, H. D., Stockmeier, C. A., Simen, A. A., ... Duman, R. S. (2010). A negative regulator of MAP kinase causes depressive behavior. *Nature Medicine*, 16(11), 1328–1332.
- Dwivedi, Y., Rizavi, H. S., Roberts, R. C., Conley, R. C., Tamminga, C. A., & Pandey, G. N. (2001). Reduced activation and expression of ERK1/2 MAP kinase in the post-mortem brain of depressed suicide subjects. *Journal of Neurochemistry*, 77(3), 916–928.
- Dzyubenko, E., Rozenberg, A., Hermann, D. M., & Faissner, A. (2016). Colocalization of synapse marker proteins evaluated by STED-microscopy reveals patterns of neuronal synapse distribution in vitro. *Journal of Neuroscience Methods*, 273, 149–159. 1
- El-Husseini, A. E., Schnell, E., Chetkovich, D. M., Nicoll, R. A., & Bredt, D. S. (2000). PSD-95 involvement in maturation of excitatory synapses. *Science*, 290(5495), 1364–1368.
- Elhwuegi, A. S. (2004). Central monoamines and their role in major depression. *Progress in Neuro-Psychopharmacology and Biological Psychiatry*, 28(3), 435–451.
- Farhy-Tselnicker, I., & Allen, N. J. (2018). Astrocytes, neurons, synapses: A tripartite view on cortical circuit development. *Neural Development*, 13(1), 1–12.
- Farmer, W. T., Abrahamsson, T., Chierzi, S., Lui, C., Zaelzer, C., Jones, E. V., ... Murai, K. K. (2016). Neurons diversify astrocytes in the adult brain through sonic hedgehog signaling. *Science*, 351(6275).
- Fatemi, S. H., Folsom, T. D., Reutiman, T. J., Pandian, T., Braun, N. N., & Haug, K. (2008). Chronic psychotropic drug treatment causes differential expression of connexin 43 and GFAP in frontal cortex of rats. *Schizophrenia Research*, 104(1–3), 127–134.
- Ferreira, T.A., Blackman, A.V., Oyrer, J., Jayabal, S., Chung, A.J., Watt, A.J., Sjöström, P.J., and van Meyel, D.J. (2014). Neuronal morphometry directly from bitmap images. *Nat Methods* 11, 982-984.
- Fields, J., Cisneros, I. E., Borgmann, K., & Ghorpade, A. (2013). Extracellular Regulated Kinase 1/2 Signaling Is a Critical Regulator of Interleukin-1 β -Mediated Astrocyte Tissue Inhibitor of Metalloproteinase-1 Expression. *PLoS ONE*, 8(2).
- Glantz, L. A., Gilmore, J. H., Hamer, R. M., Lieberman, J. A., & Jarskog, L. F. (2007). Synaptophysin and postsynaptic density protein 95 in the human prefrontal cortex from mid-gestation into early adulthood. *Neuroscience*, 149(3), 582–591.
- Goers, L., Freemont, P., & Polizzi, K. M. (2014). Co-culture systems and technologies: taking synthetic biology to the next level. *J. R. Soc. Interface*, 11: 201400.
- Gosselin, R. D., Gibney, S., O'Malley, D., Dinan, T. G., & Cryan, J. F. (2009). Region specific decrease in glial fibrillary acidic protein immunoreactivity in the brain of a rat model of depression. *Neuroscience*, 159(2), 915–925.

Greenbaum, D., Colangelo, C., Williams, K and Gerstein M. (2003). Comparing protein abundance and mRNA expression levels on a genomic scale. *Genome Biol* 4, 117.

Hajszan, T., MacLusky, N. J., & Leranth, C. (2005). Short-term treatment with the antidepressant fluoxetine triggers pyramidal dendritic spine synapse formation in rat hippocampus. *European Journal of Neuroscience*, 21(5), 1299–1303.

Hajszan, T., Szigeti-Buck, K., Sallam, N. L., Bober, J., Parducz, A., MacLusky, N. J., ... Duman, R. S. (2010). Effects of Estradiol on Learned Helplessness and Associated Remodeling of Hippocampal Spine Synapses in Female Rats. *Biological Psychiatry*, 67(2), 168–174.

Hamon, Y., Trompier, D., Ma, Z., Venegas, V., Pophillat, M., Mignotte, V., ... Chimini, G. (2006). Cooperation between engulfment receptors: The case of ABCA1 and MEGF10. *PLoS ONE*, 1(1).

Harmer C.J., Duman R.S., and Cowen P.J. (2017). How do antidepressants work? New perspectives for refining future treatment approaches. *Lancet Psychiatry*. 4(5): 409–418.

Heshmati, M., & Russo, S. J. (2015). Anhedonia and the Brain Reward Circuitry in Depression. *Current Behavioral Neuroscience Reports*, 2(3), 146–153.

Hisaoka, K., Takebayashi, M., Tsuchioka, M., Maeda, N., Nakata, Y., & Yamawaki, S. (2007). Antidepressants increase glial cell line-derived neurotrophic factor production through monoamine-independent activation of protein tyrosine kinase and extracellular signal-regulated kinase in glial cells. *Journal of Pharmacology and Experimental Therapeutics*, 321(1), 148–157.

Hol, E. M., & Pekny, M. (2015). ScienceDirect Glial fibrillary acidic protein (GFAP) and the astrocyte intermediate filament system in diseases of the central nervous system. *Current Opinion in Cell Biology*, 32, 121–130.

Holtzheimer, P., & Nemeroff, C. (2008). Novel targets for antidepressant therapies. *Current Psychiatry Reports*, 10(6), 465–473.

Ippolito, D. M., & Eroglu, C. (2010). Quantifying synapses: An immunocytochemistry-based assay to quantify synapse number. *Journal of Visualized Experiments*, (45), 2–9.

John, C. S., Smith, K. L., Van'T Veer, A., Gompf, H. S., Carlezon, W. A., Cohen, B. M., ... Bechtholt-Gompf, A. J. (2012). Blockade of astrocytic glutamate uptake in the prefrontal cortex induces anhedonia. *Neuropsychopharmacology*, 37(11), 2467–2475.

John Lin, C. C., Yu, K., Hatcher, A., Huang, T. W., Lee, H. K., Carlson, J., ... Deneen, B. (2017). Identification of diverse astrocyte populations and their malignant analogs. *Nature Neuroscience*, 20(3), 396–405.

Kang, H. J., Voleti, B., Hajszan, T., Rajkowska, G., Stockmeier, C. A., Licznarski, P., ... Duman, R. S. (2012). Decreased expression of synapse-related genes and loss of synapses in major depressive disorder. *Nature Medicine*, 18(9), 1413–1417.

Kanter, J. W., Busch, A. M., Weeks, C. E., & Landes, S. J. (2008). The nature of clinical depression: Symptoms, syndromes, and behavior analysis. *Behavior Analyst*, 31(1), 1–21.

References

- Katarzyna, M. (2015). Zinc in the Glutamatergic Theory of Depression. *Curr Neuropharmacol.* 505–513.
- Kim, H. J., & Bar-Sagi, D. (2004). Modulation of signalling by sprouty: A developing story. *Nature Reviews Molecular Cell Biology*, 5(6), 441–450.
- King, P. D., Zylberberg, J., & Dewese, M. R. (2013). Inhibitory interneurons decorrelate excitatory cells to drive sparse code formation in a spiking model of V1. *Journal of Neuroscience*, 33(13), 5475–5485.
- Kong, H., Sha, L. L., Fan, Y., Xiao, M., Ding, J. H., Wu, J., & Hu, G. (2009). Requirement of AQP4 for antidepressive efficiency of fluoxetine: Implication in adult hippocampal neurogenesis. *Neuropsychopharmacology*, 34(5), 1263–1276.
- Kong, H., Zeng, X. N., Fan, Y., Yuan, S. T., Ge, S., Xie, W. P., ... Hu, G. (2014). Aquaporin-4 Knockout Exacerbates Corticosterone-Induced Depression by Inhibiting Astrocyte Function and Hippocampal Neurogenesis. *CNS Neuroscience and Therapeutics*, 20(5), 391–402.
- Krishnan, V., & Nestler, E. J. (2011). Animal Models of Depression: Molecular Perspectives Vaishnav. *Curr Top Behav Neurosci.*, 121–147.
- Kucukdereli, H., Allen, N. J., Lee, A. T., Feng, A., Ozlu, M. I., Conatser, L. M., ... Eroglu, C. (2011). Control of excitatory CNS synaptogenesis by astrocyte-secreted proteins Hevin and SPARC. *Proceedings of the National Academy of Sciences*, 108(32), E440–E449.
- Kumar, V., Zhang, M. X., Swank, M. W., Kunz, J., & Wu, G. Y. (2005). Regulation of dendritic morphogenesis by Ras-PI3K-Akt-mTOR and Ras-MAPK signaling pathways. *Journal of Neuroscience*, 25(49), 11288–11299.
- Lawson, L. J., Perry, V. H., Dri, P., & Gordon, S. (1990). Heterogeneity in the distribution and morphology of microglia in the normal adult mouse brain. *Neuroscience*, 39(1), 151–170.
- Li, B., Zhang, S., Zhang, H., Nu, W., Cai, L., Hertz, L., & Peng, L. (2008). Fluoxetine-mediated 5-HT_{2B} receptor stimulation in astrocytes causes EGF receptor transactivation and ERK phosphorylation. *Psychopharmacology*, 201(3), 443–458.
- Li B, Zhang S, Li Min, Hertz L & Peng L. (2009) Chronic treatment of astrocytes with therapeutically relevant fluoxetine concentrations enhances cPLA2 expression secondary to 5-HT_{2B}-induced, transactivation-mediated ERK1/2 phosphorylation. *Psychopharmacology*. 207.
- Li N, Lee B, Liu RJ, Banasr M, Dwyer JM, Iwata M, Li XY, Aghajanian G, D. R. (2010). mTOR-Dependent Synapse Formation. *Science*, 329, 959–965.
- Lima, A., Sardinha, V. M., Oliveira, A. F., Reis, M., Mota, C., Silva, M. A., ... Oliveira, J. F. (2014). Astrocyte pathology in the prefrontal cortex impairs the cognitive function of rats. *Molecular Psychiatry*, 19(7), 834–841.

- Liu, R.-J., & Aghajanian, G. K. (2008). Stress blunts serotonin- and hypocretin-evoked EPSCs in prefrontal cortex: Role of corticosterone-mediated apical dendritic atrophy. *Proceedings of the National Academy of Sciences*, 105(1), 359–364.
- Longair, M.H., Baker, D.A., and Armstrong, J.D. (2011). Simple Neurite Tracer: open source software for reconstruction, visualization and analysis of neuronal processes. *Bioinformatics* 27, 2453-2454.
- MacDonald, J. M., Beach, M. G., Porpiglia, E., Sheehan, A. E., Watts, R. J., & Freeman, M. R. (2006). The Drosophila Cell Corpse Engulfment Receptor Draper Mediates Glial Clearance of Severed Axons. *Neuron*, 50(6), 869–881.
- Magariños, A. M., Deslandes, A., & McEwen, B. S. (1999). Effects of antidepressants and benzodiazepine treatments on the dendritic structure of CA3 pyramidal neurons after chronic stress. *European Journal of Pharmacology*, 371(2–3), 113–122.
- Medina, A., Watson, S. J., Bunney, W., Myers, R. M., Schatzberg, A., Barchas, J., ... Thompson, R. C. (2016). Evidence for alterations of the glial syncytial function in major depressive disorder. *Journal of Psychiatric Research*, 72, 15–21.
- Mercier, G., Lennon, A. M., Renouf, B., Dessouroux, A., Ramaugé, M., Courtin, F., & Pierre, M. (2004). MAP kinase activation by fluoxetine and its relation to gene expression in cultured rat astrocytes. *Journal of Molecular Neuroscience*, 24(2), 207–216.
- Miller F.D. & Gauthier A.S. (2007). Timing is everything: making neurons versus glia in the developing cortex. *Neuron*, 54(3):357-69.
- Miller, A. H., & Raison, C. L. (2016). The role of inflammation in depression: From evolutionary imperative to modern treatment target. *Nature Reviews Immunology*, 16(1), 22–34.
- Mitra Heshmati and Scott J. Russo. (1993). Anhedonia and the brain reward circuitry in depression. *The American Journal of Physiology*, 264, F61-5.
- Nam, H., Clinton, S. M., Jackson, N. L., & Kerman, I. A. (2014). Learned helplessness and social avoidance in the Wistar-Kyoto rat. *Frontiers in Behavioral Neuroscience*, 1–18.
- Napoli, I., Noon, L. A., Ribeiro, S., Kerai, A. P., Parrinello, S., Rosenberg, L. H., ... Lloyd, A. C. (2012). A Central Role for the ERK-Signaling Pathway in Controlling Schwann Cell Plasticity and Peripheral Nerve Regeneration In Vivo. *Neuron*, 73(4), 729–742.
- Neumann, I. D., Wegener, G., Homberg, J. R., Cohen, H., Slattery, D. A., Zohar, J., ... Mathé, A. (2011). Animal models of depression and anxiety: What do they tell us about human condition? *Progress in Neuro-Psychopharmacology and Biological Psychiatry*, 35(6), 1357–1375.
- Neumann, Inga D., Veenema, A. H., & Beiderbeck, D. I. (2010). Aggression and anxiety: Social context and neurobiological links. *Frontiers in Behavioral Neuroscience*, 4(MAR), 1–16.

References

- Nibuya, M., Morinobu, S., & Duman, R. S. (1995). Regulation of BDNF and trkB mRNA in rat brain by chronic electroconvulsive seizure and antidepressant drug treatments. *Journal of Neuroscience*, 15(11), 7539–7547.
- Ohno, Y., Hibino, H., Lossin, C., Inanobe, A., & Kurachi, Y. (2007). Inhibition of astroglial Kir4.1 channels by selective serotonin reuptake inhibitors. *Brain Research*, 1178(1), 44–51.
- Perego, C., Vanoni, C., Bossi, M., Massari, S., Basudev, H., Longhi, R., & Pietrini, G. (2000). The GLT-1 and GLAST Glutamate Transporters Are Expressed on Morphologically Distinct Astrocytes and Regulated by Neuronal Activity in Primary Hippocampal Cocultures. *J Neurochem*. 75(3):1076-84.
- Pereira, C.M., Sattlegger, E., Jiang, H.Y., Longo, B.M., Jaqueta, C.B., Hinnebusch, A.G., Wek, R.C., Mello, L.E., and Castilho, B.A. (2005). IMPACT, a protein preferentially expressed in the mouse brain, binds GCN1 and inhibits GCN2 activation. *J Biol Chem* 280, 28316-28323.
- Pittenger, C., & Duman, R. S. (2008). Stress, depression, and neuroplasticity: A convergence of mechanisms. *Neuropsychopharmacology*, 33(1), 88–109.
- Popoli, M., Yan, Z., McEwen, B. S., & Sanacora, G. (2012). The stressed synapse: The impact of stress and glucocorticoids on glutamate transmission. *Nature Reviews Neuroscience*, 13(1), 22–37.
- Porter, J. T., & Arthy, K. E. N. D. M. C. C. (1997). Astrocytic neurotransmitter receptors in situ and in vivo. *Prog Neurobiol*. 51(4):439-55.
- Price, J. L., & Drevets, W. C. (2010). Neurocircuitry of mood disorders. *Neuropsychopharmacology*, 35(1), 192–216.
- Rajkowska, G., & Miguel-Hidalgo, J. (2007). Gliogenesis and Glial Pathology in Depression. *CNS & Neurological Disorders - Drug Targets*, 6(3), 219–233.
- Rajkowska, Grazyna, Hughes, J., Stockmeier, C. A., Javier Miguel-Hidalgo, J., & Maciag, D. (2013). Coverage of blood vessels by astrocytic endfeet is reduced in major depressive disorder. *Biological Psychiatry*, 73(7), 613–621.
- Rajkowska, Grazyna, Wei, J., Dilley, G., Pittman, S. D., Meltzer, H. Y., Overholser, J. C., ... Stockmeier, C. A. (1999). Morphometric Evidence for Neuronal and Glial Prefrontal Cell Pathology in Major Depression. *Biological Psychiatry*, 3223(99).
- Regan, M. R., Huang, Y. H., Kim, Y. S., Dykes-hoberg, M. I., Jin, L., Watkins, A. M., ... Rothstein, J. D. (2007). Variations in Promoter Activity Reveal a Differential Expression and Physiology of Glutamate Transporters by Glia in the Developing and Mature CNS. *J Neurosci*. 27(25), 6607–6619.
- Rial, D., Gonçalves, F. Q., Lemos, C., Prediger, R. D., Gonçalves, N., Duarte, J. M., ... Canas, P. M. (2016). Depression as a Glial-Based Synaptic Dysfunction. *Frontiers in Cellular Neuroscience*, 1–11.

- Rittenhouse, P. A., López-Rubalcava, C., Stanwood, G. D., & Lucki, I. (2002). Amplified behavioral and endocrine responses to forced swim stress in the Wistar-Kyoto rat. *Psychoneuroendocrinology*, 27(3), 303–318.
- Rossi, J. L., Ralay Ranaivo, H., Patel, F., Chrzaszcz, M., Venkatesan, C., & Wainwright, M. S. (2011). Albumin causes increased myosin light chain kinase expression in astrocytes via p38 mitogen-activated protein kinase. *Journal of Neuroscience Research*, 89(6), 852–861.
- Rubenstein, J. L. R., & Merzenich, M. M. (2003). Model of autism: increased ratio of excitation/ inhibition in key neural systems. *Genes Brain Behav.* 255–267.
- Sanacora, G., Treccani, G., & Popoli, M. (2012). Towards a glutamate hypothesis of depression: An emerging frontier of neuropsychopharmacology for mood disorders. *Neuropharmacology*, 62(1), 63–77.
- Santos-Rosa, H., Schneider, R., Bannister, A. J., Sherriff, J., Bernstein, B. E., Emre, N. C. T., ... Kouzarides, T. (2002). Active genes are tri-methylated at K4 of histone H3. *Nature*, 419(6905), 407–411.
- Sapolsky, R. M. (2001). Depression, antidepressants, and the shrinking hippocampus. *Proceedings of the National Academy of Sciences*, 98(22), 12320–12322.
- Sapolsky, R. M. (2015). Patterns, trends and thinking “inside” the box in medical education. *Medical Education*, 49(12), 1176–1178.
- Schildkraut J.J. (1965). The catecholamine hypothesis of affective disorders: a review of supporting evidence. *American Journal of Psychiatry*, 122(5), 509–522.
- Schroeter, M. L., Abdul-Khaliq, H., Diefenbacher, A., & Blasig, I. E. (2002). S100B is increased in mood disorders and may be reduced by antidepressive treatment. *NeuroReport*, 13(13), 1675–1678.
- Selten, M., van Bokhoven, H., & Nadif Kasri, N. (2018). Inhibitory control of the excitatory/inhibitory balance in psychiatric disorders. *F1000Research*, 7(0), 1–16.
- Shu, X., Sun, Y., Sun, X., Zhou, Y., Bian, Y., Shu, Z., ... Hu, G. (2019). The effect of fluoxetine on astrocyte autophagy flux and injured mitochondria clearance in a mouse model of depression. *Cell Death and Disease*, 10(8).
- Singh, S. K., Stogsdill, J. A., Pulimood, N. S., Dingsdale, H., Kim, Y. H., Pilaz, L. J., ... Eroglu, C. (2016). Astrocytes Assemble Thalamocortical Synapses by Bridging NRX1 α and NL1 via Hevin. *Cell*, 164(1–2), 183–196.
- Slattery, D. A., & Neumann, I. D. (2010). Chronic icv oxytocin attenuates the pathological high anxiety state of selectively bred Wistar rats. *Neuropharmacology*, 58(1), 56–61.
- Slattery, David A., & Cryan, J. F. (2014). The ups and downs of modelling mood disorders in rodents. *ILAR Journal*, 55(2), 297–309.

References

- Stevens, B., Allen, N. J., Vazquez, L. E., Howell, G. R., Christopherson, K. S., Nouri, N., ... Barres, B. A. (2007). The Classical Complement Cascade Mediates CNS Synapse Elimination. *Cell*, 131(6), 1164–1178.
- Su, S., Ohno, Y., Lossin, C., Hibino, H., Inanobe, A., & Kurachi, Y. (2007). Inhibition of Astroglial Inwardly Rectifying Kir4.1 Channels by a Tricyclic Antidepressant, Nortriptyline. *Journal of Pharmacology and Experimental Therapeutics*, 320(2), 573–580.
- Sun, J. D., Liu, Y., Yuan, Y. H., Li, J., & Chen, N. H. (2012). Gap junction dysfunction in the prefrontal cortex induces depressive-like behaviors in rats. *Neuropsychopharmacology*, 37(5), 1305–1320.
- Tabata, H. (2015). Diverse subtypes of astrocytes and their development during corticogenesis. *Frontiers in Neuroscience*, 1–7.
- Tejani-Butt, S., Kluczynski, J., & Paré, W. P. (2003). Strain-dependent modification of behavior following antidepressant treatment. *Progress in Neuro-Psychopharmacology and Biological Psychiatry*, 27(1), 7–14.
- Ullian, E. M., Sapperstein, S. K., Christopherson, K. S., Barres, B. A., & Barde, Y. (2001). Control of Synapse Number by Glia Neuronal and glial cell biology. *Curr.Opin.Neurobiol.* 10(5), 642-8.
- van Deijk, A. L. F., Camargo, N., Timmerman, J., Heistek, T., Brouwers, J. F., Mogavero, F., ... Verheijen, M. H. G. (2017). Astrocyte lipid metabolism is critical for synapse development and function in vivo. *Glia*, 65(4), 670–682.
- Varghese, F. P., & Brown, E. S. (2001). The Hypothalamic-Pituitary-Adrenal Axis in Major Depressive Disorder: A Brief Primer for Primary Care Physicians. *Prim Care Companion J Clin Psychiatry*. 3(4):151-155.
- Verkhratsky, A., Zorec, R., Parpura, V., & Neuroglia, H. (2017). Stratification of astrocytes in healthy and diseased brain. 27, 629–644.
- Wu, H. H., Bellmunt, E., Scheib, J. L., Venegas, V., Burkert, C., Reichardt, L. F., ... Carter, B. D. (2009). Glial precursors clear sensory neuron corpses during development via Jedi-1, an engulfment receptor. *Nature Neuroscience*, 12(12), 1534–1541.
- Yang, J., Yang, H., Liu, Y., Li, X., Qin, L., Lou, H., ... Wang, H. (2016). Astrocytes contribute to synapse elimination via type 2 inositol 1,4,5-trisphosphate receptor-dependent release of ATP. *ELife*, 5, 1–17.
- Yeh, T., Lee, D. A. Y., Gianino, S. M., & Gutmann, D. H. (2009). Microarray Analyses Reveal Regional Astrocyte Heterogeneity with Implications for Neurofibromatosis Type 1 (NF1) - Regulated Glial Proliferation. 1249, 1239–1249.
- Zhang, Y., Sloan, S. A., Clarke, L. E., Caneda, C., Plaza, C. A., Blumenthal, P. D., ... Barres, B. A. (2016). Purification and Characterization of Progenitor and Mature Human Astrocytes Reveals Transcriptional and Functional Differences with Mouse. *Neuron*, 89(1), 37–53.

Zhou, Z., Hartweg, E., & Horvitz, H. R. (2001). CED-1 Is a Transmembrane Receptor that Mediates Cell Corpse Engulfment in *C. elegans*. *Cell*, 104(1), 43–56.

Ziegenfuss, J. S., Biswas, R., Avery, M. A., Hong, K., Sheehan, A. E., Yeung, Y. G., ... Freeman, M. R. (2008). Draper-dependent glial phagocytic activity is mediated by Src and Syk family kinase signalling. *Nature*, 453(7197), 935–939.

WHO 2012 <http://www.euro.who.int/en/health-topics/noncommunicable-diseases/mental-health/news/news/2012/10/depression-in-europe/depression-in-europe-facts-and-figures>

WHO 2017 Depression and other common mental disorders. Global health estimates (2017) World Health Organization. Geneva. Licence: CC BY-NC-SA3.0 IGO.

Acknowledgments

Acknowledgments

First and foremost, I would like to express my gratitude to my supervisor Dr. Barbara Di Benedetto for allowing me to develop my thesis in her research group. In all these years her guidance, advice and mentoring helped me to learn more about science and to progress with my research. Thanks also to the head of the department, Prof. Dr. Rupprecht. I would like to thank Prof. Dr. Inga Neumann for her interest in my project and her support in the GRK program. I also wish to express my gratitude to the professors and colleagues of the GRK for the advice and all the opportunities I had during these years.

My special thanks go to all the people who I have shared laboratory with, especially Heike, for helping me every time that I needed and for her patience during all the very last-minute decisions. Gautami and Luisa were also very important persons during my thesis; they nicely contributed to this project with their work and support and I hope they could learn from me as much as I learned from them. Thanks also to Vladi; even if he is from a different lab he kindly tried to resolve my questions every time I was lost.

Patri, Vane and Laura need to be here. Thanks to them I felt that I had a family in Germany. They understood how hard science can be and always gave me support. You are in all the best memories I have from these three years in Regensburg.

The beginning was difficult: new city, new lab, different language... but thanks to all the new friends I made here, things became much easier. I feel that I have always been surrounded by good people. Thanks for all the lunches, evenings, Stammtische, visits to the Dult and trips you have shared with me.

Very special thanks to Enri. You have always been present whenever I needed you. I am so happy we met here and you could be part of this journey until the very end.

To all my friends from NdO, thanks for making me feel as if I had never left every time I was visiting.

Last but not least, many thanks to my family: papa, mama and Marta. Since I started to study biology, I have been in three different countries, further away than you would wish, but I could always feel your support and enthusiasm when the things were working for me. ¡Gracias!

